

NASA/TM-2013-218026



Investigation of Control Inceptor Dynamics and Effect on Human Subject Performance

*Anthony A. Stanco and Frank M. Cardullo
State University of New York, Binghamton, New York*

*Jacob A. Houck and Richard C. Grube
Langley Research Center, Hampton, Virginia*

*Lon C. Kelly
Unisys Corporation, Hampton, Virginia*

NASA STI Program . . . in Profile

Since its founding, NASA has been dedicated to the advancement of aeronautics and space science. The NASA scientific and technical information (STI) program plays a key part in helping NASA maintain this important role.

The NASA STI program operates under the auspices of the Agency Chief Information Officer. It collects, organizes, provides for archiving, and disseminates NASA's STI. The NASA STI program provides access to the NASA Aeronautics and Space Database and its public interface, the NASA Technical Report Server, thus providing one of the largest collections of aeronautical and space science STI in the world. Results are published in both non-NASA channels and by NASA in the NASA STI Report Series, which includes the following report types:

- **TECHNICAL PUBLICATION.** Reports of completed research or a major significant phase of research that present the results of NASA Programs and include extensive data or theoretical analysis. Includes compilations of significant scientific and technical data and information deemed to be of continuing reference value. NASA counterpart of peer-reviewed formal professional papers, but having less stringent limitations on manuscript length and extent of graphic presentations.
- **TECHNICAL MEMORANDUM.** Scientific and technical findings that are preliminary or of specialized interest, e.g., quick release reports, working papers, and bibliographies that contain minimal annotation. Does not contain extensive analysis.
- **CONTRACTOR REPORT.** Scientific and technical findings by NASA-sponsored contractors and grantees.

- **CONFERENCE PUBLICATION.** Collected papers from scientific and technical conferences, symposia, seminars, or other meetings sponsored or co-sponsored by NASA.
- **SPECIAL PUBLICATION.** Scientific, technical, or historical information from NASA programs, projects, and missions, often concerned with subjects having substantial public interest.
- **TECHNICAL TRANSLATION.** English-language translations of foreign scientific and technical material pertinent to NASA's mission.

Specialized services also include organizing and publishing research results, distributing specialized research announcements and feeds, providing information desk and personal search support, and enabling data exchange services.

For more information about the NASA STI program, see the following:

- Access the NASA STI program home page at <http://www.sti.nasa.gov>
- E-mail your question to help@sti.nasa.gov
- Fax your question to the NASA STI Information Desk at 443-757-5803
- Phone the NASA STI Information Desk at 443-757-5802
- Write to:
STI Information Desk
NASA Center for AeroSpace Information
7115 Standard Drive
Hanover, MD 21076-1320

NASA/TM-2013-218026



Investigation of Control Inceptor Dynamics and Effect on Human Subject Performance

Anthony A. Stanco and Frank M. Cardullo
State University of New York, Binghamton, New York

Jacob A. Houck and Richard C. Grube
Langley Research Center, Hampton, Virginia

Lon C. Kelly
Unisys Corporation, Hampton, Virginia

National Aeronautics and
Space Administration

Langley Research Center
Hampton, Virginia 23681-2199

July 2013

Available from:

NASA Center for Aerospace Information
7115 Standard Drive
Hanover, MD 21076-1320
443-757-5802

Abstract

The control inceptor used in a simulated vehicle is an important part of adequately representing the dynamics of the simulation. The force feedback sensed by the operator through the control inceptor gives the pilot important cues to maintain adequate performance. The dynamics of a control inceptor are typically based on a second order spring mass damper system with damping, force gradient, breakout force, and natural frequency parameters. Changing these parameters can have a great effect on pilot or driver control of the vehicle. The neuromuscular system has a very important role in controlling the vehicle through the control inceptor.

Many studies by McRuer ([11],[13],[14]), Aponso ([10],[16]), and Hess ([4],[5],[6],[7],[8]) have dealt with modeling the neuromuscular system and quantifying the effects of a high fidelity control loader as compared to a low fidelity control loader. Pilots are adaptive in nature and their control behavior in simulators change based on different control loader dynamics. Pilots will change their control behavior to maintain tracking bandwidth and minimize tracking error.

A quasi-transfer of training experiment was performed at the NASA Langley Research Center. The study employed a high fidelity control loader and a low fidelity control loader. Test subjects trained in both simulations and then were transferred to the high fidelity control loader simulation. This is conducted to test the difference between training on two different control loader dynamics. The parameters for the high fidelity control loader were determined from the literature. The low fidelity control loader parameters were found through testing of a simple computer joystick.

A disturbance compensatory task was employed for the quasi transfer of training experiments. The compensatory task involved implementing a simple horizon on an out the window display. A disturbance consisting of a sum of sinusoids was used. The task consisted of the pilot compensating for the disturbance on the roll rate of the aircraft. The vehicle dynamics were represented as $1/s$ and $1/s^2$. It is well known that $1/s$ plant dynamics is an easy task, but $1/s^2$ plant dynamics is a hard task. The test subject tried to maintain level flight throughout the experiment. The test subjects consisted of non-pilots to remove any effects of pilot experience. A total of 20 test subjects, 10 placed in a low fidelity control inceptor training group and 10 placed in a high fidelity control inceptor training group, were used. Each group was trained until they reached a performance asymptote, then they were transferred to the high fidelity control inceptor simulation. The effect of training on either control inceptor was analyzed.

Performance metrics such as RMS tracking error, PSD analysis, and a workload analysis were performed to quantify the transfer of training effect on both the high and low fidelity control loader simulations.

Quantitative results of the experiments show that there is no significant difference between the high fidelity and low fidelity training groups for $1/s$ plant dynamics. Both their RMS tracking error and PSD results are similar suggesting similar control behavior and tracking performance. For $1/s^2$ plant dynamics there is a greater difference in tracking performance and also the PSD. Also, for $1/s^2$ plant dynamics the test subjects are less correlated with the input disturbance function.

Contents

<i>Abstract</i>	<i>i</i>
<i>Contents</i>	<i>iii</i>
<i>List of Tables</i>	<i>v</i>
<i>List of Figures</i>	<i>vi</i>
<i>Nomenclature</i>	<i>ix</i>
<i>Acronyms</i>	<i>xi</i>
<i>Chapter 1 - Introduction</i>	<i>1</i>
1.1 Introduction.....	1
1.2 Objectives and Scope of Research.....	3
1.3 Report Organization.....	4
<i>Chapter 2 Background</i>	<i>5</i>
2.1 Fidelity Assessment.....	5
2.2 Aircraft Control System Dynamics.....	6
2.3 Neuromuscular Models.....	13
2.4 Transfer of Training.....	17
2.5 Tracking Tasks.....	18
<i>Chapter 3 - Literature Review of Control Force Feedback Dynamics</i>	<i>20</i>
3.1 Introduction.....	20
3.2 Neuromuscular/Pilot system models.....	21
3.2.1 Precision Model.....	22
3.2.2 Lateral Head Motion Model.....	23
3.2.3 Hess Structural Model.....	28
3.2.4 Neuromusculoskeletal Model.....	30
3.3 Force Feel Research.....	32
<i>Chapter 4 - Design of Transfer of Training Study</i>	<i>47</i>
4.1 Introduction.....	47
4.2 Roll Disturbance Compensation Task.....	47
4.3 Force Feel Parameter Determination.....	50
4.3.1 High Fidelity Control Loader Parameters.....	50
4.3.2 Low Fidelity Control Loader Parameters.....	52
4.4 Analysis of Control Loader Parameters.....	56
4.4.1 Experimentally Obtained High Fidelity Characteristics.....	64
4.4.2 Experimentally Obtained Low Fidelity Characteristics.....	70
4.5 Disturbance Input & Performance Metric Tests.....	73

<i>Chapter 5 - Experimental Setup</i>	79
5.1 Introduction.....	79
5.2 Background	79
5.3 Implementation of Transfer of Training Study	80
5.3.1 Protocol.....	81
5.3.2 Test Setup	83
5.3.3 Display Setup	86
5.3.4 Force Feel Parameters Implementation	88
<i>Chapter 6 - Results and Discussion</i>	91
6.1 Introduction.....	91
6.2 Performance Metrics.....	92
6.3 PSD Analysis	103
6.4 Coherence Analysis	117
6.5 Frequency Responses of Test Subjects	119
6.6 Remnant	130
<i>Chapter 7 – Conclusions and Future Recommendations</i>	131
7.1 Summary.....	131
7.2 Conclusions	132
7.3 Future Recommendations.....	135
<i>Appendices</i>	137
Appendix A: Control Loader Quasi Transfer of Training Experimental Protocol	137
Appendix B: Experimental Measured and Calculated Parameters.....	141
Appendix C: Experiment Run Time.....	142
Appendix D: Matlab [21] Code to Calculate Frequency Response	143
Appendix E: Experiment Pseudo Code	144
Appendix F: Experiment Flow Chart	147
Appendix G: Mean Square and Variance for High Fidelity and Low Fidelity Training Groups	148
Appendix H: Peak Power and Frequency for Every Test Subject	154
Appendix I: Average Tracking Error Using More Runs to Train.....	156
Appendix J: Smoothed Periodogram Matlab [21] Code	159
<i>References</i>	162

List of Tables

Table 3.2.1 Neuromuscular Subsystems Model Parameter Values	23
Table 3.2.2 Lateral Head Motion Parameter Values (Gum, 1973) [2]	23
Table 3.3.1 Force Feel Characteristics (Johnston, 1988) [10]	37
Table 3.3.2 Disturbance Sum of Cosines Parameters (Johnston, 1988) [10]	37
Table 4.4.1 Control Inceptor Characteristics	56
Table 4.4.2 Frequency Sweep Input Sinusoid Formulation	59
Table 4.4.3 Acquired High Fidelity Effective Mass with Low Damping Ratio	66
Table 4.5.1 Sum of Sines Disturbance Input	73
Table 4.5.2 Disturbance Input Implemented in MMS Laboratory	75
Table 5.3.1 McFadden Control Loader Parameter Table	88
Table 5.3.2 Implemented Control Inceptor Characteristics	90
Table 6.2.1 Average Number of Runs to Reach Asymptote	101
Table 6.5.1 Disturbance Sum of Sinusoids Parameters.....	123

List of Figures

Figure 2.2.1 Reversible Flight Control System (Takats, 2011) [18]	7
Figure 2.2.2 Fly-By-Wire Flight Control System (Takats, 2011) [18]	8
Figure 2.2.3 Position Servo Control Loader Model (Takats, 2011) [18]	10
Figure 2.2.4 Analog/Digital Control Loader System (Takats, 2011) [16]	11
Figure 2.2.5 Force Servo Control Loader Model (Takats, 2011) [18]	12
Figure 2.2.6 McFadden Control Loader Model (McFadden Systems Inc., 1999) [15]	13
Figure 2.3.1 Lateral Head Motion Block Diagram (Gum, 1973) [2]	14
Figure 2.3.2 Neuromuscular Subsystems Model (Magdaleno & McRuer, 1971) [13]	15
Figure 2.3.3 The Structural Model of the Human operator for Compensatory Tracking (Hess, 1985) [8]	16
Figure 2.3.4 Neuromusculoskeletal Model (Hosman, 2010) [9]	17
Figure 3.2.1 Antagonistic Muscle Pairs (Magdaleno & McRuer, 1968) [14]	21
Figure 3.2.2 Neuromuscular Subsystems Model (Magdaleno & McRuer, 1971) [13]	23
Figure 3.2.3 Lateral Head Motion Block Diagram (Gum, 1973) [2]	23
Figure 3.2.4 Muscle Dynamics Frequency Response	24
Figure 3.2.5 Muscle Spindle Feedback Frequency Response	25
Figure 3.2.6 Lateral Head Motion Control Frequency Response	26
Figure 3.2.7 Lateral Head Motion Control Step Response	27
Figure 3.2.8 The Structural Model of the Human operator for Compensatory Tracking (Hess, 1985) [8]	28
Figure 3.2.9 Revised Structural Model of the Human Operator for Pursuit Tracking (Hess, 2000) [4]	29
Figure 3.2.10 Neuromusculoskeletal Model (Hosman, 2010) [9]	31
Figure 3.3.1 Lateral Flying Qualities Experimental Set Up (Bailey, 1990) [1]	32
Figure 3.3.2 Roll Command Gain vs. Roll Mode Time Constant (Bailey, 1990) [1]	34
Figure 3.3.3 Roll Tracking Task Block Diagram (Johnston, 1988) [10]	36
Figure 3.3.4 Effective Controlled Element (Johnston, 1988) [10]	38
Figure 3.3.5 Amplitude Ratio Peak as a Function of Force Gradient Constant (Johnston, 1988) [10]	38
Figure 3.3.6 Task Bandwidth vs. Roll Command Gain (Johnston, 1988) [10]	39
Figure 3.3.7 Workload vs. the Reciprocal of the Product of Roll Command Gain and Task Bandwidth (Johnston, 1988) [10]	40
Figure 3.3.8 Cooper Harper Rating vs. Roll Command Gain (Johnston, 1988) [10]	41
Figure 3.3.9 Center-Stick Experimental Setup (Johnston, 1988) [10]	42
Figure 3.3.10 Task Tracking Bandwidth as a Function of Feel System Natural Frequency (Johnston, 1988) [10]	43
Figure 3.3.11 Task Tracking Error as a Function of Feel System Natural Frequency (Johnston, 1988) [10]	44
Figure 3.3.12 CHPR as a Function of Feel System Natural Frequency (Johnston, 1988) [10]	45
Figure 4.2.1 Developed Roll Disturbance Compensatory Tracking Task	48
Figure 4.3.1 Simulated High Fidelity Control Loader Step Response	51
Figure 4.3.2 Logitech Computer Joystick Transient Response Obtained from MMS Laboratory	54

Figure 4.3.3 Logitech Computer Joystick Transient Response Obtained using Labview [20].....	55
Figure 4.4.1 Force Servo Control Loader Model (Takats, 2011) [18]	57
Figure 4.4.2 Frequency Sweep Configuration (Takats, 2011) [18]	59
Figure 4.4.3 Simulated High Fidelity Frequency Response	62
Figure 4.4.4 Simulated Low Fidelity Frequency Response	63
Figure 4.4.5 High Fidelity Force vs. Displacement	64
Figure 4.4.6 High Fidelity Free Release Response with Low Damping Ratio	65
Figure 4.4.7 Experimental High Fidelity Free Release Response	67
Figure 4.4.8 Experimental High Fidelity Frequency Response with Low Damping Ratio	69
Figure 4.4.9 Experimental Low Fidelity Force vs. Displacement	70
Figure 4.4.10 Experimental Low Fidelity Free Release Response	71
Figure 4.4.11 Experimental Low Fidelity Frequency Response	72
Figure 4.5.1 Plot of Roll Angle Disturbance	74
Figure 4.5.2 RMS Tracking Error Obtained from Test within MMS Laboratory	75
Figure 4.5.3 Slope of RMS Tracking Error Obtained from Test within MMS Laboratory	76
Figure 4.5.4 RMS Control Inceptor Deflection Obtained from Test within MMS Laboratory	77
Figure 4.5.5 Slope of RMS Control Inceptor Deflection Obtained from Test within MMS Laboratory	78
Figure 5.2.1 Cockpit Motion Facility (NASA LaRC).....	80
Figure 5.3.1 Quasi Transfer of Training Experimental Configuration	84
Figure 5.3.2 Out-the-Window Display Setup	88
Figure 6.2.1 Average Tracking Error for High Fidelity Training Group (1/s Plant Dynamics)	92
Figure 6.2.2 Average Tracking Error for Low Fidelity Training Group (1/s Plant Dynamics)	93
Figure 6.2.3 Average Tracking Error Results for Both Training Groups (1/s Plant Dynamics)	94
Figure 6.2.4 Average Tracking Error Results for High Fidelity Training Group (1/s ² Plant Dynamics)	95
Figure 6.2.5 Average Tracking Error for Low Fidelity Training Group (1/s ² Plant Dynamics)	97
Figure 6.2.6 Average Tracking Error Results for Both Training Groups (1/s ² Plant Dynamics)	97
Figure 6.2.7 Average Tracking Error with Greater Amount of Runs (Test Subject HF001 1/s Plant Dynamics)	99
Figure 6.2.8 Average Tracking Error with Greater Amount of Runs (Test Subject LF009 1/s Plant Dynamics)	100
Figure 6.2.9 Average Tracking Error (1/s Plant Dynamics)	102
Figure 6.2.10 Average Tracking Error (1/s ² Plant Dynamics).....	102
Figure 6.3.1 Variance of Roll Stick Deflection 1 st Run (High Fidelity Group 1/s Plant Dynamics)	104

Figure 6.3.2 Variance of Roll Stick Deflection 1 st Run (Low Fidelity Group 1/s Plant Dynamics)	104
Figure 6.3.3 Average Peak Power (1/s Plant Dynamics)	105
Figure 6.3.4 Average Peak Frequency (1/s Plant Dynamics)	106
Figure 6.3.5 Average Peak Power (1/s ² Plant Dynamics)	108
Figure 6.3.6 Average Peak Frequency (1/s ² Plant Dynamics)	109
Figure 6.3.7 PSD of Disturbance Forcing Function	110
Figure 6.3.8 Average PSD for High Fidelity and Low Fidelity Training Test Subjects Last Run Training (1/s Plant Dynamics)	111
Figure 6.3.9 Average PSD for High Fidelity and Low Fidelity Training Test Subjects First Run Transfer (1/s Plant Dynamics)	111
Figure 6.3.10 Average PSD for High Fidelity and Low Fidelity Training Test Subjects Last Run Transfer (1/s Plant Dynamics)	112
Figure 6.3.11 Average PSD for High Fidelity and Low Fidelity Training Test Subjects Last Run Training (1/s ² Plant Dynamics)	113
Figure 6.3.12 Average PSD for High Fidelity and Low Fidelity Training Test Subjects First Run Transfer (1/s ² Plant Dynamics)	113
Figure 6.3.13 Average PSD for High Fidelity and Low Fidelity Training Test Subjects Last Run Transfer (1/s ² Plant Dynamics)	114
Figure 6.3.14 PSD of Control Inceptor Deflection for Best and Worst Test Subjects (High Fidelity 1/s Plant Dynamics)	115
Figure 6.3.15 PSD of Control Inceptor Deflection for Best and Worst Test Subjects (Low Fidelity 1/s Plant Dynamics)	115
Figure 6.3.16 PSD of Control Inceptor Deflection for Best and Worst Test Subjects (High Fidelity 1/s ² Plant Dynamics)	116
Figure 6.3.17 PSD of Control Inceptor Deflection for Best and Worst Test Subjects (Low Fidelity 1/s ² Plant Dynamics)	116
Figure 6.4.1 Coherence between Control Inceptor Deflection and Disturbance Forcing Function (1/s Plant Dynamics)	117
Figure 6.4.2 Coherence between Control Inceptor Deflection and Disturbance Forcing Function (1/s ² Plant Dynamics)	118
Figure 6.5.1 Single Sided Amplitude Spectrum of Disturbance	123
Figure 6.5.2 Test Subject HF002 Experimental Frequency Response	124
Figure 6.5.3 Test Subject HF002 Experimental Frequency Response Averaged Over Four Runs	125
Figure 6.5.4 Coherence Between Roll Error and Control Inceptor Deflection for One Run (Test Subject HF002)	126
Figure 6.5.5 Coherence Between Roll Error and Control Inceptor Deflection Average over Four Runs (Test Subject HF002)	126
Figure 6.5.6 Frequency Response for LTI System (Original Disturbance Forcing Function)	128
Figure 6.5.7 Frequency Response for LTI System (Finer Frequency Vector Input)	128
Figure 6.5.8 Frequency Response for LTI System (Chirp Input Signal)	129
Figure 6.6.1 PSD of Control Inceptor Deflection for Test Subject HF002	130
Figure 6.6.2 PSD of Control Inceptor Deflection for Test Subject HF005	131

Nomenclature

Symbol:	Definition:	Units:
ω	Frequency	rad/s
ζ	Damping ratio	dimensionless
τ	Time constant	seconds
m or M	Mass	kg or lb•s ² /in
c, b, or β	Damping coefficient	lb•s/in
θ	Generic Angle	degrees
ϕ	Bank Angle	degrees
k or K_{FS}	Force gradient	lb/in
K	Generic Gain	non-dimensional
L'_{Fas}	Roll Rate Command Gain	deg/s ² /lb
P/F_{as}	Roll Sensitivity	deg/s/lb
σ_e	Roll Tracking Error	degrees
σ_c	Manipulator Control Effort (Force or Position)	lb or in
I	Inertia	kg•m ²
g	Gravity	m/s ² or ft/s ²
ρ	Roll Rate	deg/s or rad/s
δ_{ac}	Aileron Deflection Command	degrees
δ_{as}	Output Lateral Deflection of Control Inceptor	inches

Subscripts	Definition
() _N	Relates to Natural Frequency
() _P	Relates to the Pilot
() _e	Relates to Equalization or Effort
() _{sp}	Relates to the Muscle Spindle
() _j	Relates to the Joint
() _g	Relates to Gravity
() _h	Relates to the Head
() _m	Relates to the Muscle
() _i	Relates to Input
() _o	Relates to Output
() _{NM}	Relates to Neuromuscular System
() _{FS}	Relates to the Feel System
() _C	Relates to Control or Manipulator Contact Dynamics of a Task
() _{PF}	Relates to the Proprioceptive Feedback
() _{int}	Relates to the Limb Dynamics
() _{ms}	Relates to the Muscle Spindle
() _{gto}	Relates to the Golgi Tendon
() _{act}	Relates to Muscle Activation
() _v	Relates to a Velocity
() _p	Relates to a Position

- ()_a Relates to an Acceleration
- ()_r Relates to a Rate

Acronyms

CMF	Cockpit Motion Facility
CHPR	Cooper Harper Pilot Rating
CHR	Cooper Harper Rating
CTFT	Continuous Time Fourier Transform
DFT	Discrete Fourier Transform
DTFT	Discrete Time Fourier Transform
EMG	Electromyography
FFT	Fast Fourier Transform
FRF	Frequency Response Function
GFD	Generic Flight Deck Simulator
HFOV	Horizontal Field of View
HQR	Handling Qualities Rating
HUD	Head Up Display
IFD	Integration Flight Deck Simulator
Labview	Laboratory Virtual Instrumentation Engineering Workbench
LATHOS	Lateral High Order System
MMS	Man Machine Systems
PIO	Pilot Induced Oscillation
PO	Percent Overshoot
PSD	Power Spectrum Density
RFD	Research Flight Deck Simulator
RMS	Root Mean Square
SIMES	Simulation Evaluation System
STD	Standard Deviation
STI	System Technology Inc.
USAF	United States Air Force
VFOV	Vertical Field of View

Chapter 1 - Introduction

1.1 Introduction

Vehicle simulation is employed to train operators of various vehicles to reach a performance level adequate to operate the real-world vehicle. Simulation uses fewer resources than the real-world vehicle to train for the same task. With the real-world vehicle, the amount of cost and time to perform tasks is not optimal for training operators. With a simulation, different environments and tasks can be interchanged without losing time and resources. The goal of training is for operators to have good transfer of training where operator performance is maintained when transferring to the real-world vehicle. Training in simulators helps to train operators efficiently without the possibility of accidents.

Before simulators, operators trained in the real-world vehicles and some small number still do. With the introduction of complicated control systems in vehicles today, training is necessary in a safe environment before operators enter the real world vehicle. This helps prevent accidents during training and helps to train operators to prevent accidents from occurring in normal operation of the vehicle. Simulation provides the necessary practice to prevent unwanted circumstances occurring in real-world vehicle training. Simulators can be used in research to test different tasks not achievable and not safe in the real-world vehicle. Using simulator research, real-world vehicles can be improved, a better understanding of human control can be sought and future accidents can be prevented. Simulators have to provide realistic cues to the operator in order to train them effectively (Wiener, 1988) [19].

Vehicle simulation uses principles of human perception to closely replicate the vehicle it is simulating. Visual, vestibular, and proprioceptive feedback are the main components of human perception employed for vehicle control. These components work together with the cognitive system to stimulate a characteristic human control strategy. The fidelity of the simulation depends on how closely the performance of the simulator matches the vehicle. The purpose of simulation is to maintain high fidelity while keeping within the constraints of the simulator. The simulator has motion limitations that make it difficult to recreate the same accelerations, velocities, and displacements experienced in the vehicle.

A vehicle simulator uses cueing algorithms, i.e. control laws which stimulate perceptions in the simulator sufficient to produce a pilot control strategy similar to the criterion vehicle. The visual system on a simulator should also have high fidelity, recreating the scenery with details necessary for training preserved. The motion system should be correlated with visual cues otherwise the cues will conflict and provide misleading information to the pilot. Another system component involved in simulation is the force feel feedback in the vehicle. The fidelity of the control loader has fewer limitations than both the motion and visual systems. The control inceptor is the main interface of the pilot with the vehicle dynamics. Therefore, control loader force feedback can have a significant impact on the control strategy of the human operator. The control loader force feedback effect on human test subject performance is the primary focus of the research discussed in this report.

1.2 Objectives and Scope of Research

The control inceptor is the main operator-vehicle interface. Control loader systems provide the force feel feedback necessary to train test subjects efficiently. Initially, control loaders used mechanical springs, dashpots, cams, and friction brakes. As aircraft flight controls systems became more complicated, control loader systems had to provide more realistic force feedback cues (Takats, 2011) [18]. The updated control loader systems are able to match the non-linear parameters involved in vehicle control. Maintaining a high fidelity control inceptor wherein the control inceptor dynamics in the real world vehicle are accurately reproduced in the simulated vehicle is important. A quasi transfer of training experiment was conducted in order to investigate the effect of training operators on either a high fidelity or low fidelity control inceptor simulation.

The real-time training experiment which was conducted at NASA Langley Research Center provides the necessary data for analysis. Using objective metrics, an in depth analysis of test subject performance is discussed in the final chapters. Also, any future recommendations will be discussed to improve the control loader experimentation. The main objectives of these experiments are listed below.

Objectives of this research:

- Fundamental objective is to determine if the fidelity of a control loader affects training
- Define high and low fidelity control loader parameters
- Verify control loader parameters
- Develop a compensatory disturbance tracking task
- Develop the quasi-transfer of training study

- Implement experimental task on fixed base simulator
- Run test subject experiments and analyze results
- Develop test plans for future experimentation

1.3 Report Organization

This report is organized as follows. The second chapter gives a brief background on control systems in aircraft, control loader systems, the neuromuscular system, transfer of training experiments, and compensatory tasks. Chapter 3 presents a review of literature on different neuromuscular models and the different experiments to test the effect of the control loader system dynamics on human control performance. Chapter 4 describes the design of the quasi-transfer of training roll disturbance compensatory task. In this chapter, the two control loader dynamics representing a high fidelity and low fidelity control loader system were defined and implemented on a simulator located at NASA Langley Research Center. Frequency responses and step responses were obtained to verify the implemented force gradient, natural frequency, damping ratio, and breakout force. This chapter is important to understand how the experiment was performed.

In Chapter 5, the test setup of the experiment is discussed. The protocol, experimental measurements, experimental pseudo code as well as the simulator used for experiments are presented here. This is a useful chapter for those that need to recreate the experiment presented in this research. Chapter 6 discusses the results of test subject performance and control strategy using RMS tracking error and PSD analysis. Chapter 7 gives conclusions for this research and future recommendations to improve the experiment.

Chapter 2 Background

2.1 Fidelity Assessment

The force feedback cues provided to the operator are very important for the control strategy within different vehicles. The effect of training on a control inceptor with different force feedback characteristics than the real world vehicle is unknown. This report will ascertain important information on these force feedback cues and the significance of control inceptor fidelity.

Fidelity has been defined by Hess (1991) [6] as “the degree to which characteristics of perceivable states induce adequate pilot psychomotor and cognitive behavior for a given task and environment.” Typically, simulators cannot match the full motion capabilities of the vehicle being simulated. Therefore, simulators rely on the principles of human perception to provide the cues which induce proper operator control of the vehicle. This is a key component in maintaining motion fidelity and part of the difficulty to obtain adequate simulator fidelity. On the other hand, the visual system fidelity is obtained by replicating the simulator visual scene as closely as possible to the real-world visual scene. Maintaining visual fidelity requires synchronizing the visual to the motion characteristics. A conflicting visual and motion cue can have adverse effects on test subject’s control of the simulated vehicle. The force feel system dynamics are easily replicated although there are still limitations. The limitations include non-linear effects such as friction and the ability to maintain sufficient bandwidth while preserving the force gradient. In the research conducted, the control behavior between the high fidelity and low fidelity simulation is investigated to ascertain if force feedback is necessary for adequate control behavior.

There has been considerable focus for fidelity assessment on motion systems and visual systems. Hess (2000) [4] proposed the Handling Qualities Sensitivity Function (HQSF) as a method for assessing simulator fidelity. This function uses the Hess structural model (Hess, 1985) [8] of the human pilot to determine how the input power is transferred to output control power of the pilot. It is consistent with a transfer function which relates the input to the output of the pilot. The fidelity metric relates the area below the HQSF between the real world vehicle and the simulated vehicle. As the value of the fidelity metric becomes larger, the simulator fidelity is lower. Another approach is the Sinacori technique (Schroeder, 1999) [17], which compares the gain and phase distortion between the nominal vehicle and the simulated vehicle. The gain and phase distortion should be minimal for the simulation to be considered high fidelity.

2.2 Aircraft Control System Dynamics

Many new aircraft have moved to mechanical hydraulically boosted and fly-by-wire force feel control systems which have unknown effects on pilot performance. The mechanical hydraulically boosted and fly-by-wire control systems do not have any direct physical connection to the control surfaces of the aircraft. Both mechanical hydraulically boosted and fly-by-wire control systems use hydraulics to reduce the forces required to move the control surfaces. Mechanical hydraulically boosted and fly-by-wire control systems utilize an artificial force feel device to create the force feedback cues that arrive from the aerodynamic forces on the control surfaces. In the same manner, simulators use a control loader system to simulate the control inceptor dynamics in the real world vehicle. Within this section, there is a discussion on the background of aircraft and simulator flight control systems.

The flight control systems in aircraft prior to World War I consisted of direct mechanical linkages to the control surfaces (Takats, 2011) [18]. This type of flight control system is referred to as a reversible flight control system whereby the aerodynamic forces on the control surfaces are felt directly by the pilot. An example of a reversible flight control system is shown below in Figure 2.2.1.

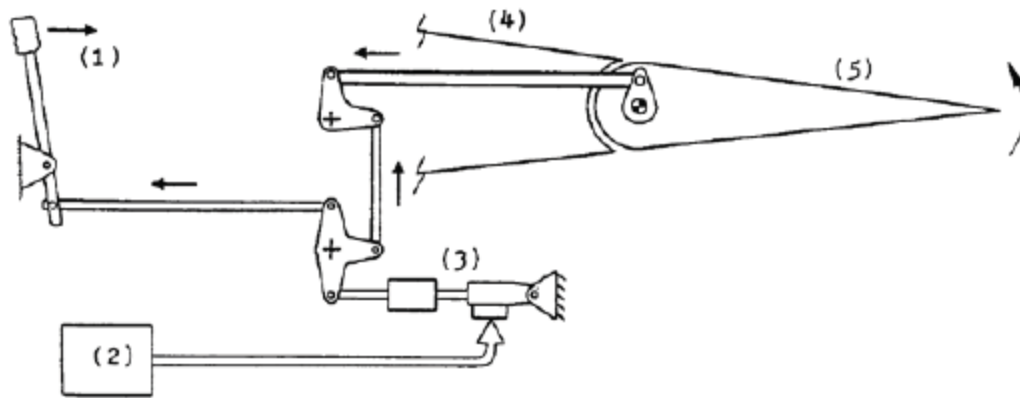


Figure 2.2.1 Reversible Flight Control System (Takats, 2011) [18]

In Figure 2.2.1, the input force by the operator causes the control inceptor (1) to deflect. Through a series of direct linkages and hinges, a hinge moment is applied to the control surface (5). This causes an increased aerodynamic force on the control surface (5) which is directed back to the control inceptor via the linkages and hinges. The gearing of the linkages provides a certain amount of mechanical advantage but is limited by the space available within the aircraft. Also shown in Figure 2.2.1 is the autopilot (2) system. The autopilot applies a signal to a servo valve to increase hydraulic flow, therefore increasing the applied force. The force from the hydraulic actuator is applied by way of linkages to deflect the control surface (5).

On larger aircraft, hydraulically boosted flight control systems are typically used. Two types of hydraulically boosted flight control systems exist: mechanical and fly-by-

wire. The mechanical hydraulically boosted flight control system utilizes mechanical linkages to control a hydraulic valve actuator instead of direct connection to the control surfaces. For the fly-by-wire systems either an analog circuit or a digital computer is used to measure pilot control inceptor inputs and apply a command to an actuator to drive the control surfaces. The fly-by-wire and mechanical hydraulically boosted control systems are examples of irreversible flight control systems. For both systems, the aerodynamic forces cannot be felt by the pilot because of the absence of the direct linkage to the control surfaces. For these systems, an artificial feel system is implemented to simulate any force feedback characteristics (Takats, 2011) [18]. An example of a fly-by-wire flight control system is shown in Figure 2.2.2.

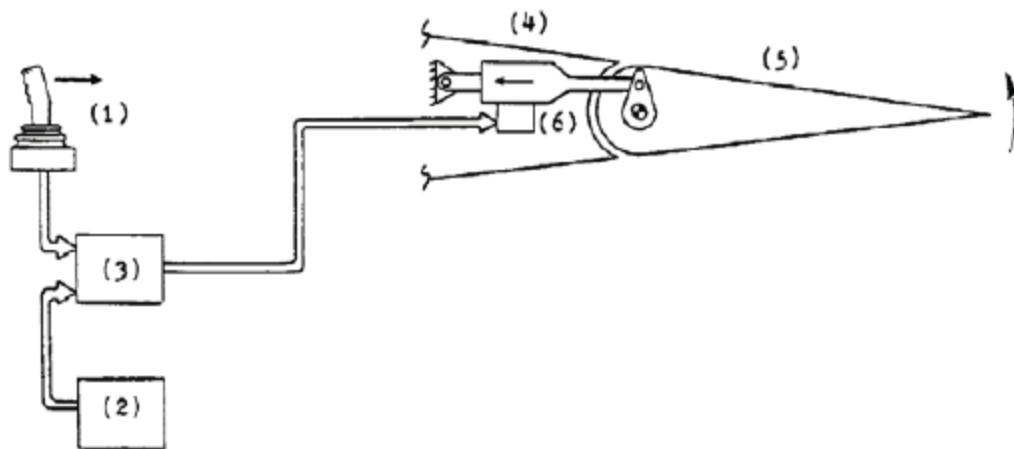


Figure 2.2.2 Fly-By-Wire Flight Control System (Takats, 2011) [18]

In Figure 2.2.2, the deflection of the control inceptor (1) from the operator is analyzed by an analog or digital computer. The computer then sends the proper command to a hydraulic valve actuator (6) which provides the hinge moment to deflect the control surface (5). An autopilot system (2) can bypass the control by the operator by directly controlling the command to the hydraulic valve actuator (6).

The flight control system characteristics are divided into two groups; the aft mass and the forward mass. For an irreversible flight control system, the forward mass includes the control inceptor and the linkages to the control surfaces. The aft mass includes any linkages, hinges, and aerodynamic forces on the control surface itself. Some of the components to consider when modeling the aircraft control system are the spring and damping forces due to the linkages and the mass attached. Also, the hinge moments due to aerodynamic forces are considered for the aft mass model. When modeling a hydraulically boosted system, the dynamics of the hydraulic actuator must be included. The forward mass simulation for most irreversible systems represents a spring mass damper system with: force gradient, natural frequency, and a damping coefficient term. With modern fly-by-wire systems, nonlinear characteristics can be present such as breakout force, friction, and detents. The fly-by-wire system allows for the choice of certain characteristics, which can affect the stability of the aircraft. This is why many aircraft have digital systems that help stabilize the aircraft (Takats, 2011) [18].

Control loader systems are utilized in simulators to simulate the control inceptor characteristic dynamics. These dynamics include the force gradient, damping, natural frequency, friction, detents, breakout force, and any other nonlinear dynamics. Early control loader systems used a position feedback control loop. An example of a position feedback control loader system is shown in Figure 2.2.3. As the control inceptor is moved, both the force and position on the control inceptor are measured. The force is fed through the aft mass and forward mass simulations, which creates the appropriate dynamics.

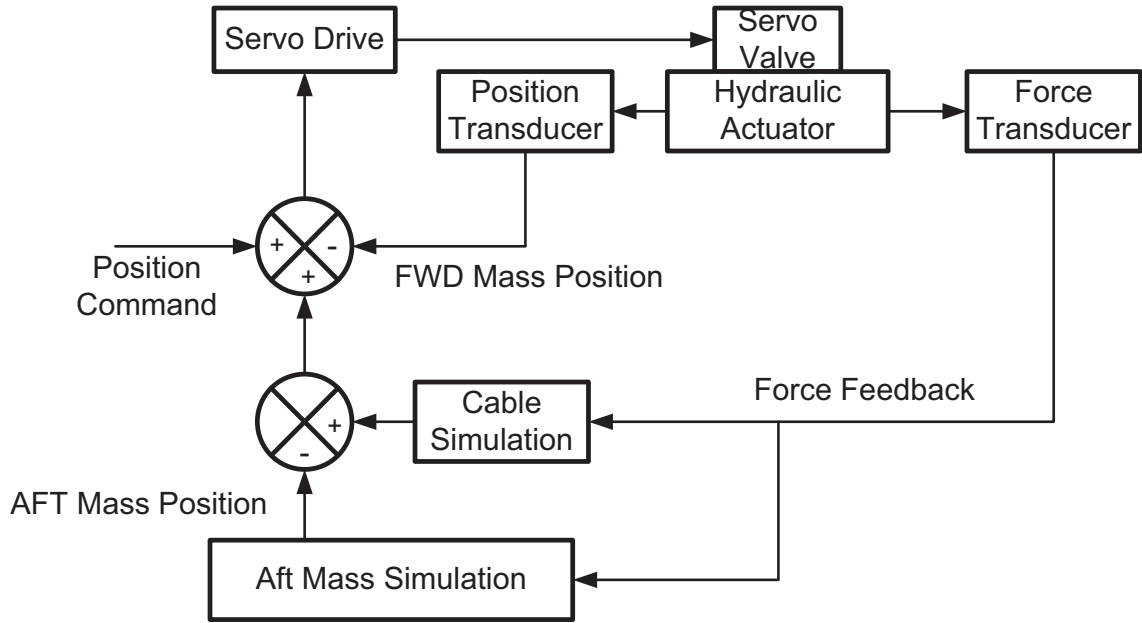


Figure 2.2.3 Position Servo Control Loader Model (Takats, 2011) [18]

The combination of the aft and forward mass simulation results in a commanded position. The servo drive command is produced when the position of the control inceptor is subtracted from the commanded position. The position servo control loader has limits on the achievable bandwidth. Therefore, force feedback control loader systems were implemented to obtain a higher bandwidth and because human test subjects predominantly use force to control a vehicle (Takats, 2011) [18].

The forward mass simulation can either be computed in the control loader computer or a similar analog circuit. In Figure 2.2.4, a hybrid analog/digital control loader system is shown. In this system, an analog circuit computes the forward mass dynamics such as the force gradient, damping, and natural frequency while the control loader computer computes the cable and aft mass simulation. As the control inceptor is deflected, a force transducer measures the force applied by the operator. This force is fed through the forward mass simulation to produce a commanded velocity. The velocity

command computed is then multiplied by the damping coefficient (C) to produce the damping force. The position of the control inceptor goes through the control loading computer, which applies a force gradient calculated from the cable and aft mass simulation. The cable and aft mass simulations depend upon the aircraft being simulated. If a specific aircraft is not being simulated, a linear force gradient can be set without implementing the cable or aft mass simulation.

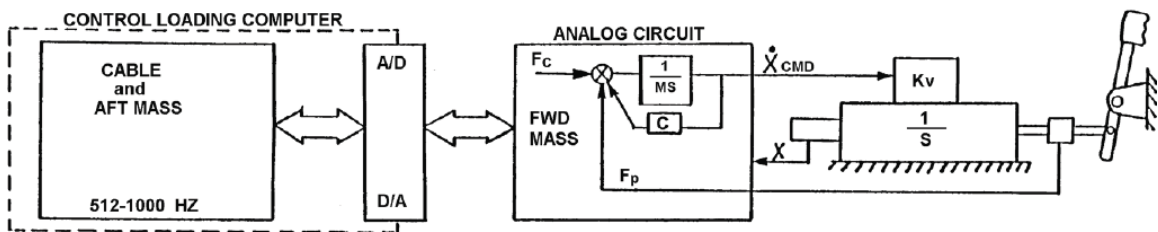


Figure 2.2.4 Analog/Digital Control Loader System (Takats, 2011) [16]

The force feedback control loader, Figure 2.2.5, uses a force command to drive the servo. As the control inceptor is deflected, both the position and force are measured. The position of the control inceptor is implemented through the forward mass, aft mass, and cable simulations to produce a force command to the servo valve. The servo drive command is produced when the force of the control inceptor is subtracted from the calculated commanded position. A control loader system commands the control inceptor to the proper position based on the force applied by the operator.

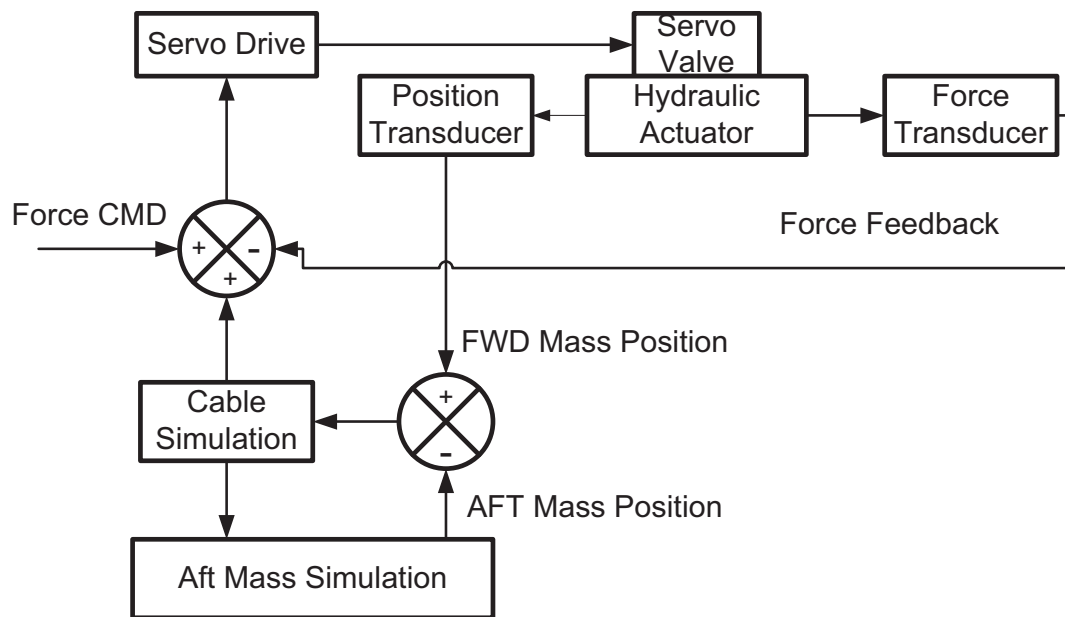


Figure 2.2.5 Force Servo Control Loader Model (Takats, 2011) [18]

The control loader system used in the experiments is a force feedback control loader system developed by McFadden Simulator Systems. The block diagram of its internal control structure is shown in Figure 2.2.6. When the test subject applies a force, the position of the control inceptor is fed back through the implemented dynamics. The parameters that create the force feel dynamics consist of the forward damping, the force gradient, the breakout force, and forward stop force. The position is fed through the force gradient to produce a force command which could be non-linear. The velocity of the control inceptor is fed through the damping coefficient to produce a force due to the damping. The breakout force applies a high force gradient and a certain force level around the neutral position of the control inceptor. The control inceptor will not move until the breakout force level is reached. The forward stop position sets the maximum deflection of the control inceptor in either direction.

The force that is applied to the control inceptor by the operator is first summed with the force command developed from the characteristic forward mass dynamics to produce an applied force. The applied force is then subtracted from the measured force on the control inceptor, which produces a force error command that drives the servo to the correct position. A force can be developed by a computer or analog circuitry and then injected in the control loader system at the same summing junction where operator force input is usually added. This allows for frequency sweep and step response data to be collected from the control loader system.

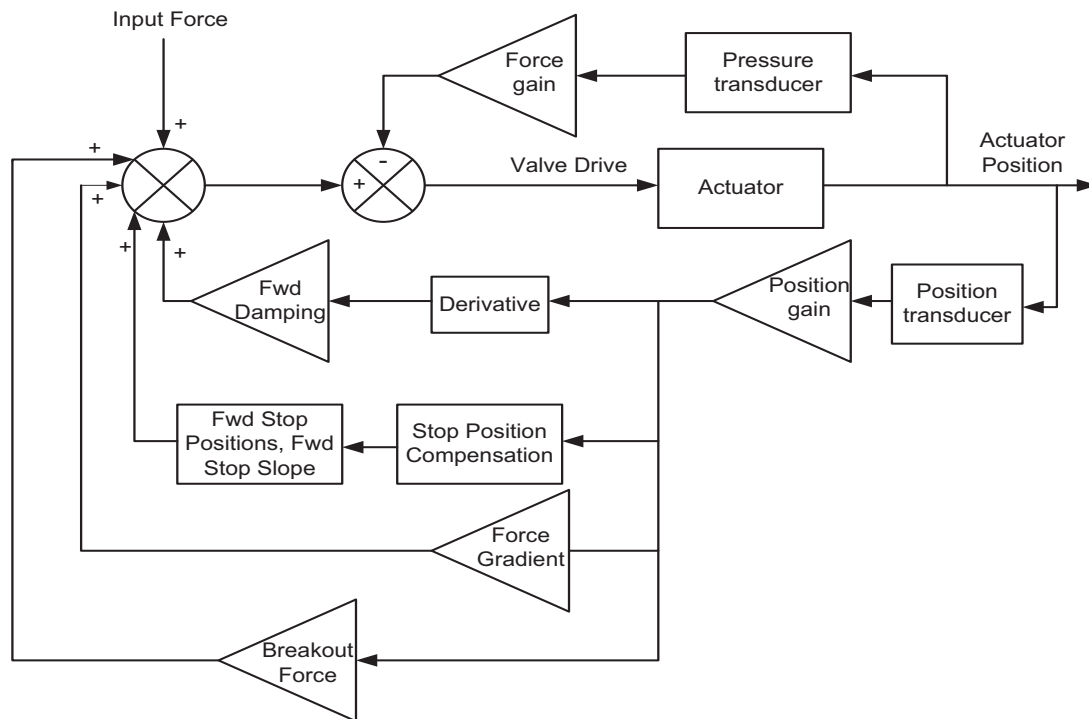


Figure 2.2.6 McFadden Control Loader Model (McFadden Systems Inc., 1999) [15]

2.3 Neuromuscular Models

The neuromuscular system is an important component in the control of a vehicle. The visual, vestibular, and somatosensory systems give feedback to the operator and

relay important information regarding vehicle control. The information is processed by the central nervous system and a command is applied by the neuromuscular system. The output of the neuromuscular system is a force. The neuromuscular system has its own internal feedback loop. The Golgi tendons and muscle spindle relay information on the muscle extension and force applied by the muscles in the limbs. This allows for coarse as well as fine motor control within a task. This allows the pilot to be adaptable and able to control many varying dynamic tasks. One question brought up by the study of the neuromuscular system is the limitation of the neuromuscular system and the situations that cause a task to be uncontrollable.

Don R. Gum (1973) [2] proposed a lateral head motion model. This model includes the muscle dynamics, head dynamics, and muscle spindle feedback. The transfer function for the muscle is defined as a first order system. The muscle spindle represents a lead/lag and the head dynamics represents a typical spring mass damper second order system. The lateral head motion model is shown in Figure 2.3.1.

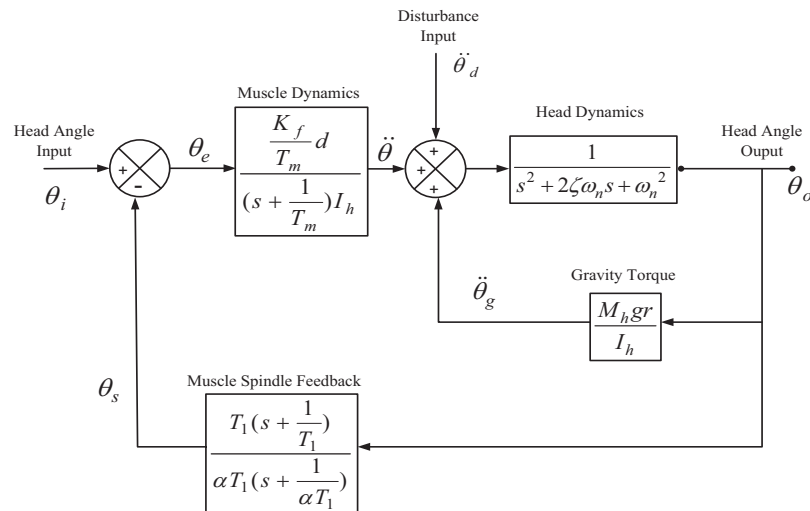


Figure 2.3.1 Lateral Head Motion Block Diagram (Gum, 1973) [2]

R. E. Magdaleno and D. T. McRuer (1971) [13] have also investigated many aspects of the neuromuscular system and proposed similar neuromuscular models. One such model is the neuromuscular subsystems model which was developed using test subject describing functions using an input/output relationship. To obtain a specific model for the muscle and muscle spindle feedback, EMG signals were recorded from each test subject. This allowed for the measurement of the effective muscle activation signal and average tension in the muscle. The neuromuscular subsystems model is shown in Figure 2.3.2.

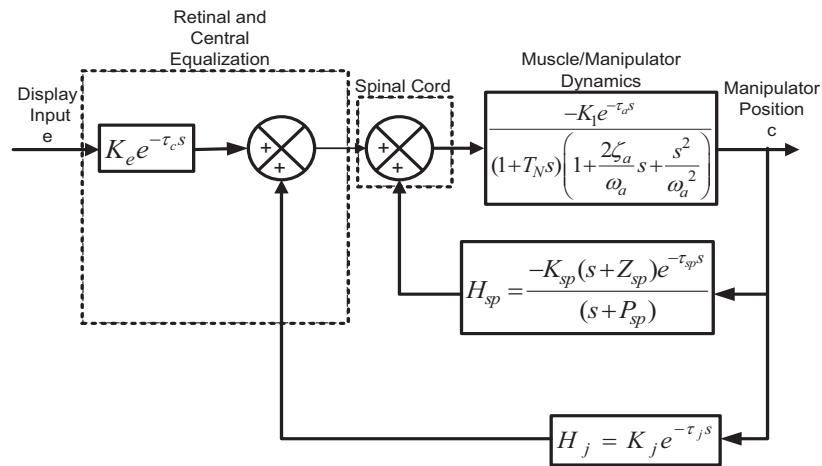


Figure 2.3.2 Neuromuscular Subsystems Model (Magdaleno & McRuer, 1971) [13]

Another model proposed is from Ronald A. Hess (1985) [8]. Hess developed a structural model in which each transfer function is defined for the components of the neuromuscular system. The model is then matched to pilot input/output relationships through various tasks. Hess uses the crossover model to equalize the structural model and chose parameters to have K/s dynamics around 2 rad/s. The structural model proposed by Hess (1985) [8] is shown in Figure 2.3.3.

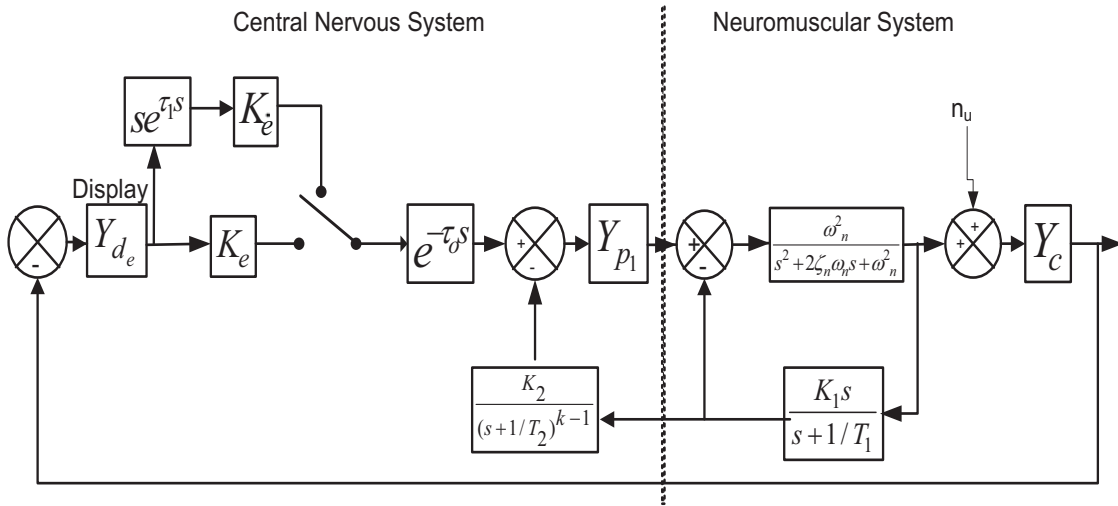


Figure 2.3.3 The Structural Model of the Human operator for Compensatory Tracking (Hess, 1985) [8]

A neuromuscular model has recently been proposed by Ruud Hosman and David Abbink (Hosman, 2010) [9]. This model also takes a structural approach by using test subject input/output relationships to define the parameters. The neuromuscular model proposed by Hosman (2010) [9] is shown in Figure 2.3.4. A detailed description of the neuromuscular models presented above is discussed within the Literature Review.

Many performance effects are noted throughout the research when the control loader dynamics are changed. It is shown that phase lag due to the control force feel dynamics has less impact since both the input and output of the control inceptor are known to the test subject. The natural frequency of the neuromuscular system is typically around 14 rad/s. It seems that reducing the natural frequency of the control loader below that of the neuromuscular system causes roll ratchet tendencies. Also, the sensitivity of the control loader can cause pilot induced oscillations (Johnston, 1988) [10]. The reason for many of these effects is not very clear, and this is a matter for continuing research.

of training study can be conducted. A quasi-transfer of training differs in that a simulator is used to test both training and transfer tasks. One group will train on a high fidelity simulator and another group will train on a simulator with certain variables altered. The two groups will then transfer to the same high fidelity simulator which represents the real-world vehicle. A quasi-transfer of training study is easily replicable and can be performed for a wide variety of tasks.

An example of a quasi-transfer training study is an experiment conducted by William H. Levison (1979) [12]. Five groups of test subjects trained on a roll-axis tracking task. One group trained with only visual cues. A second group trained with synchronized visual and motion cues. The other three groups trained with motion cues delayed 80, 200 and 300 msec. The groups were trained on the Roll Axis Tracking Simulator (RATS) at the Aerospace Medical Research Laboratory. One group trained with no motion in the RATS and then transferred to the RATS with synchronized motion and visual cues turned on. Another group trained with the synchronous motion and visual turned on and then transferred to the synchronous motion and visual simulation. The groups that trained on the delayed motion cues, trained in the RATS with motion delayed 80, 200 and 300 msec and then transferred to the synchronous motion and visual simulation. The test subjects all trained to an asymptotic mean square tracking error before transferring to the synchronous motion and visual simulation.

2.5 Tracking Tasks

Tracking tasks are implemented most of the time when determining human control strategy because of their simplicity and transportability to multiple simulators. There are two types of tracking tasks, compensatory and pursuit.

In a compensatory tracking task, a forcing function moves an indicator on a display. An indicator and a zero reference point are shown on the display. The indicator can represent a bank angle, altitude, or deflection in the horizontal direction. The operator is required to maintain the indicator on the zero reference point. This task is similar to driving on a road, a wind gust moves the car off course, and you have to return the car on course again. The compensatory task employed in experiments is usually a roll disturbance or pitch disturbance compensatory task. In the roll disturbance compensatory task, the test subject tries to return the cursor back to level flight or zero degrees bank angle. For the pitch disturbance compensatory task, the test subject nulls the forcing function in the vertical direction returning the cursor back to a target altitude labeled on the display.

In a pursuit tracking task, the operator is presented with a display consisting of two indicators, the target and the follower. The target moves according to the defined forcing function. The operator has to follow the target to keep the follower superimposed on the target indicator. This task can be utilized for horizontal and vertical motion. Usually, the percent on target and tracking error are used to measure test subject performance.

For a compensatory tracking task, the tracking error is the difference between the indicator and the reference point. For a pursuit tracking task, the tracking error is the difference between the target and the follower position. Typically, the forcing function is a pseudo-random disturbance employed by a sum of sinusoids. This mitigates operators from recalling the disturbance in previous runs.

Chapter 3 - Literature Review of Control Force Feedback Dynamics

3.1 Introduction

Research involving simulator dynamics and controls has improved simulator training and the transfer of training to real-world vehicles for pilots. Research exists for the different mechanisms that the human uses to control a vehicle. These mechanisms involve the visual system, the vestibular system, and the somatosensory system. Much of the knowledge is focused on the visual and vestibular systems. Vestibular cues are the main source for motion sensation, but somatosensory cues could offer additional information that could be beneficial to the pilot's control of the vehicle.

Simulators create the effect that the pilot is controlling the real-world vehicle. A high fidelity simulator matches the response of the vehicle's motion closely. Simulators cannot duplicate the actual dynamics of the vehicle but use basic principles of human perception to create cueing algorithms to allow the pilot to perceive the same vehicle motion. To create a high fidelity simulator, human perception of motion has to be well understood. In particular, this research focuses on the somatosensory system and the effect of control inceptor dynamics on a human test subject.

Within this literature review, both an understanding of the somatosensory system involvement in stick control of the aircraft, and the different effects that the control stick dynamics have on pilots was sought. The first topic discussed is the somatosensory system, particularly the neuromuscular system involved with limb movement and the different pilot models involving this system. The second topic discussed is the

experiments that have been conducted in the past to clarify the effects of changing the control inceptor dynamics.

This literature review together with knowledge on human in the loop control tasks has provided the necessary information to design and conduct experiments to test the effect of force feedback cues on human test subjects.

3.2 Neuromuscular/Pilot system models

The neuromuscular system is a complex system consisting of the neural pathways, the motor neurons, the muscle fibers, and many proprioceptors. Two of the most important proprioceptors are the muscle spindle and the Golgi tendon. The muscle spindle is responsible for sensing the change of length and the rate of change of length in the muscle fiber. This gives a sense of the position of the limb. The Golgi tendon has a linear relationship with the muscle force. These two sensors are very important in controlling the position of the limb. The muscles within the limbs have both damping and spring characteristics. The muscle works in antagonistic pairs to move the limb. An example of antagonistic pairs working to move a control stick is shown in Figure 3.2.1.

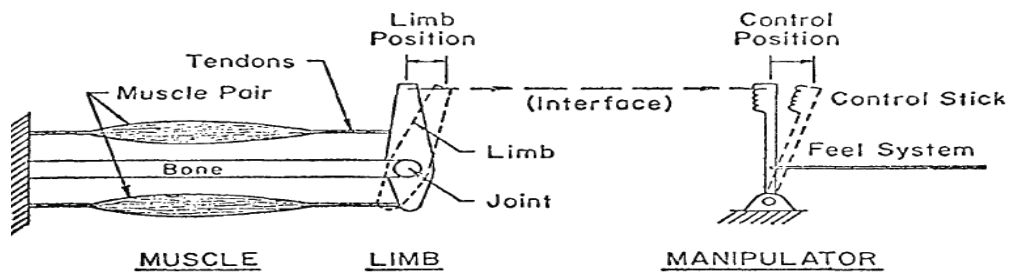


Figure 3.2.1 Antagonistic Muscle Pairs (Magdaleno & McRuer, 1968) [14]

A motor neuron creates a firing rate that causes the overlapping muscles to contract. This causes tension in the muscle which moves the limb. Some of the major neuromuscular models that have been described in the literature will be discussed within this section.

3.2.1 Precision Model

A neuromuscular model for limb dynamics that was proposed by Magdaleno and McRuer (1968) [14] is the precision model. The transfer function representation of this neuromuscular model is presented in Equation 3.2.1 (Magdaleno and McRuer, 1968) [14].

$$Y_p = \underbrace{K_p \left(\frac{T_L s + 1}{T_I s + 1} \right)}_{\text{Equalization Term}} e^{-s\tau} \underbrace{\left\{ \left(\frac{T_K s + 1}{T_{K'} s + 1} \right) \frac{\omega_N^2}{(T_{N_1} s + 1) [s^2 + 2\zeta_N \omega_N s + \omega_N^2]} \right\}}_{\text{Neuromuscular System}} \quad \text{Equation 3.2.1}$$

The K_p term is a gain used to adjust the open loop crossover frequency. The equalization term is used to allow the open loop frequency response to have a slope of -20 dB/decade at the crossover frequency. There is also a delay term which represents the delay of the nervous system. A lead/lag term exists which represents the low frequency phase lag seen by higher order aircraft dynamics.

To accurately describe each subsystem of the neuromuscular system, Magdaleno and McRuer (1971) [13] conducted experiments to determine the describing function for the muscle/manipulation actuation element. These experiments involved both hand and leg control manipulators. The experiment performed was a tracking compensation task in which the describing functions were obtained. The results obtained led to the block diagram of the neuromuscular system with muscle spindle and effective joint sensor feedback shown below in Figure 3.2.2. The values for each parameter are shown below in Table 3.2.1.

Values for Neuromuscular Subsystems Model	
T_n	1/30 sec
ζ_a	.8
ω_a	10 rad/sec
τ_a	.017 sec
Z_{sp}	11 rad/sec
P_{sp}	40 rad/sec
τ_{sp}	.023 sec

Table 3.2.1 Neuromuscular Subsystems Model Parameter Values (Magdaleno & McRuer, 1971) [13]

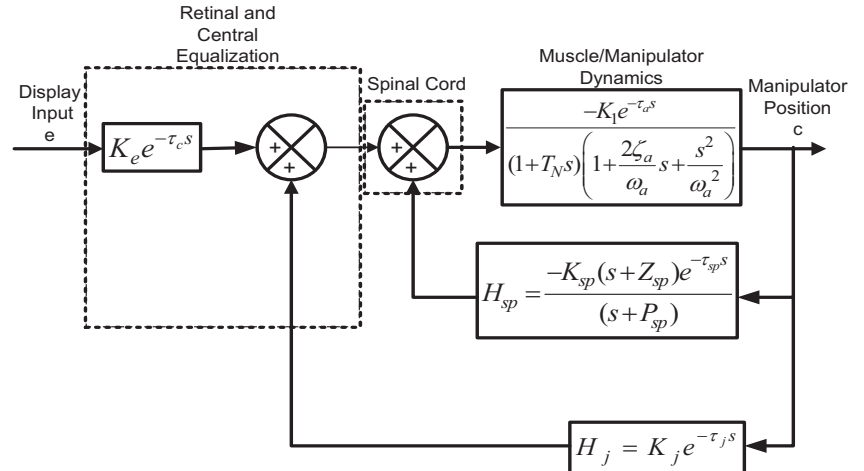


Figure 3.2.2 Neuromuscular Subsystems Model (Magdaleno & McRuer, 1971) [13]

3.2.2 Lateral Head Motion Model

Another neuromuscular model presented is a lateral head motion control model developed by Gum (1973) [2]. This model represents the motion of the head in response to an input from the nervous system. Head motion consists of multiple components. These components are the muscle dynamics, the head dynamics, and muscle spindle feedback. The block diagram of the lateral head motion control model by Gum (1973) [2] is shown in Figure 3.2.3. The values for the terms within the lateral head motion control block diagram are shown in Table 3.2.2.

Values for Lateral Head Motion Block Diagram	
K_f	43 N
d	0.075 m
T_m	0.08 s
I_h	0.0304 kg-m ²
ζ	0.64
ω_n	7.81 rad/s
M_h	4.6 kg
g	9.8 m/s ²
r	0.0498m
α	0.2
T_1	0.25 s

Table 3.2.2 Lateral Head Motion Parameter Values (Gum, 1973) [2]

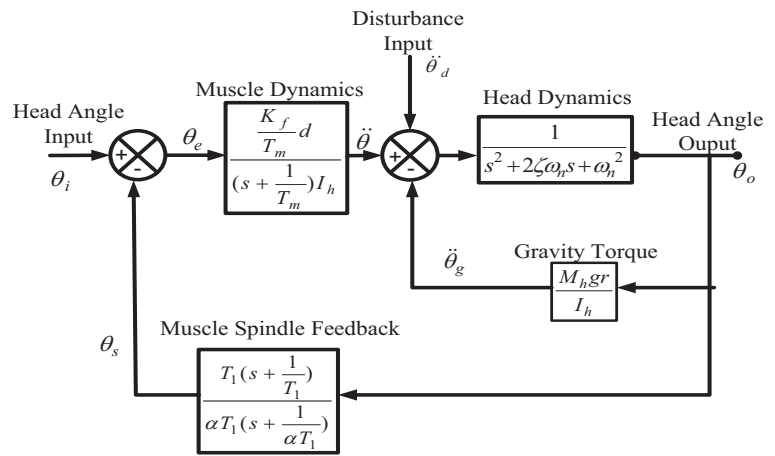


Figure 3.2.3 Lateral Head Motion Block Diagram (Gum, 1973) [2]

The system input is a commanded head angle input (θ_i) from the nervous system. The sensed angular output of the head (θ_s) is subtracted from (θ_i) to create the error (θ_e) which drives the system. At this summation point gravity applies a torque on the head through an angular acceleration which is represented by ($\ddot{\theta}_g$). The gravity torque constant has units of rad/s^2 . These angular accelerations from the muscle dynamics, disturbance input, and gravity torque are applied to the head, which creates a head angle output (θ_o).

The control of muscle dynamics is a low pass filter. At low frequencies the magnitude is about 40 dB and has a corner frequency of 12.5 rad/sec. The frequency response for the muscle dynamics along with its transfer function is shown in Figure 3.2.4.

$$\frac{\ddot{\theta}}{\theta_e} = \frac{1326}{(s + 12.5)}$$

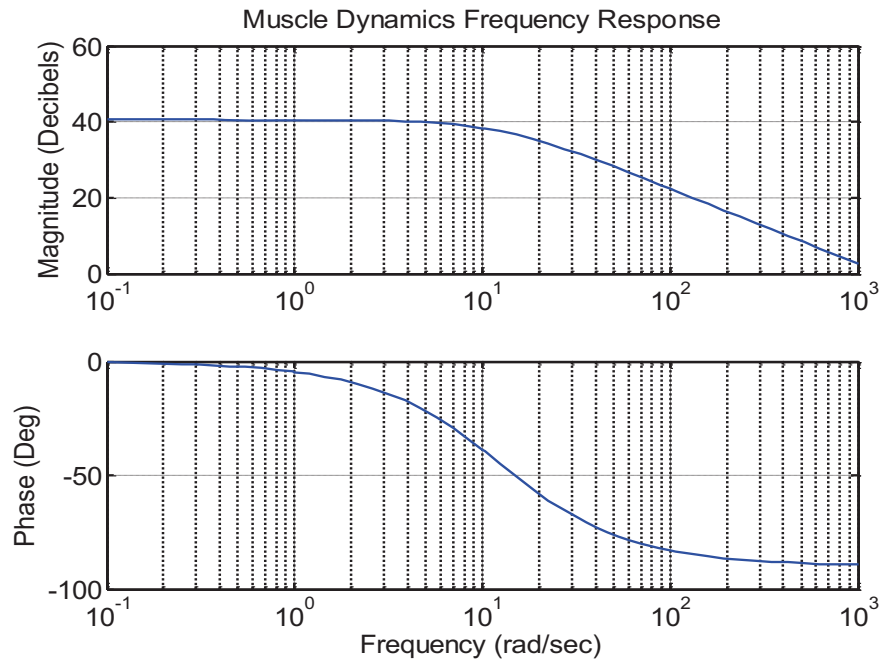


Figure 3.2.4 Muscle Dynamics Frequency Response

At low frequencies the muscle has zero phase. At high frequencies the muscle has a phase lag of 90 degrees. The muscle has more sensitivity to slower movements and will drop down to a gain of 0 dB at 1,000 rad/sec. Between 0.1 and 1 rad/sec, there is a constant gain and zero phase lag.

In the neuromuscular model proposed by Gum (1973) [2] the muscle spindle feedback is represented as a high pass filter. The muscle spindle is more sensitive to smaller muscle movements at higher frequencies since it increases its gain at frequencies beyond 1 rad/s. The phase of the muscle spindle dynamics seems to peak at 10 rad/sec at a phase angle of about 45 degrees. The frequency response of the muscle spindle along with its transfer function is shown in Figure 3.2.5.

$$\frac{\theta_s}{\theta_o} = \frac{5(s + 4)}{(s + 20)}$$

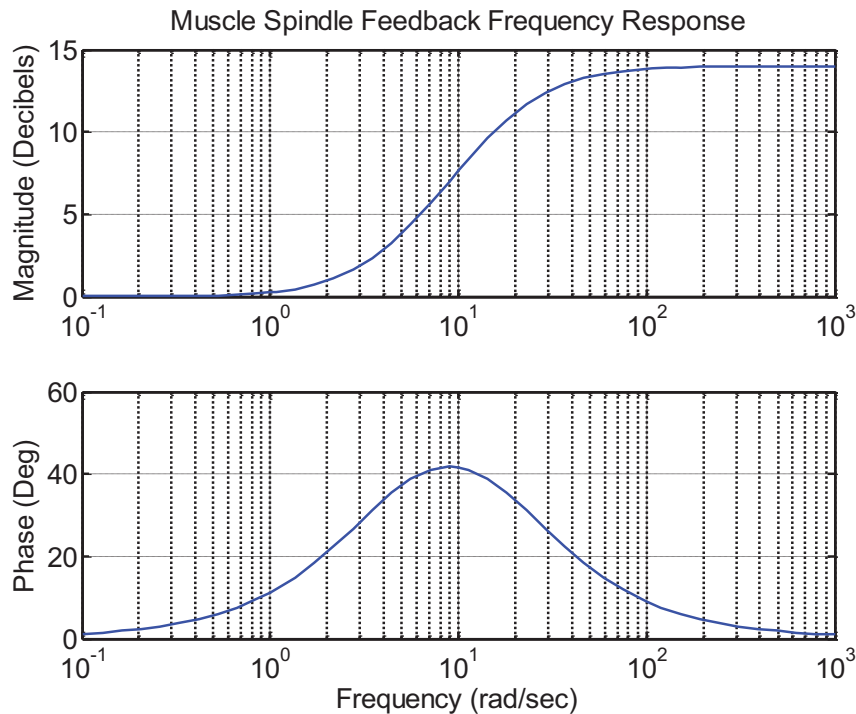


Figure 3.2.5 Muscle Spindle Feedback Frequency Response.

The frequency response of the total lateral head motion control is shown in Figure 3.2.6. The frequency response acts as a low pass filter allowing for a constant gain sensation at lower frequencies. The system has a gain margin of 6.43 dB and a phase margin of 149 degrees. In the head motion range of 0.1 Hz (0.628 rad/sec) and 1 Hz (6.283 rad/sec), the movement of the head has zero phase and zero gain. At frequencies above 100 rad/s, the output lags the input by 270 degrees. An increase in gain by a factor of 2.4 times or a phase lag of 149 degrees will cause instability. The total head motion control has a peak frequency of 14 rad/s. If you increase the damping ratio, a smaller peak occurs which leads to less head motion ratcheting.

$$\frac{\theta_o}{\theta_i} = \frac{1326s + 26,520}{s^4 + 42.5s^3 + 562.2s^2 + 8,714s + 23,320}$$

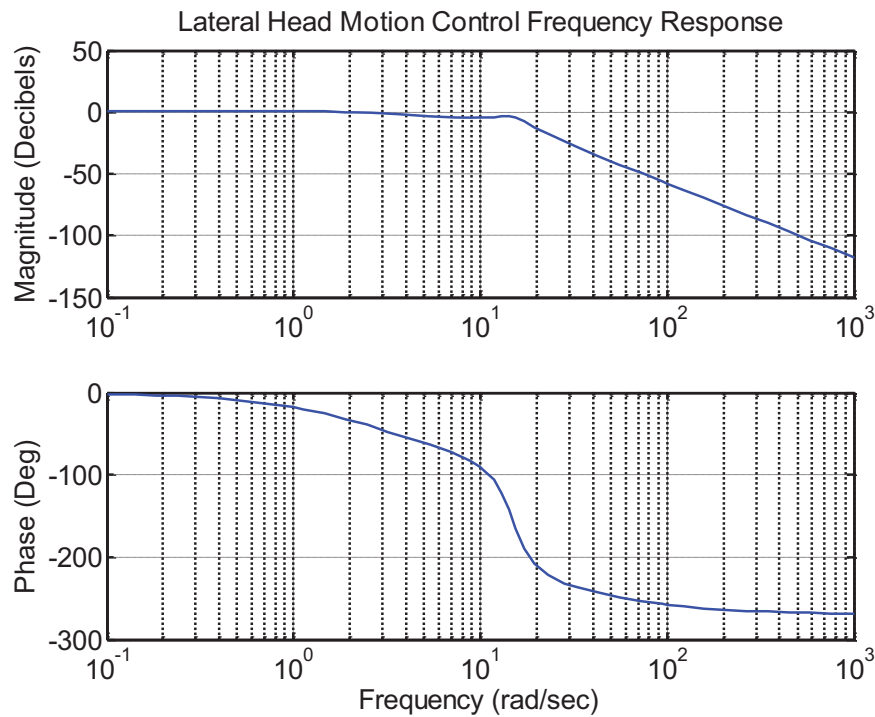


Figure 3.2.6 Lateral Head Motion Control Frequency Response

The step response for the total head motion control is shown in Figure 3.2.7. This response has a rise time of 0.583 seconds and a settling time of 1.15 seconds. The response has an oscillation that is not sinusoidal in nature. This behavior is due to a second order peaking shown in the total lateral head motion frequency response (Figure 3.2.6). The neuromuscular peaking in pilot control of a center stick on an airplane is shown to cause roll ratcheting. The final value of the system is 1.13 degrees which is greater than the commanded head angle of 1 degree. The step response shows a slight muscle ratcheting which occurs when the neuromuscular peak magnitude is above 0 dB at -180 degrees of phase.

$$\frac{\theta_o}{\theta_i} = \frac{1326s + 26,520}{s^4 + 42.5s^3 + 562.2s^2 + 8,714s + 23,320}$$

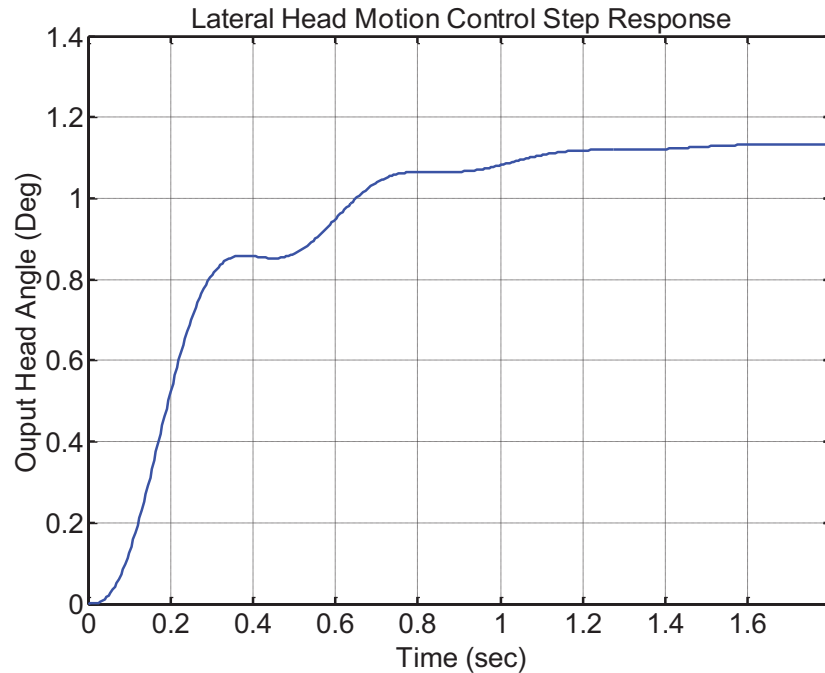


Figure 3.2.7 Lateral Head Motion Control Step Response

3.2.3 Hess Structural Model

A structural pilot model was proposed by Hess (1985) [8]. The model is shown in Figure 3.2.8. This model includes muscle manipulator dynamics, muscle spindle feedback, and Golgi tendon feedback. The model represents the response of the pilot's neuromuscular system via visual feedback. It is a disturbance compensation task in which the pilot compensates for a disturbance. The error between the disturbance and the output of the plant are visualized by the human. In this model, the human operator tries to minimize this error through visual and proprioceptive feedback cues.

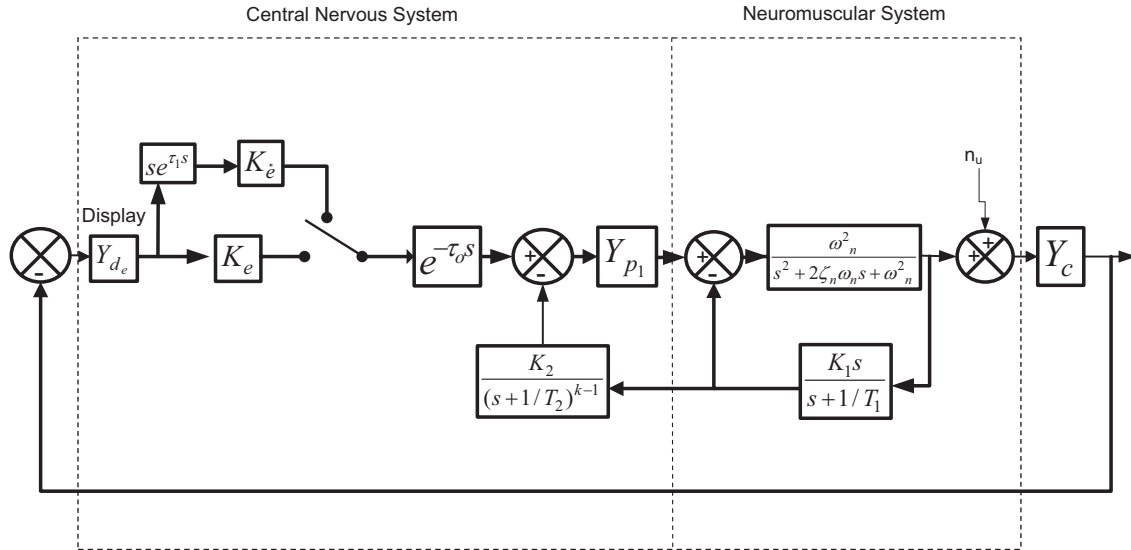


Figure 3.2.8 The Structural Model of the Human operator for Compensatory Tracking (Hess, 1985) [8]

The parameters T_1 , K_1 , K_2 , and K_e are chosen using the crossover model proposed by Johnston & McRuer (1986) [11]. The crossover model states that the form of the combined open loop transfer function for the pilot and the plant should be K/s for the crossover frequency. The crossover frequency of the pilot model is the frequency at which the response crosses 0 dB or a magnitude of one. Typically the crossover frequency is between 3 and 6 rad/s.

The crossover model is used by Hess to determine the proper proprioceptive feedback which equalizes the plant to have K/s dynamics. When the dynamics of the system are equal to K/s^2 , the pilot adapts to the different dynamics by applying different control strategies and these are typically compensated within the feedback of the system.

An updated structural model presented by Hess (2000) [4] is shown in Figure 3.2.9. In contrast to the original structural pilot model proposed by Hess, the revised model includes one term for the proprioceptive feedback. The revised model also includes a vestibular feedback loop. The equations presented below in Section 3.2.3 are obtained from Hess (2000) [4].

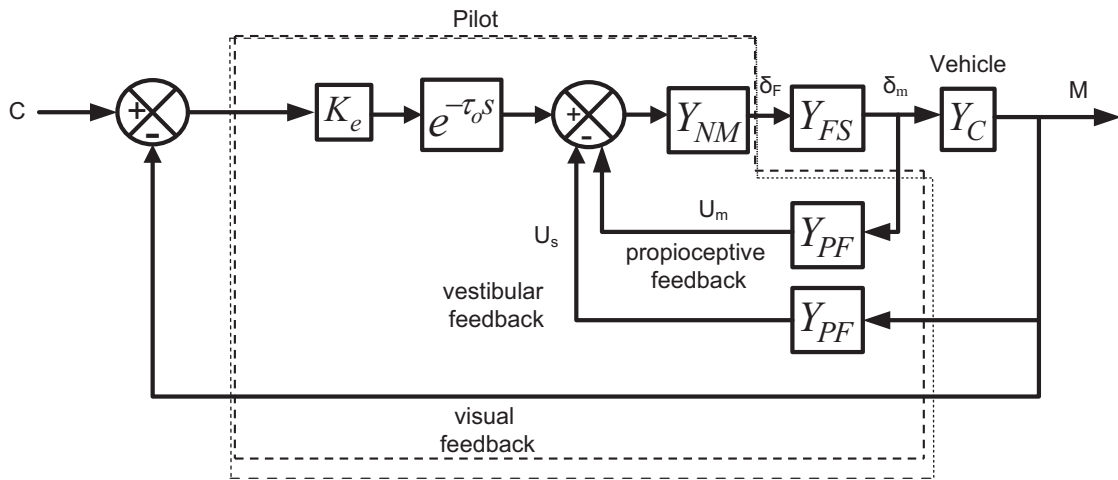


Figure 3.2.9 Revised Structural Model of the Human Operator for Pursuit Tracking (Hess, 2000) [4]

The term Y_{NM} is represented by the transfer function in Equation 3.2.2.

$$Y_{NM} = \frac{\omega_{NM}^2}{s^2 + 2\zeta_{NM}\omega_{NM}s + \omega_{NM}^2} \quad \text{Equation 3.2.2}$$

The nominal parameters for the neuromuscular transfer function (Y_{NM}) are equal to a damping ratio (ζ_{NM}) equal to 0.7 and a natural frequency (ω_{NM}) equal to 10 rad/s. The force feel system term (Y_{FS}) is typically represented as a second order spring mass damper system with the transfer function represented by Equation 3.2.3.

$$Y_{FS} = \frac{\omega_{FS}^2}{s^2 + 2\zeta_{FS}\omega_{FS}s + \omega_{FS}^2} \quad \text{Equation 3.2.3}$$

The proprioceptive feedback term (Y_{PF}) is in the form of $K_{PF}(s+a)$, K_{PF} , or $K_{PF}/(s+a)$ when the vehicle dynamics are equal to K_c , K_c/s , and K_c/s^2 respectively. The proprioceptive gain (K_{PF}) is chosen so that the minimum damping ratio of 0.15 is obtained for any of the closed-loop poles. The equalization term (K_e) is chosen to allow ($Y_p Y_c$) to have a crossover frequency of 2 rad/sec. The parameter “a” is chosen so that ($Y_p Y_c$) represents K/s dynamics around a crossover frequency of 2 rad/s. The transfer function (Y_p) is represented by Equation 3.2.4.

$$Y_p = K_e e^{-\tau_o s} \left(\frac{Y_{NM} Y_{FS}}{1 + Y_{NM} Y_{FS} Y_{PF}} \right) \quad \text{Equation 3.2.4}$$

The term K_e and $e^{-\tau_o s}$ represent the pilot equalization term and the central processing time delay respectively. The term τ_o is equal to 0.2 seconds.

3.2.4 Neuromusculoskeletal Model

A neuromusculoskeletal model presented in the American Institute of Aeronautics and Astronautics (AIAA) 2010 Modeling and Simulation Technologies Conference is shown in Figure 3.2.10 (Hosman, 2010) [9]. This model represents motion of the neuromusculoskeletal system in response to an externally applied force disturbance. The equations presented below in Section 3.2.4 are obtained from Hosman (2010) [9]. The model includes feedback from both the muscle spindle and the Golgi tendon. As shown in this model, the Golgi tendon receives force feedback from the muscle as opposed to receiving feedback from the muscle extension.

The terms k_p , k_v , and k_a represent the position feedback gain, the velocity feedback gain, and the acceleration feedback gain respectively. The control inceptor transfer function (H_e) is represented by Equation 3.2.7.

$$H_e = \frac{1}{m_e s^2 + b_e s + k_e} \quad \text{Equation 3.2.7}$$

The limb dynamics (H_{int}) are also described by a second order system in Equation 3.2.8.

$$H_{int} = \frac{1}{m_q s^2 + b_q s + k_q} \quad \text{Equation 3.2.8}$$

In this case the terms b_q and k_q represent the passive viscosity and passive elasticity of the muscle within the limb. The term (m_q) represents the mass in kilograms of the arm.

3.3 Force Feel Research

Bailey (1990) [1] conducted experiments on how force feel characteristics affected pilot performance. The experiments consisted of using a USAF variable stability NT-33A aircraft. Pilots tested 200 configurations in which the roll-mode time constant, roll command gain, time delay, and the roll pre-filter break frequency were changed. The block diagram showing the implementation of the experiment is shown in Figure 3.3.1. Equation 3.3.1, Equation 3.3.2, and Equation 3.3.3 below are obtained from Bailey (1990) [1].

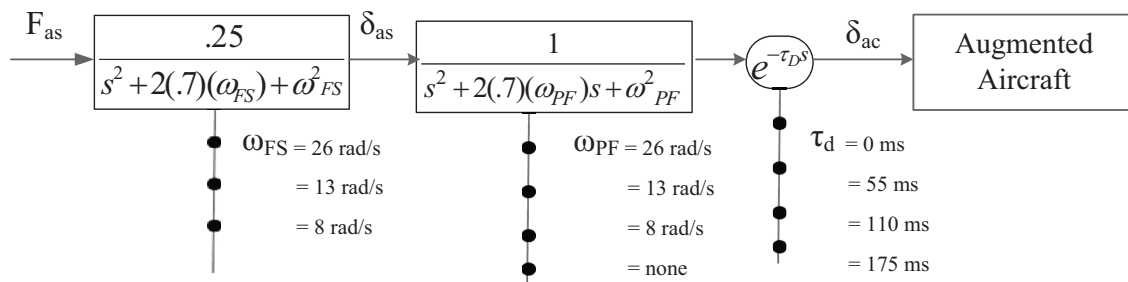


Figure 3.3.1 Lateral Flying Qualities Experimental Set Up (Bailey, 1990) [1]

In Figure 3.3.1, the feel system dynamics are represented by a second order transfer function shown in Equation 3.3.1.

$$\frac{\delta_{as}}{F_{as}} = \frac{k_{FS}\omega_{FS}^2}{s^2 + 2(.7)(\omega_{FS})s + \omega_{FS}^2} \quad \text{Equation 3.3.1}$$

Equation 3.3.1 represents the output lateral deflection of the control inceptor (δ_{as}) due to the input lateral force applied to the control inceptor (F_{as}). The term (k_{FS}) represents the force gradient. Two force gradients of 2.75 lb/in and 4 lb/in were tested within this experiment. The term (ω_{FS}) represents the natural frequency. The natural frequencies tested were 8 rad/s, 13 rad/s, and 26 rad/s. The damping ratio was held constant at 0.7. The pre-filter shown directly after the command type can either be in terms of a second order system transfer function shown in Equation 3.3.2 or a simple time delay (τ_{PF}).

$$\frac{\delta_{ac}}{\delta_{as}} = \frac{\omega_{PF}^2}{s^2 + 2(.7)(\omega_{PF})s + \omega_{PF}^2} \quad \text{Equation 3.3.2}$$

The pre-filter natural frequencies were chosen as 8 rad/s, 13 rad/s, and 26 rad/s. The augmented aircraft dynamics are shown below in Equation 3.3.3.

$$\frac{\rho}{\delta_{ac}} = \frac{L'_{Fas} \tau_R}{\tau_R s + 1} e^{-.04s} \quad \text{Equation 3.3.3}$$

The term (L'_{Fas}) and (τ_R) are referred to as the roll rate command gain and the roll mode time constant respectively. The units of the roll rate command gain are deg/sec²/lb and the units of the roll mode time constant are seconds. The roll mode time constant and roll rate command are chosen based on a specified roll sensitivity (P/F_{as}) which is the slope of the roll rate command gain divided by the roll mode time constant. The units of

the roll sensitivity (P/F_{as}) are deg/sec/lb. The roll sensitivity represents the roll rate of the augmented aircraft with respect to the force input. Figure 3.3.2 shows this correlation of the roll mode time constant and the roll gain.

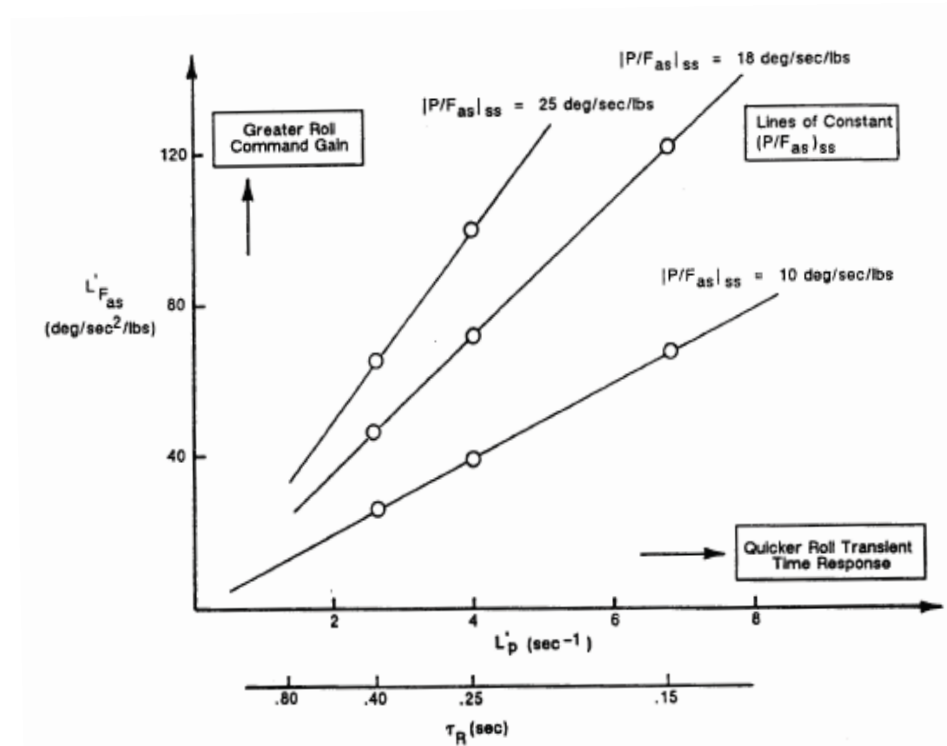


Figure 3.3.2 Roll Command Gain vs. Roll Mode Time Constant (Bailey, 1990) [1]

The roll mode time constants used in this experiment were 0.15, 0.25, and 0.40 sec. The roll sensitivities used were 10, 18 and 25 deg/sec/lb. For the different configurations, the roll command gain was chosen based on Figure 3.3.2 above.

The two experiments conducted were a power approach and an up-and-away task. The power approach task involved a visual landing task with a lateral offset. The up-and-away task consisted of a Heads Up Display (HUD) generated tracking task. The experimental data consists of pilot ratings, pilot comments, and task performance records. The pilot ratings were obtained using the Cooper-Harper pilot rating scale.

The results show that performance decreases when the roll mode time constant decreases from 0.40 to 0.15 sec. Also a change in the feel system natural frequency from 26 rad/sec to 8 rad/sec and all other parameters fixed causes performance degradation. The reduction of the natural frequency produces a greater chance of roll ratchet. When the feel system natural frequency is reduced from 26 rad/s to 13 rad/s, very little change in the pilot's flying qualities occurs. When the force gradient was decreased from 4 lb/inch to 2.75 lb/inch an improvement was seen. The phase lag caused by force feel dynamics has less effect on the pilot's performance as compared to other control system phase lags. The force feel is a part of the control system in which the pilot can sense both the input and output of the control inceptor.

High performance flight control system bandwidths could be affecting the neurological system of the pilot. Some of the issues in new control loader systems include high roll control sensitivity, pilot induced oscillations, and roll ratchet in precision control.

Dynamic models for the pilot and the closed loop Arm/Manipulator/Feel system are obtained from the frequency responses obtained within experiments conducted by Johnston (1988) [10]. The experiment consisted of a roll tracking task where the pilot matched the bank angle of the plant with the target, which was defined by a pseudo random motion. The pseudo random motion was created from a sum of cosines waveform. The difference between the target bank angle and the plant bank angle was recorded. The block diagram for the experiment is shown in Figure 3.3.3.

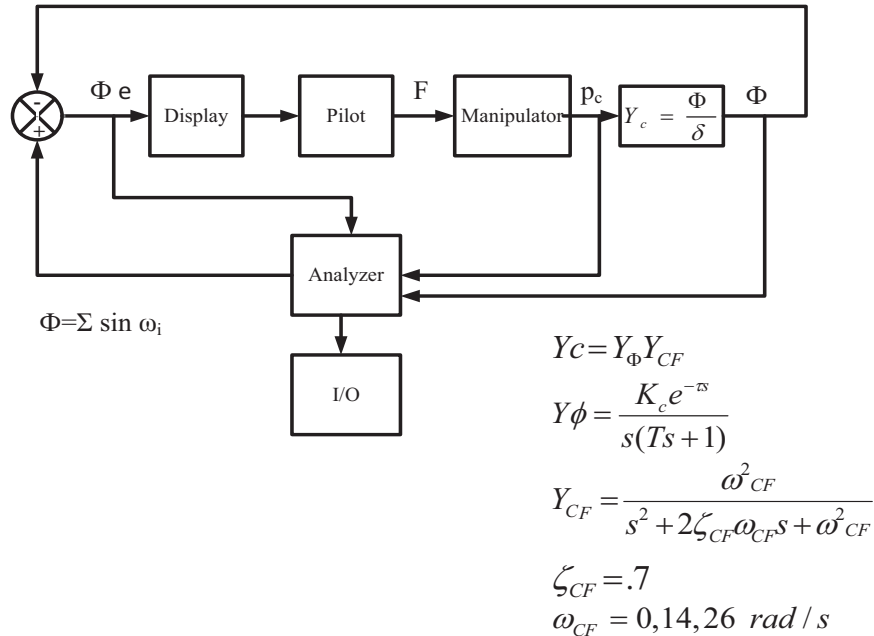


Figure 3.3.3 Roll Tracking Task Block Diagram (Johnston, 1988) [10]

The control plant (Y_c) is equal to the transfer function (Y_ϕ) multiplied by an optional pre-filter (Y_{CF}). The output of the manipulator above was converted into digital signals that were analyzed using STI's (System Technology Inc.) describing function analyzer program. This allowed pilot/vehicle transfer functions to be extracted from the experiments. The transfer functions were used to analyze the effect of the force feel system on the neuromuscular system.

The manipulators used were McFadden force loader systems. Both a center stick and a side stick were used for the different configurations. Different sets of feel system dynamic characteristics were implemented. These characteristics are shown in Table 3.3.1. The disturbance that was implemented was a sum of different cosine waves at different frequencies and amplitudes. The form of the sum of cosines is $\phi = \Sigma A_i \cos(\omega_i t)$. This created a pseudo random target for the pilot to follow. The parameters for the frequencies and amplitudes of each cosine wave are shown in Table 3.3.2.

Sidestick	Y_{FS1}	Y_{FS2}	Y_{FS3}
K_{FS} (lb/in)	14	7.5	3.75
(lb/deg)	1.22	0.65	0.33
(deg/lb)	0.82	1.53	3.1
ω_{FS} (rad/sec)	31.4	22.4	18
ζ_{FS}	0.7	0.6	0.6
Breakout (lb)	0.75	0.75	0.75
Centerstick	Y_{FS4}	Y_{FS5}	
ω_{FS} (rad/sec)	4	4	
ζ_{FS}	26	14	
Breakout (lb)	1	1	

Table 3.3.1 Force Feel Characteristics (Johnston, 1988) [10]

Cosine Wave	1	2	3	4	5	6	7	8	9
Frequency (ω_i rad/s)	0.467	0.701	1.17	1.87	3.51	7.01	11/2	14	18.7
Amplitude (A_i)	15.2	15.2	15.2	7.6	3.04	0.76	0.38	0.228	0.152
Relative Amplitude	1	1	1	0.5	0.2	0.05	0.025	0.015	0.01

Table 3.3.2 Disturbance Sum of Cosines Parameters (Johnston, 1988) [10]

The performance level to be met by each pilot was short periods of 1 to 2 degrees tracking error and peak errors less than 22 degrees. A Cooper Harper Pilot Rating (CHPR) was given by each pilot after each task was performed.

A simple block diagram, shown in Figure 3.3.4 below, represents the control apparatus used by the test subject to create a commanded roll angle. The block diagram includes the force feel system, a command gain which represents a roll rate per unit force, and the vehicle dynamics. This block diagram represents a position sensing control effort in which the deflection of the control inceptor controls the vehicle. The input to the vehicle dynamics is a commanded roll rate and the output is a roll angle of the vehicle. The roll rate is converted into a roll angle of the vehicle by the s term in the denominator of the vehicle dynamics. This acts as an integrator, which integrates a velocity (roll rate) into a displacement (roll angle).

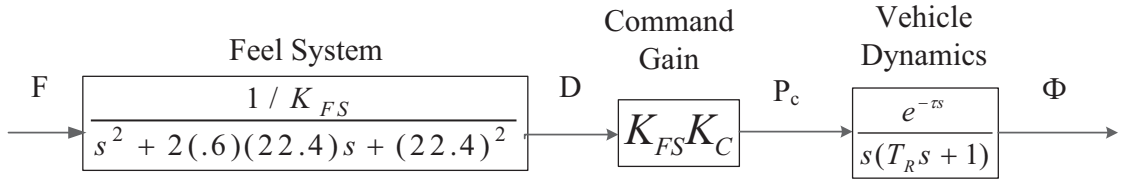


Figure 3.3.4 Effective Controlled Element (Johnston, 1988) [10]

For the two test subjects that performed these experiments, the neuromuscular natural frequency was around 14 rad/s. The peak magnitude for the neuromuscular system was affected slightly by the feel system gradient. By increasing the control stick stiffness, a small increase in the peaking of the neuromuscular system occurred. It was shown that if the neuromuscular peak goes above the 0 db line at a phase angle close to -180 degrees, roll ratchet could occur. Figure 3.3.5 represents the neuromuscular amplitude ratio peaking as a function of frequency from the range of 11-19 rad/s.

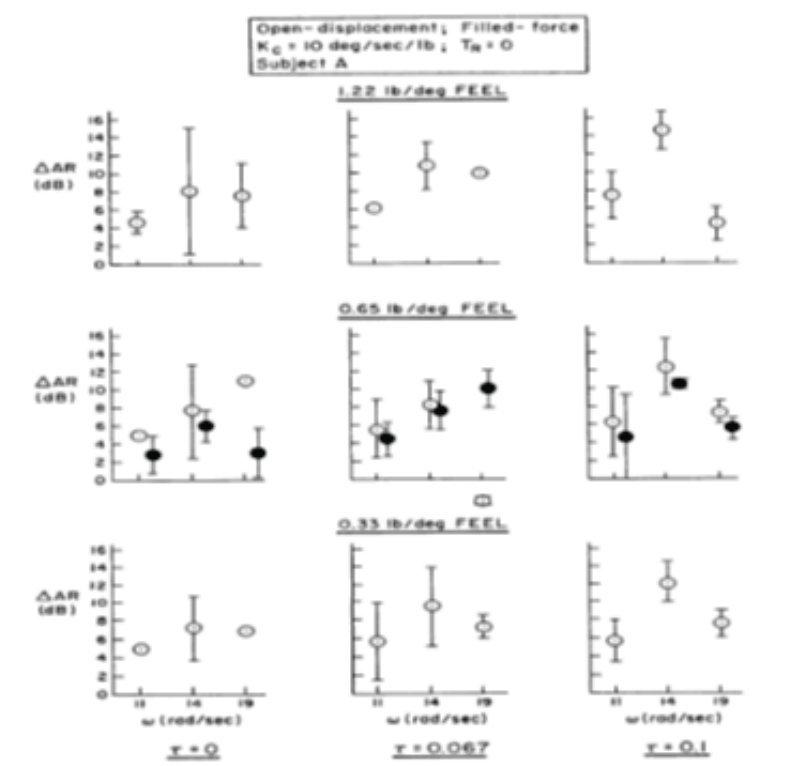


Figure 3.3.5 Amplitude Ratio Peak as a Function of Force Gradient Constant (Johnston, 1988) [10]

Figure 3.3.5 compares three different force gradients along with three different time delays added. The roll rate per unit force was kept at 10 deg/sec/lb and the vehicle dynamics were K/s dynamics. As shown, increasing the force gradient increases the neuromuscular peaking slightly. Also, the displacement sensing cases presented for the 0.65 lb/deg force gradient case show greater neuromuscular peaking as opposed to force sensing configurations.

Tracking performance for the experiments was measured from the RMS roll error (σ_e) and the crossover frequency (ω_c). The crossover frequency is the frequency at which the Pilot/Vehicle frequency response crosses the 0 db line. A higher crossover frequency corresponds with lower root mean square (RMS) tracking error. The manipulator control effort (σ_c) was also recorded as a performance measure. The Cooper Harper rating was used to obtain pilot ratings. The tracking bandwidth increased as the roll rate per unit force increased. At around 10 deg/sec/lb, the tracking bandwidth remains constant. This is shown in Figure 3.3.6.

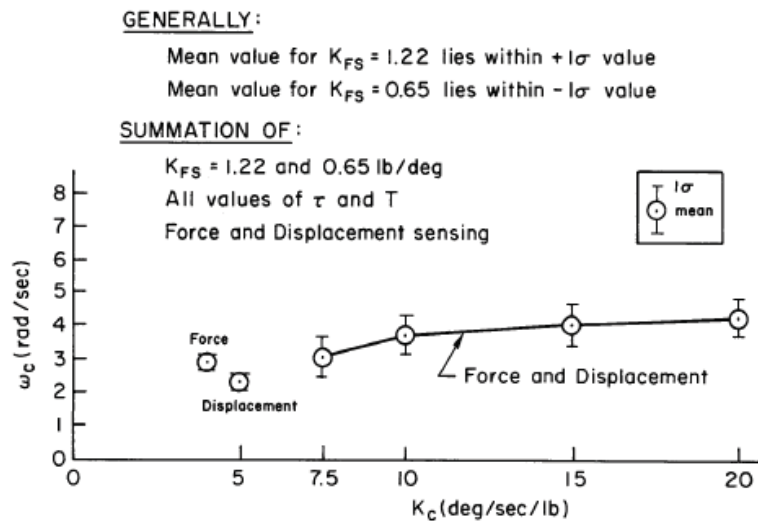


Figure 3.3.6 Task Bandwidth vs. Roll Command Gain (Johnston, 1988) [10]

Figure 3.3.6 represents the crossover frequency as a function of the roll rate per unit force gain. At a low roll rate per unit force, the pilot has a hard time moving the control inceptor to the proper position in a short time. The optimal command gains reported by Johnston (1988) [10] are between 10 and 20 deg/sec/lb. This report suggests that high stick forces, particularly consistent with the force gradient, limit how fast the pilot can compensate. For a higher force gradient, a higher roll rate per unit force is needed to allow for higher bandwidth control.

The measure of pilot workload was conducted using both the root mean square tracking error and the root mean square manipulator displacement or force input. A good measure of pilot workload is done by plotting the product of the tracking error and the manipulator input versus the reciprocal of the crossover frequency and the command gain. A plot of the pilot workload versus the reciprocal of the product of the command gain and the crossover frequency is shown in Figure 3.3.7.

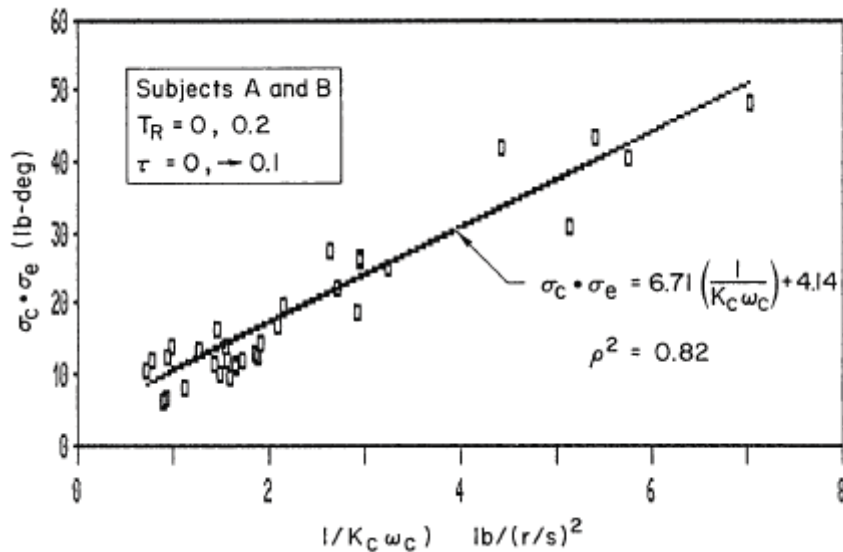


Figure 3.3.7 Workload vs. the Reciprocal of the Product of Roll Command Gain and Task Bandwidth (Johnston, 1988) [10]

The workload parameter is equal to the product of the tracking error and the manipulator input. Decreasing the crossover frequency or the command gain causes the pilot workload to increase. The Cooper-Harper ratings also show that a decrease in the command gain causes performance degradation.

The highest force gradient of 1.22 lb/deg causes higher pilot workload at a low roll command gain of 10 deg/sec/lb. The forces were too high to command fast maneuvers. The lower force gradient of 0.33 lb/deg caused large stick deflections and the command gain was increased to avoid the control stick going beyond the travel limits. The force gradient that had the best Cooper-Harper ratings from pilots was 0.65lb/deg. This trend is shown in Figure 3.3.8 below. As shown, the increase in command gains for the different force gradient cases corresponds to a lower Cooper-Harper rating. This suggests that increasing the command gain results in typically better pilot ratings within these experiments. For the highest feel gradient of 1.22 lb/deg, increasing the roll command gain leads to pilot induced oscillation PIO.

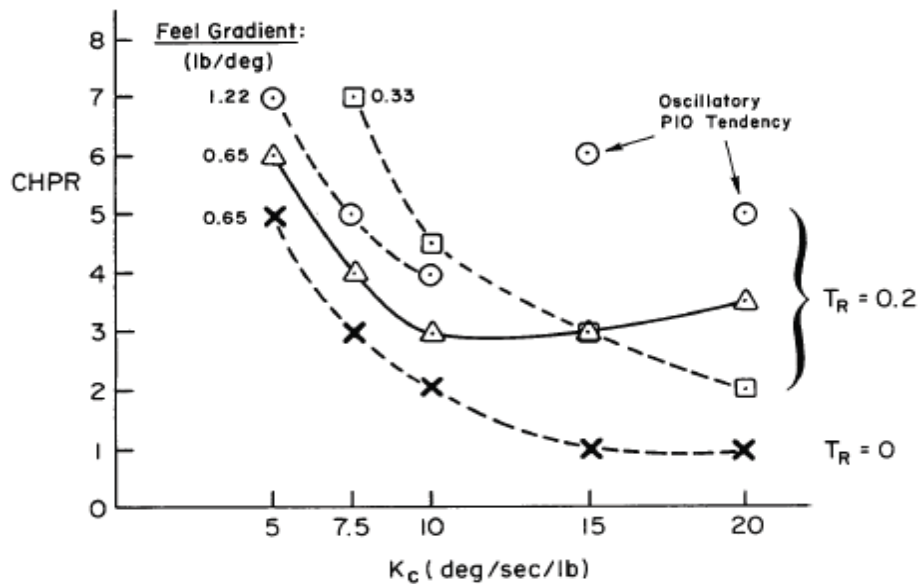


Figure 3.3.8 Cooper Harper Rating vs. Roll Command Gain (Johnston, 1988) [10]

Experiments were conducted on a center stick installed in the USAF NT-33 aircraft, and were presented in Johnston (1988) [10]. The block diagram describing the experiments performed on the center-stick is shown in Figure 3.3.9.

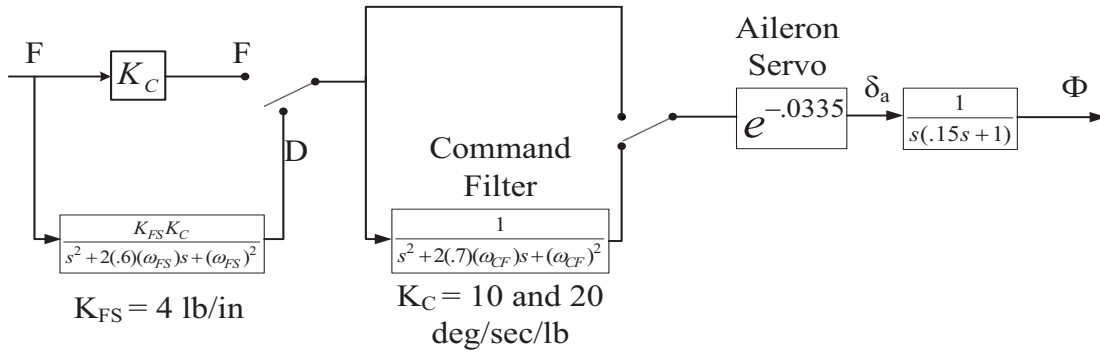


Figure 3.3.9 Center-Stick Experimental Setup (Johnston, 1988) [10]

The input into this system is a force. A force sensing or displacement sensing task can both be performed. A force sensing configuration is where the force applied to the control inceptor commands the plant and a displacement sensing configuration involves the displacement of the control inceptor commanding the plant. For the displacement sensing configuration, the force feel dynamics convert the force input into a displacement of the control inceptor. The force system dynamics are represented by a second order system shown in Equation 3.3.4 (Johnston, 1988) [10] below.

$$\frac{\delta}{F} = \frac{K_{fs} K_c}{s^2 + 2(.7)(\omega_{fs})s + \omega_{fs}^2} \quad \text{Equation 3.3.4}$$

The term (K_{fs}) represents the feel system force gradient. The term (K_c) represents the roll command gain with units of deg/sec/lb. The term (ω_{fs}) represents the force feel natural frequency. In this block diagram a command filter is optional. The command filter represents a second order transfer function in the form of Equation 3.3.5 (Johnston, 1988) [10].

$$\frac{\delta_{cf}}{F_{cf}} = \frac{1}{s^2 + 2(.7)(\omega_{cf})s + \omega_{cf}^2}$$

Equation 3.3.5

The aileron servo block represents a delay added to the system. The $1/(s(.15s+1))$ block represents the plant dynamics. The result of the effect that the feel system and filter dynamics has on the tracking bandwidth is shown below in Figure 3.3.10.

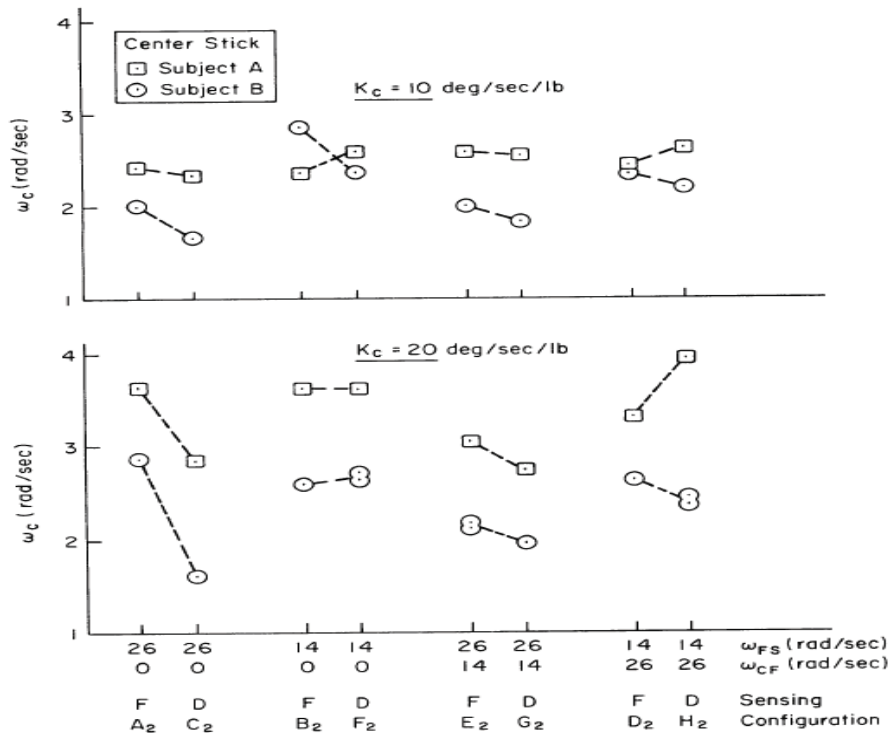


Figure 3.3.10 Task Tracking Bandwidth as a Function of Feel System Natural Frequency (Johnston, 1988) [10]

As shown, as the command is increased from 10 deg/sec/lb to 20 deg/sec/lb the tracking bandwidth increases. When the natural frequency of the force feel system is increased from 14 rad/s to 26 rad/s the tracking bandwidth decreases for the displacement sensing configuration. An increase in tracking bandwidth allows for better control of the plant dynamics. Although the tracking bandwidth changes dramatically when the natural frequency is increased, the tracking error does not change much between the two. The tracking error as a result of each configuration is shown below in Figure 3.3.11.

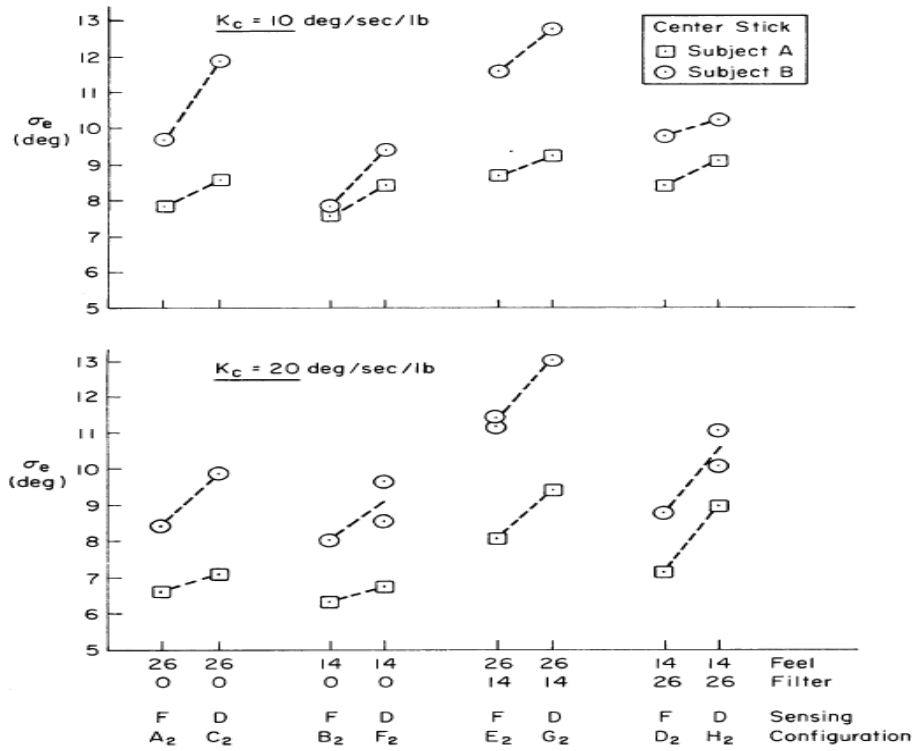


Figure 3.3.11 Task Tracking Error as a Function of Feel System Natural Frequency (Johnston, 1988) [10]

The tracking error does improve with an increase in the roll command gain from 10 deg/sec/lb to 20 deg/sec/lb. The Cooper-Harper rating also corresponds with these results. As the roll command is increased, the Cooper-Harper rating improves. The Cooper-Harper ratings for each configuration are shown in Figure 3.3.12. The two configurations that have the best Cooper-Harper ratings and lowest tracking errors are the force feel system with a natural frequency of 14 rad/sec and 26 rad/sec, a roll command gain of 20 deg/sec/lb, force sensing configuration, and no command filter.

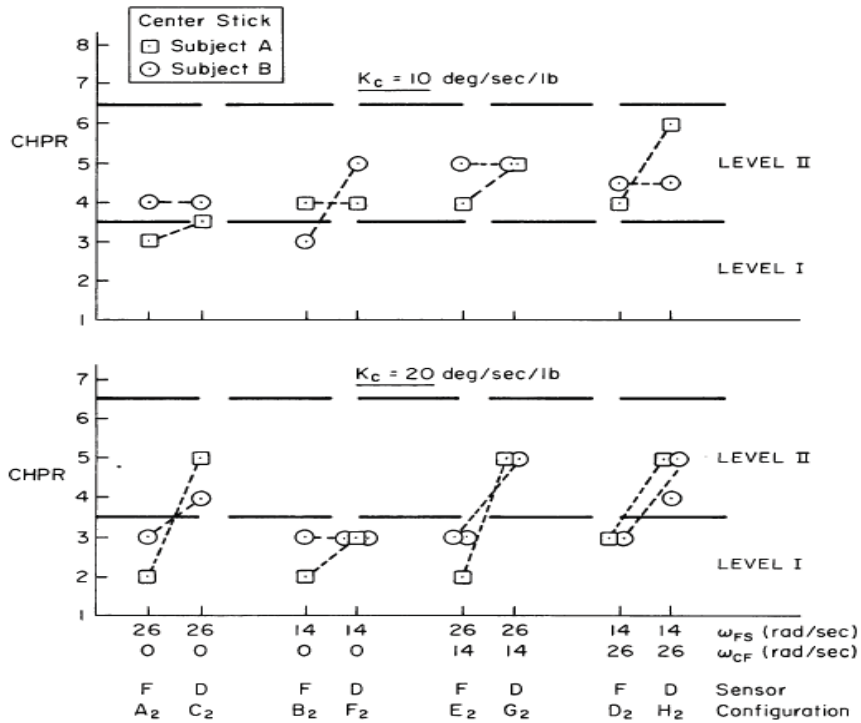


Figure 3.3.12 CHPR as a Function of Feel System Natural Frequency (Johnston, 1988) [10]

The case for the 10 deg/sec/lb command gain shows a lower bandwidth for the higher natural frequency case, but shows a similar tracking error and a better Cooper rating than the lower natural frequency case. Test subject A consistently held a higher tracking bandwidth and lower tracking error. Also, test subject A held a more consistent control strategy. Looking at the performance of test subject A, it seems that the 14 rad/s feel system with no pre-filter has a slightly better tracking performance, and a higher bandwidth. Changing the force gradient to cause a lower control inceptor natural frequency can affect tracking performance.

Mitchell (1992) [16] reported that in order to obtain a Level 1 Handling Qualities Rating (HQR), a minimum control inceptor natural frequency should be set to 10 rad/s for a control inceptor mass of 5 lbm ($0.0133 \text{ lb}\cdot\text{s}^2/\text{in}$). Typically with a low force gradient, a high natural frequency is not obtainable for a low control inceptor mass. Most

experimental aircraft show that a higher frequency control inceptor with a low mass typically has a higher force gradient. If the mass of the control inceptor is very light, then more inceptor deflection will occur.

LATHOS is an abbreviation for Lateral High Order System Experiments which are discussed by Mitchell (1992) [16]. A USAF NT-33 aircraft was used during these experiments. The best reported system had 1.5 lb control inceptor breakouts, a 3.81 lb/in force gradient and an optimal command gain of 6.6 to 8.4 deg/sec/lb. In this report it was suggested that the command gain should be set just above 8 deg/sec/lb, the force gradient should be set just below 4 lb/in, and to use some nonlinearity in the force gradient.

In the literature, it was shown that the neuromuscular system can be characterized with a transfer function that matches results from experiments involving human test subjects. The proposed characteristics of a roll compensatory task found throughout the literature were utilized when designing a quasi-transfer of training study discussed in Chapter 4. In conclusion, a natural frequency between 14 and 26 rad/s and a damping ratio of 0.7 leads to high performance from each test subject. The roll command of the control inceptor should be set just above 8 deg/sec/lb and the force gradient should be set to 4 lb/in for the high fidelity control inceptor. It was shown that these characteristics produce the best tracking error and task bandwidth for the compensatory tasks conducted. By increasing control inceptor roll command gain to 20 deg/sec/lb it was shown to improve tracking bandwidth. The increased roll command gain was shown to increase pilot induced oscillation (PIO). To avoid neuromuscular ratcheting and PIO, a control inceptor sensitivity of 10 deg/sec/lb is chosen.

Chapter 4 - Design of Transfer of Training Study

4.1 Introduction

The design of the experimental task to test the effectiveness of transfer of training on a simulator will be discussed within this chapter. This particular transfer of training experiment is focused on the control loader system and its interaction with the neuromuscular system. To focus in on the particular effect of the neuromuscular system by altering the control loader dynamics, the simulator is fixed base and a simple out the window display is used. A roll disturbance compensatory task is used within the experiments. A description of the roll compensatory task as well as the parameters that were determined to design the experiment is presented within this chapter.

4.2 Roll Disturbance Compensation Task

A quasi transfer of training experiment is conducted where a high and low fidelity control inceptor is interchanged to test transfer of training effectiveness. The reason for pursuing a study in the force feel system provided by a control loader is to develop an understanding of the prominence of force feedback cues to the pilot. To test each human test subject, a disturbance compensatory roll tracking task with $1/s$ and $1/s^2$ plant dynamics will be used. The quasi transfer of training study consists of training test subjects to null a roll disturbance maintaining level flight using a high and low fidelity control loader simulation. The reason for using a roll disturbance compensatory task is to keep the task as simple as possible to mitigate effects other than those caused by the neuromuscular system of the human test subject. Implementation of the experiment will be described in the following sections.

The roll disturbance compensatory task used in the experiment is shown in Figure 4.2.1. A disturbance consisting of a sum of nine sinusoids deflects a bank angle line viewed on the display. The disturbance input that is applied is discussed in section 4.5.

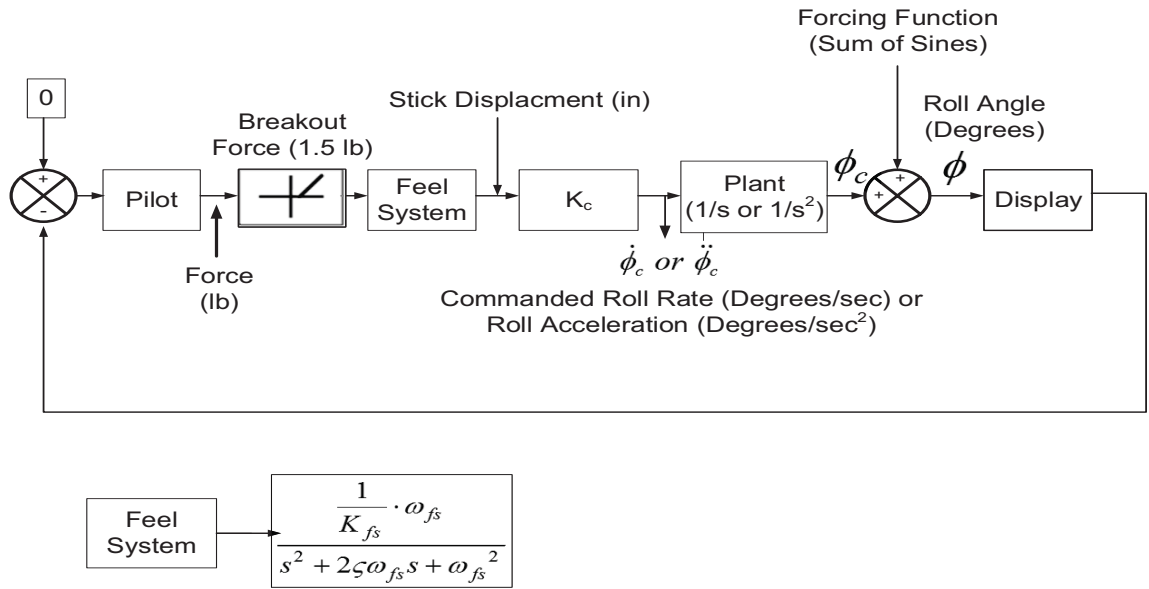


Figure 4.2.1 Developed Roll Disturbance Compensatory Tracking Task

The commanded plant input is equal to the test subject control inceptor deflection multiplied by a roll rate per inceptor deflection command gain (K_c). The commanded plant input is then passed through plant dynamics to produce a roll angle. The roll angle of the vehicle is displayed as an angle displaced from an artificial horizon line representing level flight. The visual feedback and proprioceptive feedback are the main cues to the test subject. The test subject will have to compensate for this disturbance and maintain level flight, an angle of zero degrees from the horizon line. For $1/s^2$ dynamics the roll command gain (K_c) of the plant will represent roll acceleration per unit deflection of the control inceptor.

The displayed roll angle causes the test subject to output a force from muscle activation on the control inceptor. The deflection of the control inceptor in inches is multiplied by a roll command gain (K_c). The roll command gain converts the deflection of the control inceptor to a roll rate command ($\dot{\phi}_c$) and roll acceleration command ($\ddot{\phi}_c$) for $1/s$ and $1/s^2$ plant dynamics respectively. The roll rate command ($\dot{\phi}_c$) and roll acceleration command ($\ddot{\phi}_c$) are displayed as a roll angle (ϕ) after being passed through $1/s$ and $1/s^2$ dynamics respectively.

The roll command gain K_c will be set initially to a value of 40 deg/in•s and 40 deg/in•s² for plant dynamics of $1/s$ and $1/s^2$ respectively. When the deflection output of the control inceptor in inches is multiplied by the roll command gain it creates a roll rate given in deg/s and roll acceleration in deg/s² for $1/s$ and $1/s^2$ dynamics respectively. For both $1/s$ and $1/s^2$ plant dynamics, the roll command gain is adjusted during pre-experiment trials. The roll command gain is kept constant for both $1/s$ and $1/s^2$ plant dynamics.

In section 4.3, the determination and implementation of the force feel parameters on the McFadden control loader are discussed. The K_{ξ} in the block diagram represents the force gradient and K_c represents the roll command gain. When the test subject deflects the control inceptor, a roll rate command or roll acceleration command is produced which will then be integrated once for the $1/s$ plant dynamics or integrated twice for the $1/s^2$ plant dynamics. The integration of the roll rate command or roll acceleration command can be obtained using the Euler numerical integration method represented by Equation 4.2.1.

$$\phi_{n+1} = \phi_n + \phi'_n \cdot h \quad \text{Equation 4.2.1}$$

The term (ϕ_{n+1}) represents the new calculated roll angle at every time step. The current roll angle (ϕ_n) is summed with the current roll rate (ϕ'_n) multiplied by the step size (h). The roll angle output (ϕ_c) commanded by the pilot is summed with the disturbance which drives the image generation. The roll rate at each time step (ϕ'_n) is represented by Equation 4.2.2. The term X_c represents the commanded control inceptor displacement in inches. The term K_c represents the roll command gain in deg/s•in and deg/s²•in for 1/s and 1/s² plant dynamics respectively.

$$\phi'_n = X_c \cdot K_c \quad \text{Equation 4.2.2}$$

4.3 Force Feel Parameter Determination

4.3.1 High Fidelity Control Loader Parameters

The high fidelity control loader parameters were adapted from the literature presented in the literature review. These parameters were determined to produce a good task performance from test subjects within the many experiments conducted in the literature. Two of the characteristics that determined good flying performance were test subject tracking error and tracking bandwidth. Throughout the literature, many experiments were conducted in which different control inceptor characteristics were tested. The parameters were chosen that produced the smallest tracking error, and the highest tracking bandwidth.

The parameters that defined a high fidelity control inceptor were a force gradient of 4 lb/in, a damping ratio of 0.7, a natural frequency of between 14 and 26 rad/s, and a

breakout force of 1.5 lb. These parameters lead to a system that has a small peak overshoot and that settles to its final value fairly quick. A step response of the high fidelity control inceptor with a natural frequency set to 26 rad/s is shown below in Figure 4.3.1.

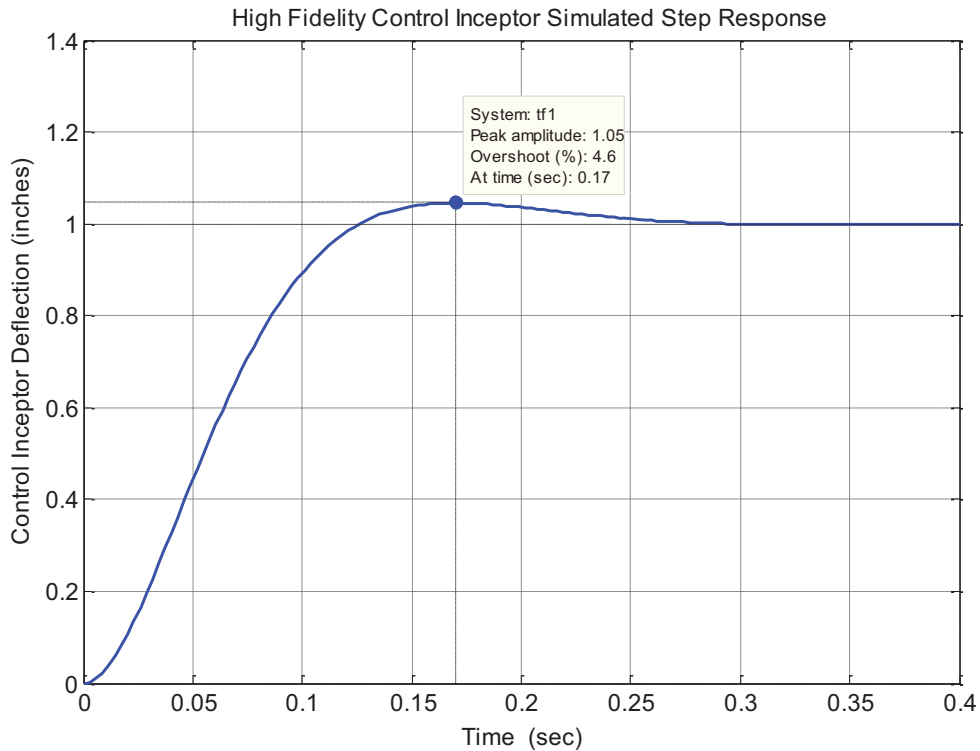


Figure 4.3.1 Simulated High Fidelity Control Loader Step Response

Shown in Figure 4.3.1, an overshoot of around 4.6 corresponds to a damping ratio of 0.7. The natural frequency is difficult to measure using the time response so the frequency response method is used. The natural frequency of the system should be anywhere between 14 rad/s and 26 rad/s to be considered a high fidelity control inceptor. Since the mass changes from simulator to simulator it will be difficult to maintain the natural frequency without changing the inertia of the control inceptor. The inertia of a

system can only be increased; therefore only allowing the natural frequency to be decreased while maintaining the force gradient.

4.3.2 Low Fidelity Control Loader Parameters

For the control loader quasi transfer of training experiment, the low fidelity parameters are determined from a computer joystick. The computer joystick used is a Logitech Force 3D Pro and is used frequently in flight simulator games. These parameters are all measured in the horizontal direction of the computer joystick. The final measured parameters of the computer joystick are a natural frequency of 34.5 rad/s, a damping ratio of 0.135, and a force gradient of 0.7 lb/in. The damping ratio and corresponding natural frequency are found using the log decrement.

The first step in determining the natural frequency is to calculate two successive peak times. In this case, two successive zero crossings on each of the peaks are used to find the period of the transient decay of the computer joystick. The damped frequency is found using the formula $2\pi/T$ where T is the period of transient oscillation. The natural frequency is then calculated using $\omega_n = \omega_d / \sqrt{1-\zeta^2}$ where (ω_d) is the damped natural frequency and (ζ) is the damping ratio found using the log decrement. The force gradient is found using a force gauge to measure the maximum force at the maximum deflection of the joystick.

To obtain the time response of the computer joystick, the program MMS (Man Machine Systems) Laboratory was used as a baseline test. The MMS Laboratory software was created to test different compensatory tasks. The program runs a simple background with a cursor and a target box in which the person has to compensate for a disturbance of the plant. The program has the ability for keyboard, mouse, or joystick input from the

subject performing the tests. The measured response from the program is the power spectral density of the input and output, input response from the joystick, and the tracking error. The computer joystick is held at its maximum deflection in either direction. It is then released when the program is run to obtain the transient behavior of the joystick. This type of test is referred to as a free release response.

Using the time response of the computer joystick, the natural frequency and the damping ratio is calculated. To find the force gradient, the force is found at the maximum deflection of the joystick using a force gauge. The force gradient is then found by dividing the maximum force by the maximum deflection of the joystick. The output of the joystick is not known since it communicates through USB. The USB accepts packets of data in bits, which can represent a voltage, current, or resistance from the joystick. Since the log decrement is utilized to obtain the damping ratio and natural frequency, the ratio between two successive peak amplitudes should be the same if a voltage, current or resistance is being read by the computer.

The MMS Laboratory software gave results that were not consistent for each run. Successive peak times varied between 0.21seconds and 0.25 seconds which changed the damped frequency and therefore natural frequency. From 0.21 seconds to 0.25 seconds successive peak time, the difference in natural frequency differs by 4.83 rad/s. The time response obtained using MMS Laboratory software is shown in Figure 4.3.2. The maximum deflection of the computer joystick is normalized in the MMS Laboratory software by dividing the response by the maximum deflection. The results for the MMS Laboratory software show a damping ratio of 0.133, and a natural frequency of 26.18 rad/s.

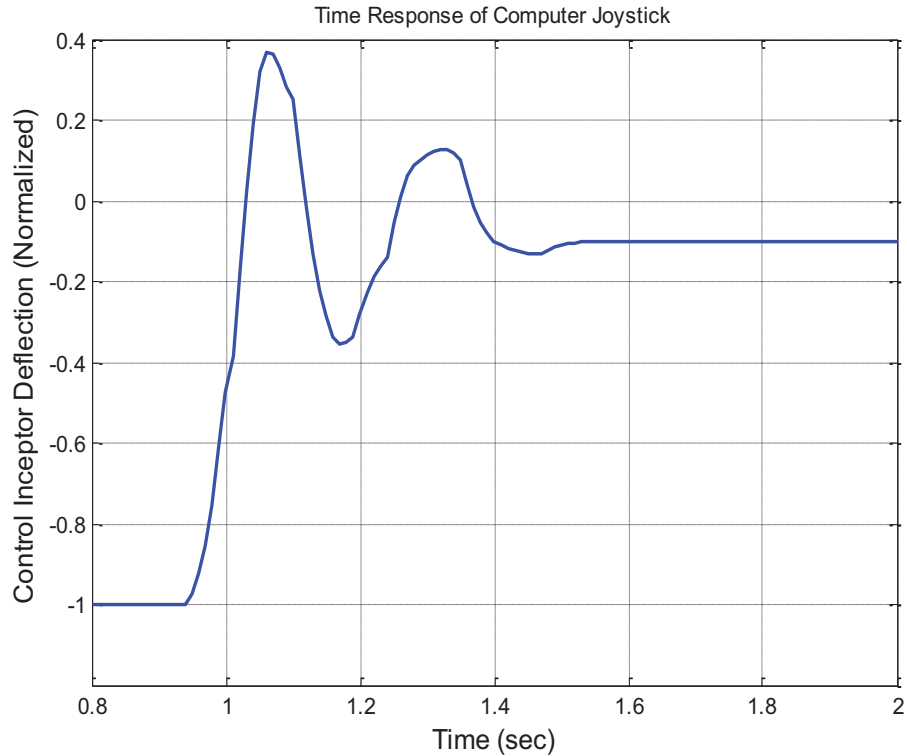


Figure 4.3.2 Logitech Computer Joystick Transient Response Obtained from MMS Laboratory

To obtain a more accurate measurement of the computer joystick, a built-in program in Labview [20] that measures the input of the joystick was used. A built-in function was used to measure the length of time the program ran. This timer was verified against a stopwatch and computer time to make sure that it was measuring the time accurately. A while loop used a metronome device which set the duration of each iteration that occurred. This was utilized to find the sample time and to determine the accuracy of collecting data at specific time intervals.

The while loop was used to collect data at a specific time rate so that each sample of the joystick data represented a set time that had elapsed. The while loop time was compared to the time selected for each iteration. The time response for the computer joystick obtained using Labview [20] is shown in Figure 4.3.3. The y-axis is the normalized deflection of the computer joystick. The deflection of the computer joystick

was normalized by dividing the response by its maximum deflection. The x-axis represents the time in seconds.

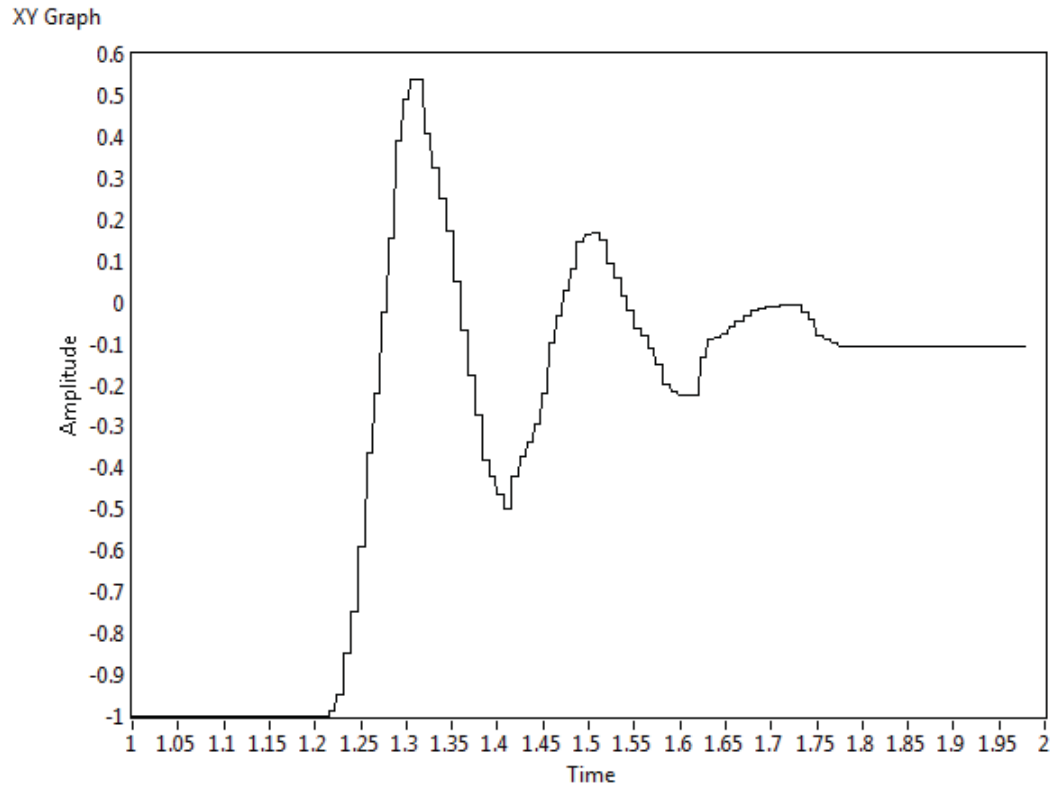


Figure 4.3.3 Logitech Computer Joystick Transient Response Obtained using Labview [20]

The results obtained using Labview [20] were more consistent for successive peak times. This gave a more accurate natural frequency. The results for the transient response obtained using Labview [20] were a damping ratio of 0.135, and a natural frequency of 34.5 rad/s. Since the mass of a control inceptor from simulator to simulator is never the same; it is important to maintain the force gradient which corresponds to the natural frequency. Since typical control inceptors in simulators have a greater mass, the obtainable natural frequency will be much lower.

The average natural frequency obtained using Labview [20] of approximately 34 rad/s might not be able to be replicated within the control loaders available with such a

low force gradient. Also, the low damping ratio of 0.135 and force gradient of 0.7 lb/in can cause the control stick to oscillate. The low fidelity control inceptor will be represented by a low force gradient, a low damping ratio, and a low natural frequency. These parameters are implemented and analyzed in Section 4.4 to ensure proper setup of the control loader for further experimental testing.

4.4 Analysis of Control Loader Parameters

To verify that the control loader parameters are implemented correctly, a frequency response and step response of the control loader for both the high fidelity and low fidelity system is required. The control inceptor dynamics have to be such that they match the characteristics that are defined below in Table 4.4.1.

McFadden Control Loader:				
Control Inceptor Fidelity:	Force Gradient:	Damping Ratio ζ	Damping Coefficient β :	Breakout Force:
High Fidelity	4 lb/in	0.7	0.25 lb•s/in	1.5 lb
Low Fidelity	0.7 lb/in	0.135	0.0243 lb•s/in	0 lb

Table 4.4.1 Control Inceptor Characteristics

To perform either a frequency response or a step response, a signal is injected into the control loader to obtain an output response. The control loader used for these experiments was manufactured by McFadden Systems. This type of control loader uses a force command servo as opposed to a position command servo. To inject a signal, the Simulation Evaluation System (SIMES) was used. The SIMES unit has the capability to output analog signals through an analog output port. Wiring from the analog output on the SIMES unit is connected to the control loader circuitry. The SIMES unit analog

output is connected at the force command summing junction within the control loader circuitry shown below in Figure 4.4.1.

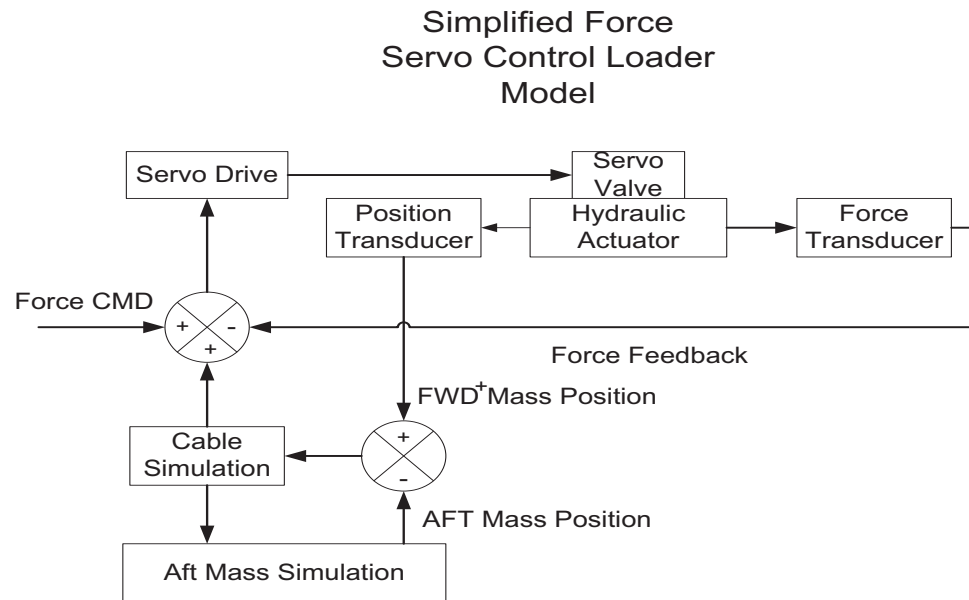


Figure 4.4.1 Force Servo Control Loader Model (Takats, 2011) [18]

The input voltage to the control loader circuitry is chosen so that the control inceptor deflects 10% of its maximum travel in one direction. The maximum travel of the control inceptor was set to 2 inches in either direction so 10% of travel is equal to 0.2 inches. The input analog signal is created within Matlab [21] as digital data. This data then passes through a digital to analog converter which then goes into the control loader circuitry.

The step response input that was created in Matlab [21] is actually a series of pulses with a 10 second pulse width. The response of the control loader to the pulse train results in a sharp spike right when the signal is injected. The reason for a sharp spike when injecting a step input is that a step input has a large change in amplitude very quickly and the control loader system might not be able to handle a fast changing input. To simplify the results, a free release response is used instead. A free release response

consists of manually deflecting the control inceptor to its maximum deflection in one direction and releasing the control inceptor. The SIMES unit is used to record the position of the control inceptor straight from the position transducer within the control inceptor.

To calculate the damping ratio using the free release response either the maximum percent overshoot or the logarithmic decrement method is utilized. To find the damping ratio (ζ) using the maximum percent overshoot, Equation 4.4.1 is used. The term PO refers to the maximum percent overshoot.

$$\zeta = \frac{-\ln(PO/100)}{\sqrt{\pi^2 + (\ln(PO/100))^2}} \quad \text{Equation 4.4.1}$$

To obtain the damping ratio using the logarithmic decrement method, Equation 4.4.2 is used first. The term (δ) represents the logarithmic decrement. The term (n) refers to the number of periods between two successive peaks. The terms (x_0) and (x_n) refer to the first peak amplitude and the successive peak amplitude n periods away.

$$\delta = \frac{1}{n} \ln \frac{x_0}{x_n} \quad \text{Equation 4.4.2}$$

After the logarithmic decrement is calculated, the damping ratio (ζ) is found using Equation 4.4.3.

$$\zeta = \frac{1}{\sqrt{1 + \left(\frac{2\pi}{\delta}\right)^2}} \quad \text{Equation 4.4.3}$$

To obtain the frequency response, a frequency sweep is first conducted. A frequency sweep consists of inputting a constant small amplitude sinusoid with varying

frequencies. To implement this on the McFadden controller the following procedure shown in Figure 4.4.2 is conducted.

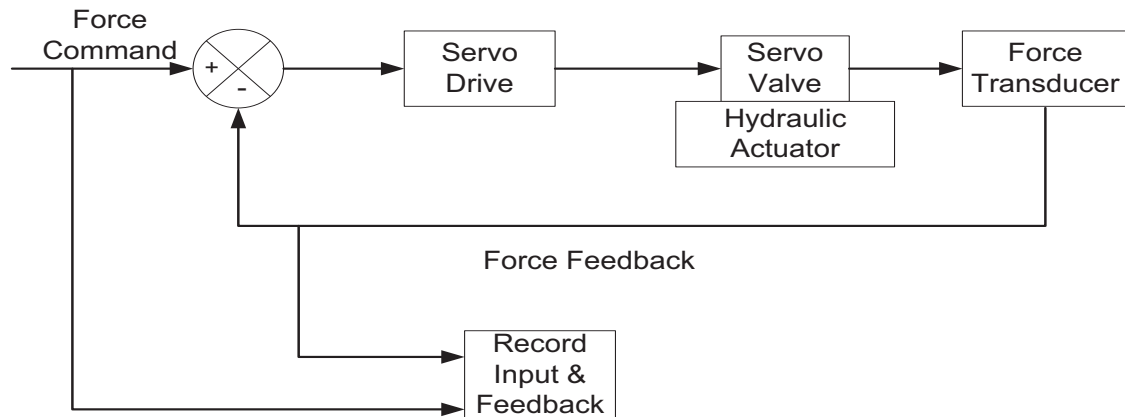


Figure 4.4.2 Frequency Sweep Configuration (Takats, 2011) [18]

A sinusoid with varying frequencies is fed into the control loader force command summing junction and the force feedback measured by the control inceptor force transducer is recorded. Two different sinusoids were chosen for the high fidelity and low fidelity frequency sweep. The amplitude and frequency range for both the high fidelity and low fidelity frequency sweep are shown in Table 4.4.2.

Control Loader Fidelity		Frequency Range			
		0.1 to 1 rad/s	1-18 rad/s	19-21 rad/s	22-25 rad/s
High Fidelity	Frequency Interval	0.1 rad/s interval	1 rad/s interval	0.1 rad/s interval	1 rad/s interval
	Amplitude	1 inch	1 inch	1 inch	1 inch

Control Loader Fidelity		Frequency Range			
		0.1 to 1 rad/s	1-7 rad/s	7-9 rad/s	9-20 rad/s
Low Fidelity	Frequency Interval	0.1 rad/s interval	1 rad/s interval	0.1 rad/s interval	1 rad/s interval
	Amplitude	1 inch	1 inch	1 inch	1 inch

Table 4.4.2 Frequency Sweep Input Sinusoid Formulation

Once the input force command and the force feedback are recorded, an offline analysis of the input/output is conducted. Using a Fast Fourier Transform technique within Matlab [21], the time domain signals are converted to the frequency domain. The

Matlab [21] code to accomplish this technique is located in Appendix D. The command in Matlab [21] referred to as spectrogram computes the Fast Fourier Transform and also applies a window function to a signal. The Fast Fourier Transform is computed for both the input and the output of the system. The cross spectrum which relates the similarity of two waveforms is then computed. The equation to compute the cross spectrum is shown in Equation 4.4.4.

$$\text{Cross Spectrum} = FFT(\text{Input})^* \times FFT(\text{Output}) \quad \text{Equation 4.4.4}$$

The auto spectrum which is equal to the cross spectrum of a signal with itself is computed for the input. The equation to compute the auto spectrum is shown in Equation 4.4.5.

$$\text{Auto Spectrum} = FFT(\text{Input})^* \times FFT(\text{Input}) \quad \text{Equation 4.4.5}$$

The term $FFT(\text{Input})^*$ denotes the complex conjugate of the Fast Fourier Transform of the Input. Next, the frequency response function (FRF) is obtained by using Equation 4.4.6.

$$FRF = \frac{\text{Cross Spectrum}}{\text{Auto Spectrum}} \quad \text{Equation 4.4.6}$$

From the frequency response function (FRF), both the magnitude ratio in dB and the phase between the Output and Input Signals can be calculated. The magnitude in dB is obtained by using Equation 4.4.7.

$$\text{Magnitude dB} = 20 \times \log_{10}(|FRF|) \quad \text{Equation 4.4.7}$$

To find the phase difference in degrees between the Input and Output Equation 4.4.8 is used.

$$Phase = \tan^{-1}(\text{imag}(FRF) / \text{real}(FRF)) \times (180 / \pi) \quad \text{Equation 4.4.8}$$

The terms $\text{imag}(FRF)$ and $\text{real}(FRF)$ represent the imaginary and real part of the FRF respectively.

To test the above signal processing technique, a frequency sweep was conducted on the control inceptor dynamics within Simulink [22]. The response using the above signal processing technique is compared with the true response using the transfer function. The simulated frequency response of the high fidelity control inceptor is shown below in Figure 4.4.3 using both the signal processing technique and the transfer function response. The transfer function used to simulate the high fidelity control inceptor is shown in Equation 4.4.9. The natural frequency was found using the square root of the defined force gradient of 4 lb/in divided by the mass of the McFadden control inceptor (0.01 lb•s²/in).

$$\frac{(20)^2}{s^2 + 2(.7)(20)s + (20)^2} \quad \text{Equation 4.4.9}$$

The frequency response is limited from 0.0159 to 4 Hz (0.1 to 25 rad/s). The frequency is limited to this range to decrease computation time for the signal processing technique. Also, the control loader is limited to a 5 Hz (31 rad/s) input signal. The average error in magnitude between the simulated and true frequency response is 0.0014 dB. The average error in phase between the signal processed and true frequency response is 0.00015 degrees.

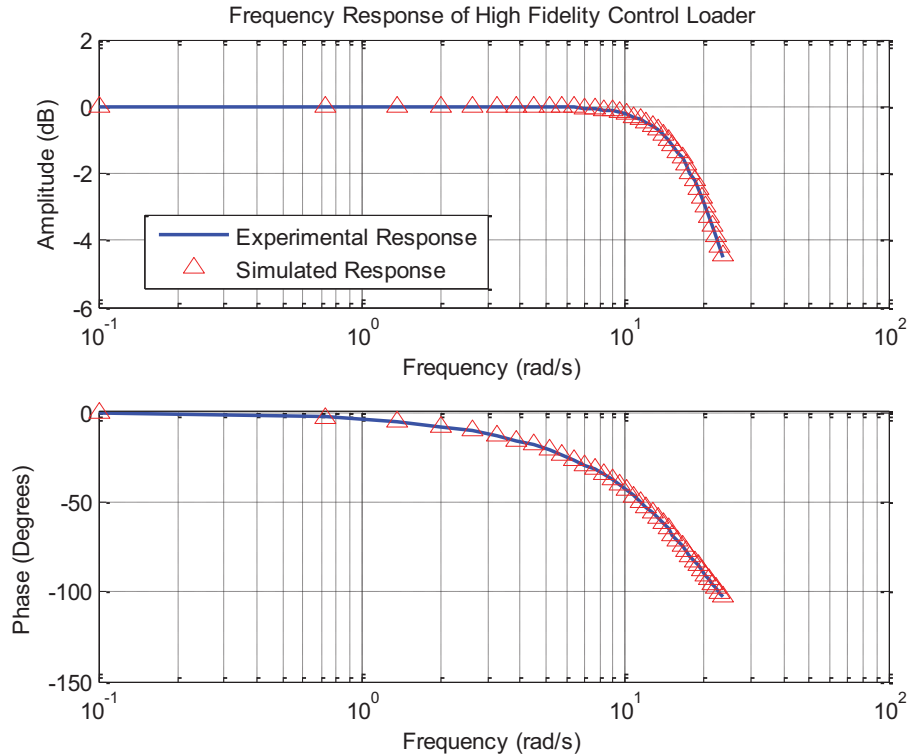


Figure 4.4.3 Simulated High Fidelity Frequency Response

The simulated frequency response for the low fidelity control inceptor is shown in Figure 4.4.4. The transfer function used to simulate the low fidelity control inceptor is shown in Equation 4.4.10. The natural frequency was obtained using a force gradient of 0.7 lb/in and the McFadden control inceptor mass of 0.01 lb•s²/in.

$$\frac{(8.366)^2}{s^2 + 2(.135)(8.366)s + (8.366)^2} \quad \text{Equation 4.4.10}$$

The response for the low fidelity control inceptor using the signal processing technique matches the true response very well. The average magnitude and phase error between the signal processed response and the true response is equal to 0.0035 dB and 0.09 deg respectively. The signal processing technique produces good results, but has issues with noisy signals.

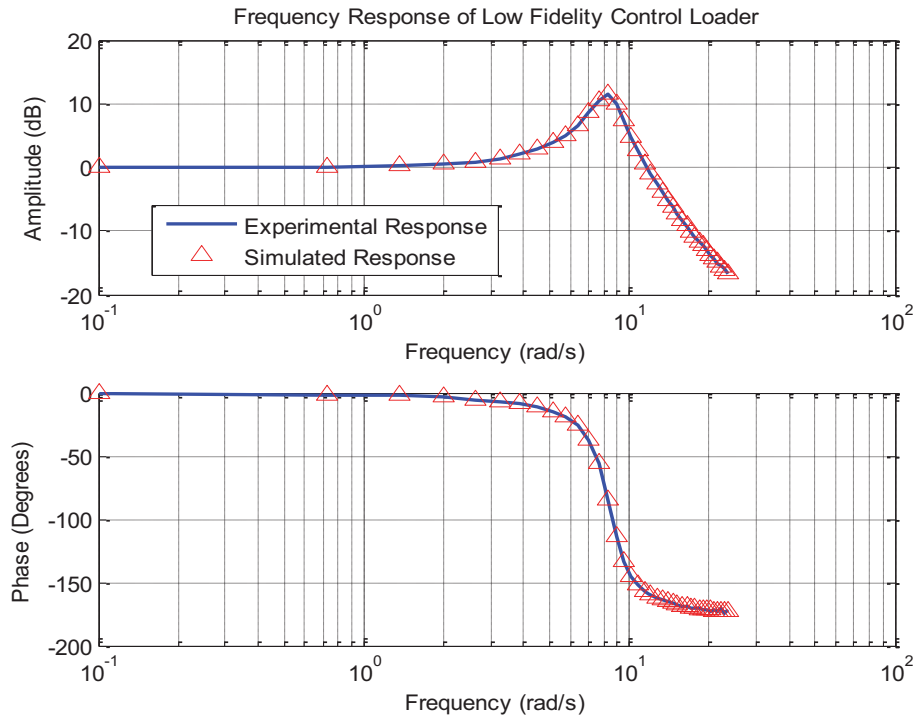


Figure 4.4.4 Simulated Low Fidelity Frequency Response

Another technique used when computing the frequency response is to select the different frequency sinusoids within the input and output of the control loader system and compare the magnitudes and phase difference between the two. This results in one value per frequency producing a smooth frequency response.

To measure the force gradient of both the high fidelity and low fidelity control inceptors, a push/pull test was conducted. To perform this test the control inceptor is pushed to its maximum deflection in one direction then pulled to its maximum deflection in the other direction. Both the force applied to the control inceptor in pounds and its position in inches are recorded. The force applied is plotted against the position of the control inceptor. The slope of this plot is equal to the force gradient.

4.4.1 Experimentally Obtained High Fidelity Characteristics

The characteristics for the high fidelity control inceptor that were experimentally measured from the McFadden control inceptor are presented within this section. The first measured characteristic is the force gradient obtained by plotting the force applied versus the displacement of the control inceptor. The force versus displacement for the high fidelity control inceptor is shown in Figure 4.4.5.

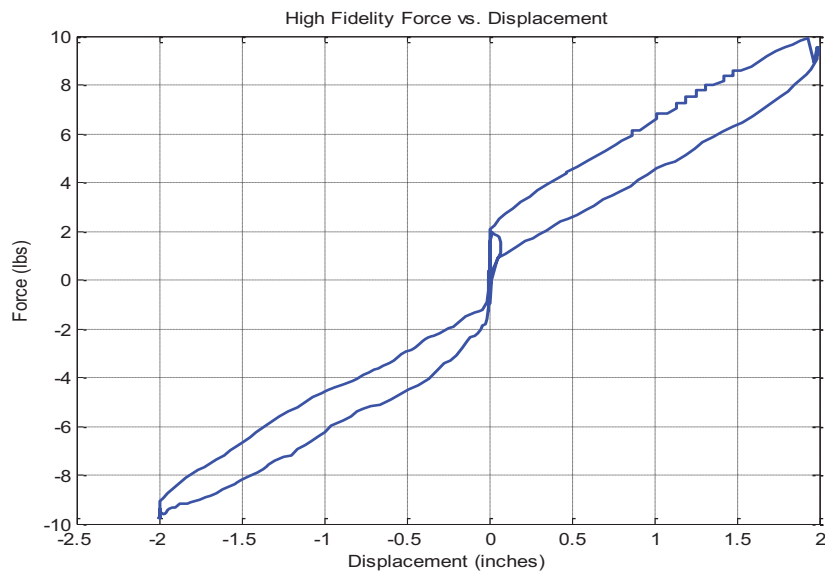


Figure 4.4.5 High Fidelity Force vs. Displacement

As shown in Figure 4.4.5, the control inceptor contains hysteresis. The control inceptor follows a different force vs. displacement path when being loaded as opposed to being unloaded. The hysteresis is caused by the difference in energy dissipation due to viscous damping when loading the control inceptor as opposed to unloading the control inceptor. The area in between the force vs. displacement hysteresis loop represents the energy loss of the system ΔE . Using the formula $\Delta E = \pi c \omega X^2$, the damping coefficient can be calculated. The term X represents the amplitude of motion, c represents the damping ratio, and ω represents the natural frequency. The loss of damping energy in one

direction makes it harder to load the control inceptor as opposed to unloading the control inceptor. The force gradient obtained from the slope in Figure 4.4.5 is equal to 4.09 lb/in. The implemented force gradient for the high fidelity control inceptor is 4 lb/in. At zero inches of deflection, there exists a non-linearity corresponding to the breakout force. The control inceptor starts deflecting when the force applied is around 1.5 lb.

To obtain an effective mass of the control inceptor and to investigate the effect that friction has on the damping, a free release was conducted with the damping coefficient set to a low value of 0.01 lb•s/in. The free release for this system is shown in Figure 4.4.6. By obtaining the effective mass, the damping coefficient corresponding to the defined damping ratio of 0.7 for the high fidelity control inceptor can be calculated. The low damping ratio allows multiple peak amplitudes to appear in the transient response allowing for the investigation of the change in damping ratio as the motion of the control inceptor decreases.

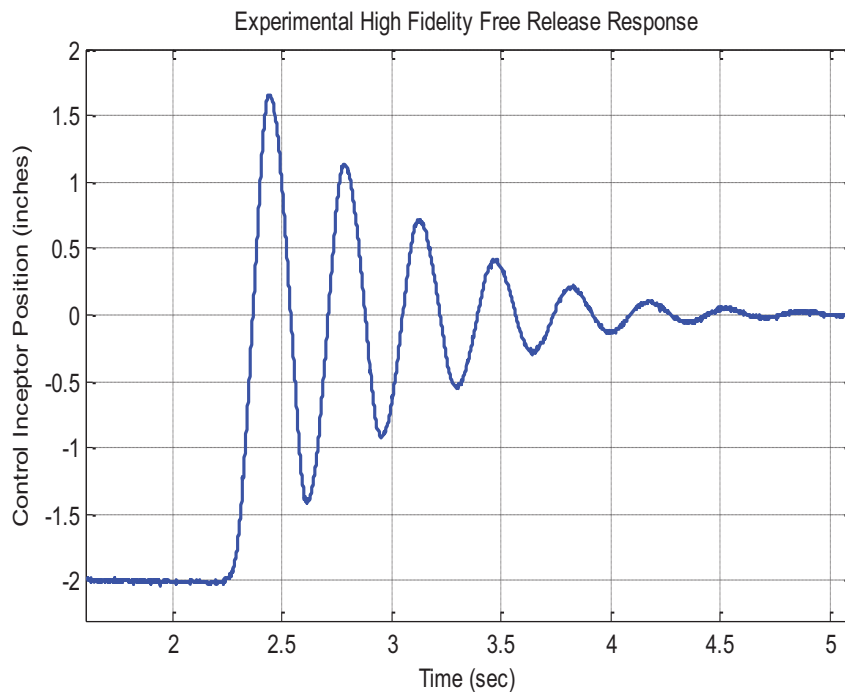


Figure 4.4.6 High Fidelity Free Release Response with Low Damping Ratio

Using every two successive peaks, the logarithmic decrement was used to determine the damping ratio as the amplitude of motion decreases. Since the force gradient of 4 lb/in was confirmed, this was used along with the natural frequency obtained from every two successive peaks to find the effective mass. The effective mass is then calculated using Equation 4.4.11.

$$m_e = \frac{k}{\omega_n^2} \quad \text{Equation 4.4.11}$$

A list of the damping ratios for different successive peaks along with the effective mass is shown in Table 4.4.3. As shown, the damping ratio increases as the motion of the control inceptor becomes smaller. This can be due to coulomb friction that exists very close to the neutral position of the control inceptor.

Successive Peaks	Logarithmic Decrement δ	Damping Ratio ζ	Natural Frequency ω_n (rad/s)
1 st	0.446	0.071	18.311
2 nd	0.537	0.085	18.493
3 rd	0.624	0.099	18.408
4 th	0.748	0.118	18.34
5 th	0.55	0.087	17.918

Successive Peaks	Effective Mass (lb*s ² /in)
1 st	0.0119
2 nd	0.0117
3 rd	0.0118
4 th	0.0119
5 th	0.0125

Table 4.4.3 Acquired High Fidelity Effective Mass with Low Damping Ratio

For larger motion, the friction does not affect the damping nearly as much as for low amplitude motion. This occurs because at a higher deflection of the control inceptor, a higher restoring force overcomes the resistance due to friction. The effective mass of the control inceptor generally stays consistent and is not affected by an increase in the

damping ratio. The effective mass was compared with previous results conducted by NASA Langley Research Center, and the average values of the effective mass have a difference $0.00197 \text{ lb}\cdot\text{s}^2/\text{in}$.

The free release response was conducted for the high fidelity control inceptor with an implemented damping coefficient of $0.0243 \text{ lb}\cdot\text{s}/\text{in}$. The response is shown below in Figure 4.4.7. As shown, the response contains a small amplitude peak and settles fairly quickly. This response is typical of a highly damped second order system. The overshoot for this system is equal to 4.022% which corresponds to a damping ratio of 0.715 . This is consistent with the damping ratio of 0.7 that is implemented for the high fidelity control inceptor. Because of friction, the measured damping ratio is slightly larger.

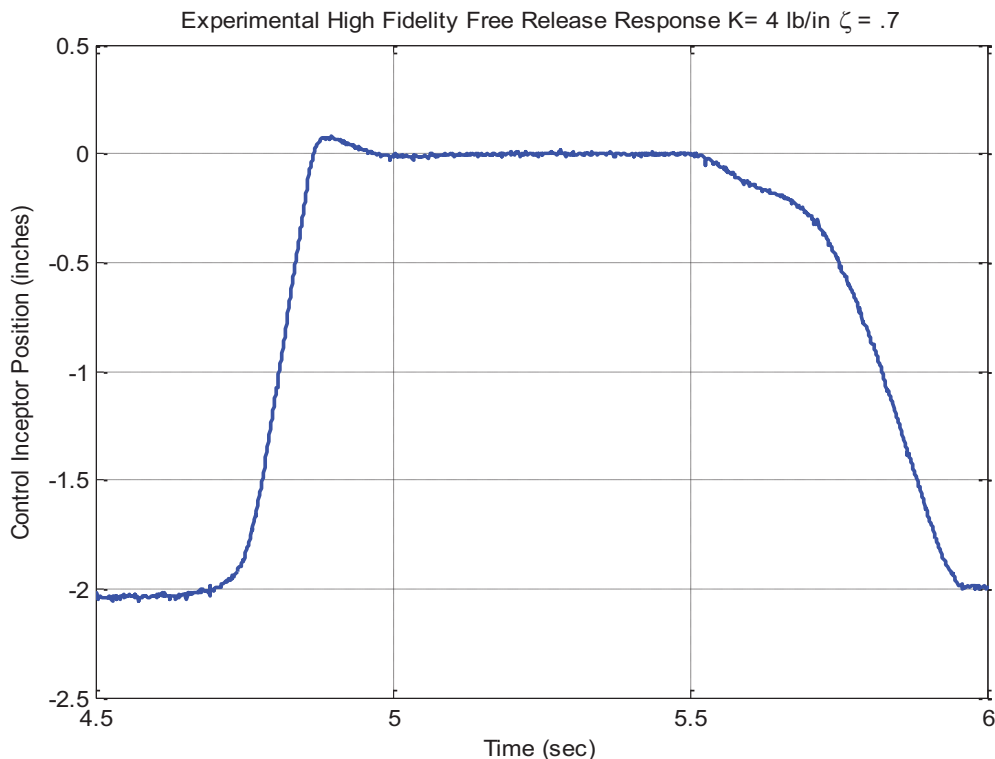


Figure 4.4.7 Experimental High Fidelity Free Release Response

The frequency sweep technique described above in Section 4.4 was implemented on a McFadden control loader to verify the control inceptor dynamics before conducting

the main transfer of training study. The input frequency sweep was developed in Matlab [21] with a force amplitude of 1.5 lbs and the frequencies of the sinusoids presented in Table 4.4.2 in Section 4.4. The input represents a force command to the force servo of the control loader. The output is the measured force from the force transducer located within the McFadden control inceptor.

Using the signal processing technique produces a noisy Bode diagram. This is mitigated by plotting only the phase and magnitude at the frequency intervals used in the frequency sweep. The damping coefficient used for the high fidelity was lowered to .01 lb•s/in. The damping coefficient was lowered so that a resonance peak can be seen around the natural frequency of the system. Otherwise, a system with a damping ratio of 0.7 has no peaking and therefore harder to locate the resonance peak.

From the free release response of the high fidelity control inceptor with the damping coefficient lowered to 0.01 lb•s/in, a damping ratio of 0.118 was obtained. Using the obtained force gradient of 4.09 lb/in and an effective mass of 0.0119 lb•s²/in, the calculated natural frequency is equal to 18.54 rad/s. A damping ratio of 0.118 along with a natural frequency of 18.54 rad/s is used when simulating the frequency response. Using the signal processing technique the following frequency response is obtained in Figure 4.4.8.

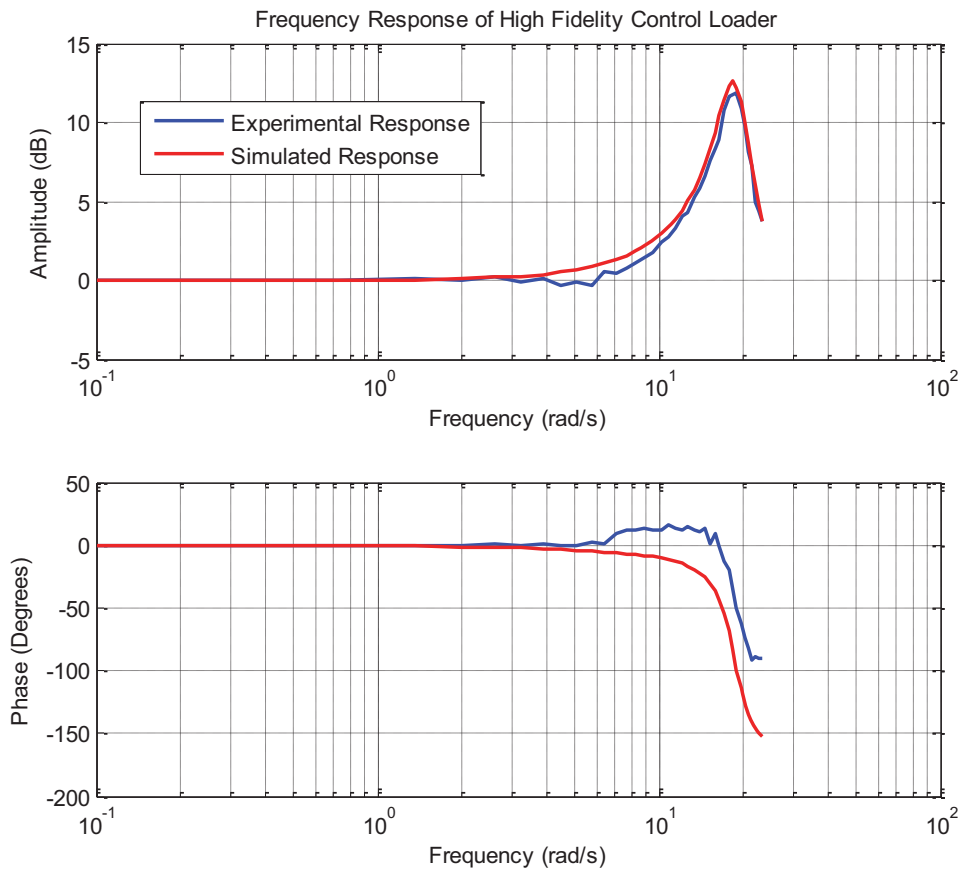


Figure 4.4.8 Experimental High Fidelity Frequency Response with Low Damping Ratio

The resonance peak frequency is equal to 18.32 rad/s, which corresponds to a natural frequency of 18.57 rad/s. This value is 0.16% different than the natural frequency obtained from the simulated frequency response.

The phase relation between the input and output obtained experimentally shows some phase lead at around 7 rad/s. There is a time shift that occurs in the output when the input sinusoid changes frequencies. It could be that the momentum of the control inceptor keeps the control inceptor from responding to a change in frequency promptly. The time response of the input and output shows the input leading the output at this frequency.

4.4.2 Experimentally Obtained Low Fidelity Characteristics

The same tests performed above for the high fidelity control inceptor were again performed for the low fidelity control inceptor. One of the tests performed was the force vs. displacement test. Shown below in Figure 4.4.9 is the force vs. displacement of the low fidelity control inceptor.

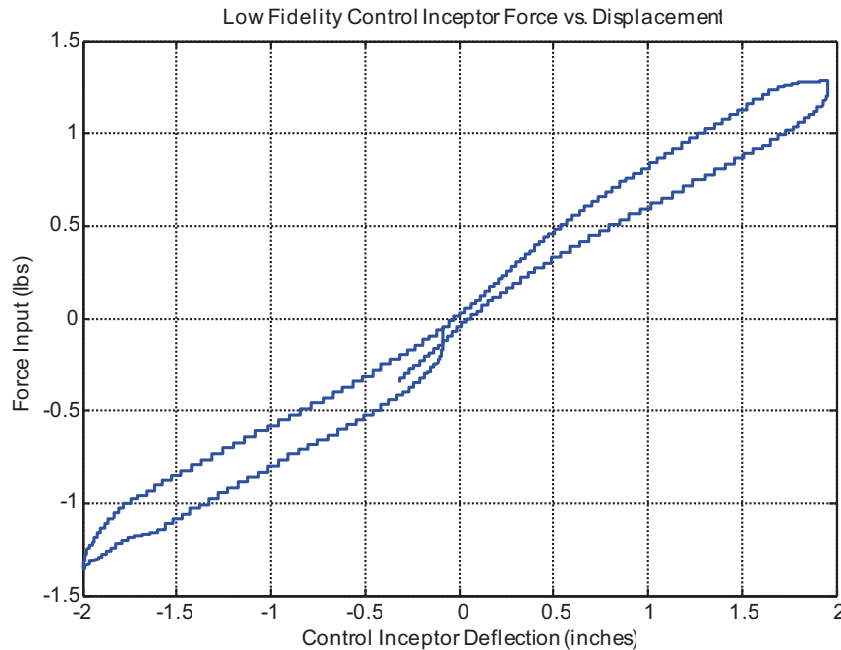


Figure 4.4.9 Experimental Low Fidelity Force vs. Displacement

The mean slope of the low fidelity control inceptor force vs. displacement was found to be 0.66 lb/in which is 0.04 lb/in different than the defined value of 0.7 lb/in. The non-linearity at 0 inches of deflection that is present for the high fidelity control inceptor is not present for the low fidelity control inceptor. The breakout force that causes the non-linearity is set to 0 lb for the low fidelity control inceptor. There still exists hysteresis for the low fidelity control inceptor caused by energy dissipation while unloading the control inceptor due to viscous damping.

The free release response was also conducted and is shown in Figure 4.4.10. As shown, the free release response for the low fidelity control inceptor represents a low damped system.

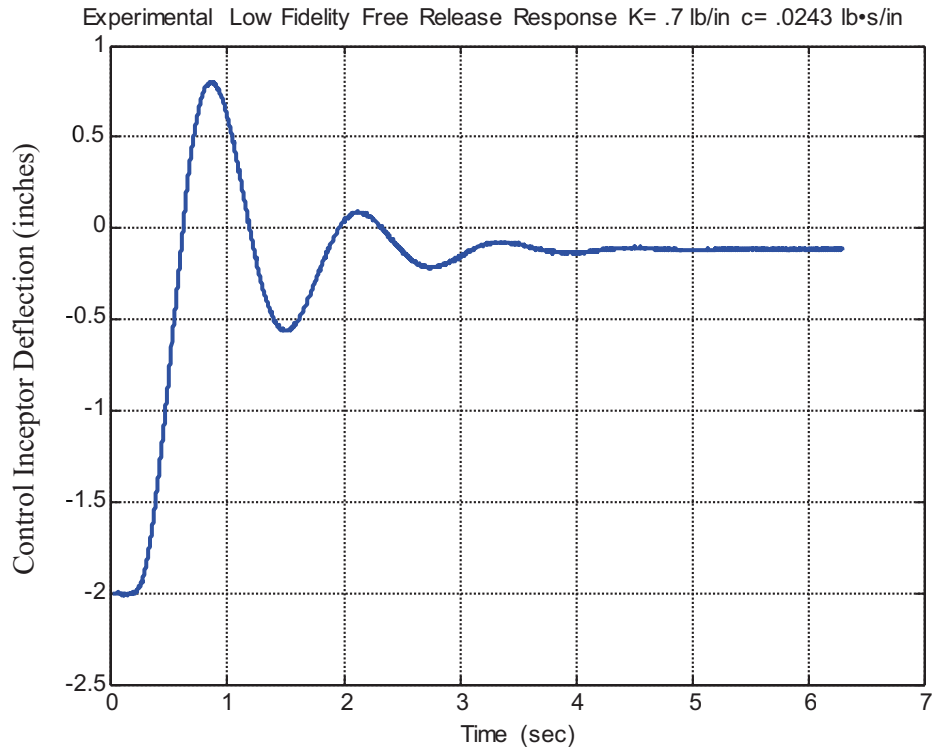


Figure 4.4.10 Experimental Low Fidelity Free Release Response

The overshoot of 48.2% corresponds to a damping ratio of 0.226. Using the log decrement on the first two successive peaks a damping ratio of 0.233 is obtained. The defined damping ratio is equal to 0.135 but because of added friction to the system, the damping ratio is larger than what is defined. The natural frequency obtained from the free release response is equal to 5.26 rad/s.

Both the experimentally obtained frequency response using a signal processing technique proposed in Section 4.4 and a simulated response are shown in Figure 4.4.11. A damping ratio of 0.226 and a natural frequency of 5.26 rad/s that are both obtained from the free release response (Figure 4.4.10) are used to simulate the frequency

response. The peak magnitude of the simulated and experimental frequency response is equal to 7.125 and 7.4 dB respectively. The peak magnitude corresponds to the damping ratio of the system. The simulated peak magnitude corresponds to a damping ratio of 0.226. A peak magnitude of 7.4 dB corresponds to a damping ratio of 0.219. Therefore the difference is equal to 3%.

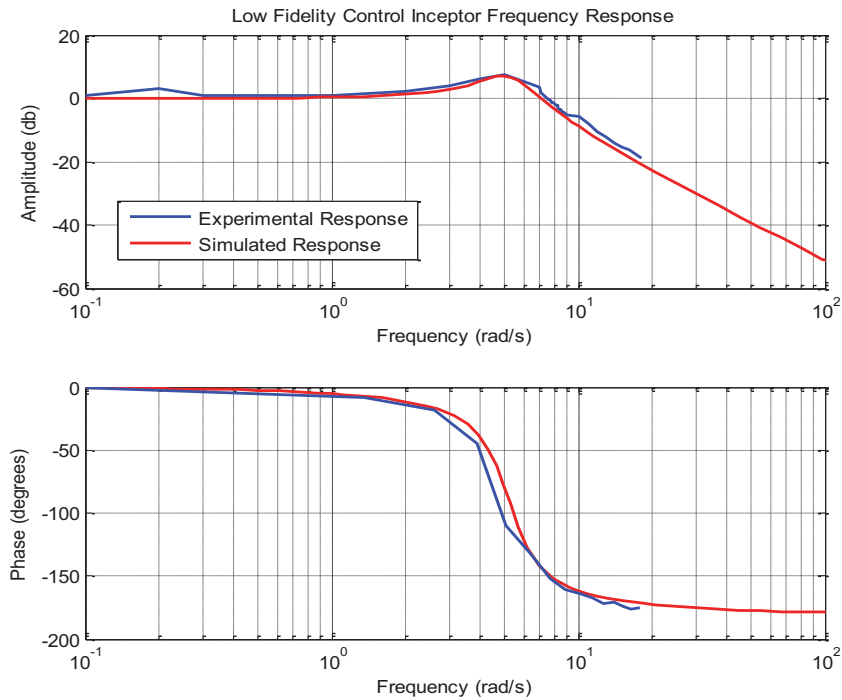


Figure 4.4.11 Experimental Low Fidelity Frequency Response

The peak magnitude for the simulated and experimental response occurs at 5 rad/s and 4.965 rad/s respectively. The natural frequencies that correspond to the peak natural frequencies for the simulated and experimental responses are equal to 5.26 rad/s and 5.24 rad/s respectively. The difference between these two natural frequencies is equal to 0.4%.

The expected natural frequency for this system using the effective mass of the control inceptor of $.0119 \text{ lb}\cdot\text{s}^2/\text{in}$ and a force gradient of $0.7 \text{ lb}/\text{in}$ is equal to 7.67 rad/s . The control inceptor contains friction which effectively damps the system which acts as an added mass. The calculated effective mass for the low fidelity control inceptor is equal

to 0.025 lb•s²/in. The effective mass for the low fidelity control inceptor is 0.0131 lb•s²/in greater than the high fidelity control inceptor.

4.5 Disturbance Input & Performance Metric Tests

The disturbance shown below in Table 4.5.1 was chosen from an experiment conducted by Bailey (1990) [1]. The disturbance consists of a series of sine waves in the form of $\sum A_i \sin(\omega_i t)$ with different amplitudes and frequencies. This allows the task to be pseudo random which tests each of the test subjects for a wide range of human performance. This also removes any effect of improved performance solely to learning the task.

Plant Dynamics	Sine Wave	1	2	3	4	5	6	7	8	9
1/s & 1/s ²	Frequency (ω_i rad/s)	.467	.701	1.17	1.87	3.51	7.01	11/2	14	18.7
	Amplitude (A_i)	15.2	15.2	15.2	7.6	3.04	.76	.38	.228	.152

Table 4.5.1 Sum of Sines Disturbance Input

The frequencies for each sinusoid were chosen to effectively test the neuromuscular system. The neuromuscular system is represented by a second order mass damper with a natural frequency typically around 14 rad/s. The sum of sines disturbance includes the frequency of 14 rad/s.

The response of the disturbance is shown below in Figure 4.5.1. The root mean square (RMS) of the disturbance over a 30 second interval is equal to 20.85 deg. The maximum roll angle that occurs from the disturbance input is 38 deg. The disturbance switches direction 10 times over the duration of 30 seconds.

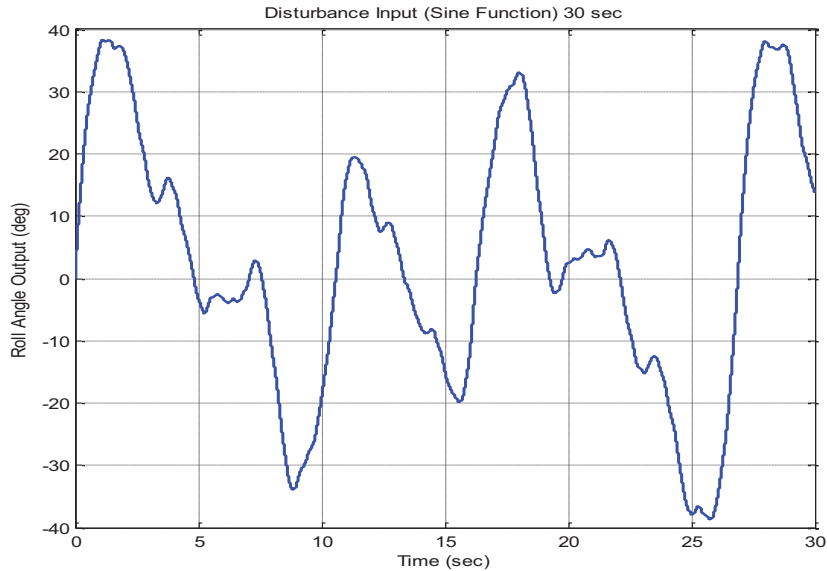


Figure 4.5.1 Plot of Roll Angle Disturbance

As shown in Figure 4.5.1, the disturbance reaches approximately the same maximum amplitude in both directions and is evenly centered around zero degrees roll angle. The disturbance contains numerous low frequencies as compared to higher frequencies.

The disturbance input was implemented within the MMS (Man Machine Systems) Laboratory software. This software allows for the testing of compensatory tracking tasks with test subjects. It has the ability to test $1/s$ and $1/s^2$ plant dynamics with a disturbance input. It can measure performance attributes such as RMS tracking error, RMS input, STD input, and time on target. A Logitech computer joystick, the same used to obtain the low fidelity control inceptor characteristics, was used to test the ability to null the disturbance.

At the same time that the disturbance was tested, the performance metric RMS tracking error was tested to determine if the test subject reached an asymptotic tracking error. To test the disturbance within the MMS Laboratory software, it was scaled down to

stay within the limits of the display. The disturbance that is implemented within the MMS Laboratory software is normalized. The full deflection of the cursor on the display is represented by an amplitude of 1. The disturbance was normalized by dividing by the maximum amplitude multiplied by a factor of 5. The disturbance that was implemented within the MMS Laboratory is shown below in Table 4.5.2.

Plant Dynamics	Sine Wave	1	2	3	4	5	6	7	8	9
$1/s$ & $1/s^2$	Frequency (ω_i rad/s)	.467	.701	1.17	1.87	3.51	7.01	11/2	14	18.7
	Amplitude (A_i)	.2	.2	.2	.1	.04	.01	.005	.003	.002

Table 4.5.2 Disturbance Input Implemented in MMS Laboratory

Using the MMS Laboratory software, the running cumulative average RMS tracking error was recorded for each run which lasted for 30 seconds. A plot of the running cumulative average RMS tracking error is shown in Figure 4.5.2.

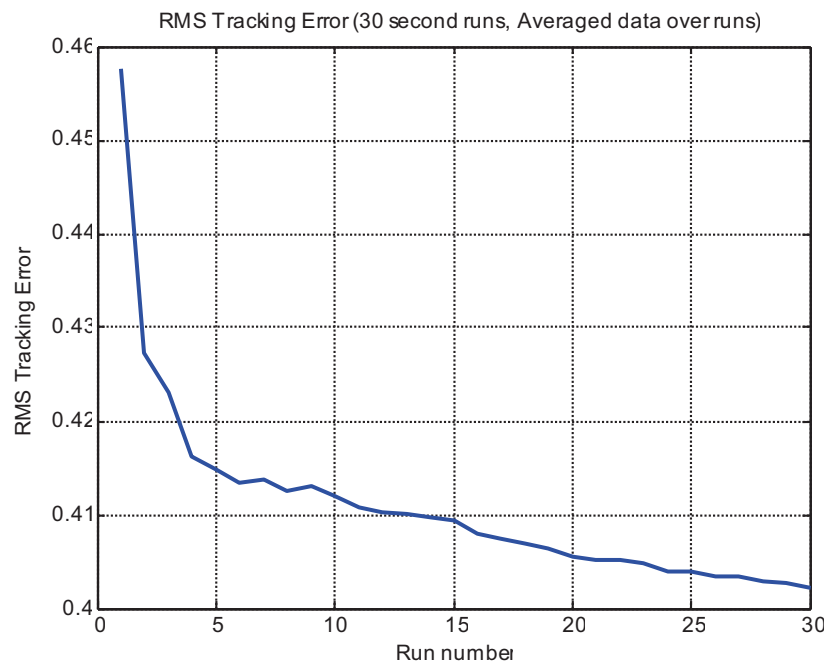


Figure 4.5.2 RMS Tracking Error Obtained from Test within MMS Laboratory

As shown in Figure 4.5.2, the running cumulative average RMS tracking error reduces drastically from the first run to the fourth run. After the fourth run it seems that the running cumulative average RMS tracking error starts to level off and approach an asymptote. This shows that the test subject has reached his/her maximum performance.

From Figure 4.5.2 it is hard to tell that the RMS tracking error has reached an asymptote. Since the RMS tracking error differs by an order of 10^{-2} between each run, the slope of the running cumulative average tracking error is obtained. The slope of the RMS tracking error is calculated between every two successive runs. The slope is shown in Figure 4.5.3.

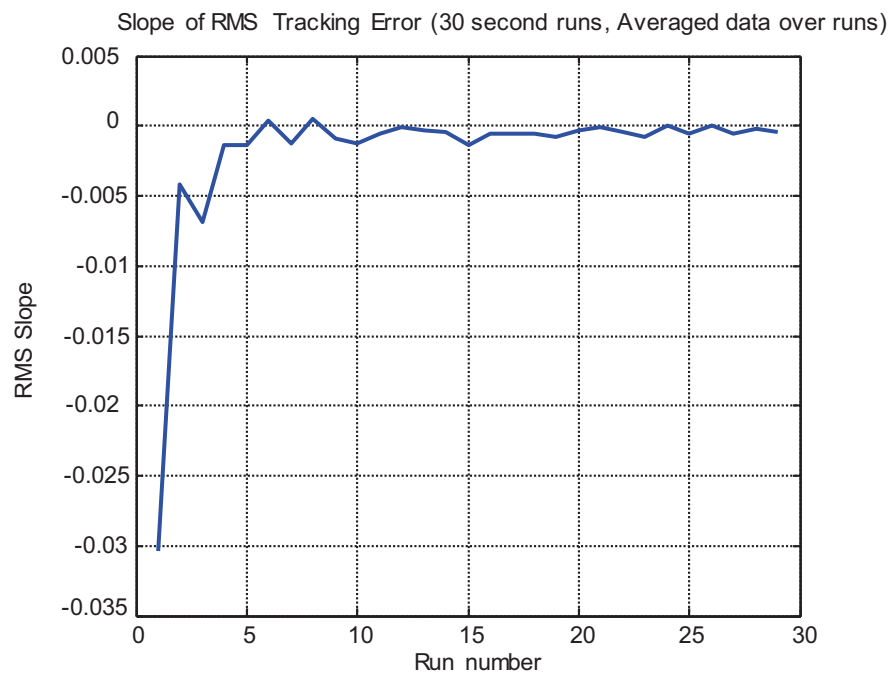


Figure 4.5.3 Slope of RMS Tracking Error Obtained from Test within MMS Laboratory

As shown, the slope in the beginning is much higher and then it eventually starts to approach a zero slope meaning that the response is reaching a horizontal asymptote. It has been determined that if a consistent slope of 0.01 or less exists for 3 runs, the test

subject has reached his/her performance asymptote and has trained successfully on the task.

The reason for using the running cumulative average of the RMS tracking error is that there exists a small fluctuation of the RMS tracking error from run to run. This distorts the behavior and the RMS tracking error appears to not reach an asymptote. The running cumulative average does not distort the values but gives a general trend for the behavior of the RMS tracking error.

The running cumulative average RMS control inceptor deflection was also considered when conducting these tests. The RMS control inceptor deflection is shown in Figure 4.5.4. It appears that the behavior of RMS control inceptor deflection is very similar to that of the RMS tracking error. The RMS control inceptor deflection also decreases in value with each successive run. This suggests that the test subject has less control inceptor movement as the task is being learned.

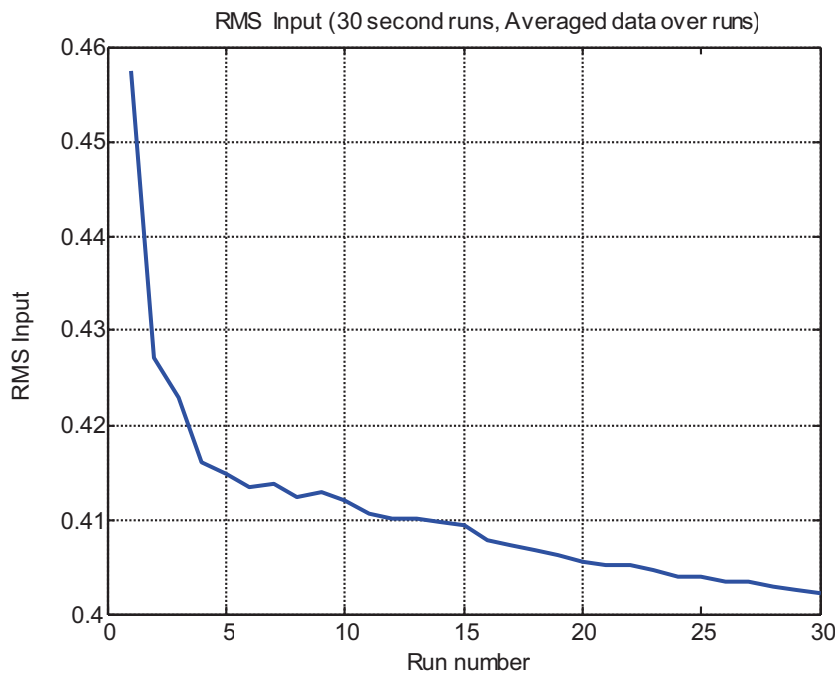


Figure 4.5.4 RMS Control Inceptor Deflection Obtained from Test within MMS Laboratory

The slope of the RMS control inceptor was calculated and plotted in Figure 4.5.5. Although the RMS input shows a general trend of reaching an asymptote, less control inceptor deflection does not necessarily show an improvement in performance. It does show an improvement in test subject workload. More important is the bandwidth of the test subject input. Higher bandwidth corresponds to increased test subject performance.

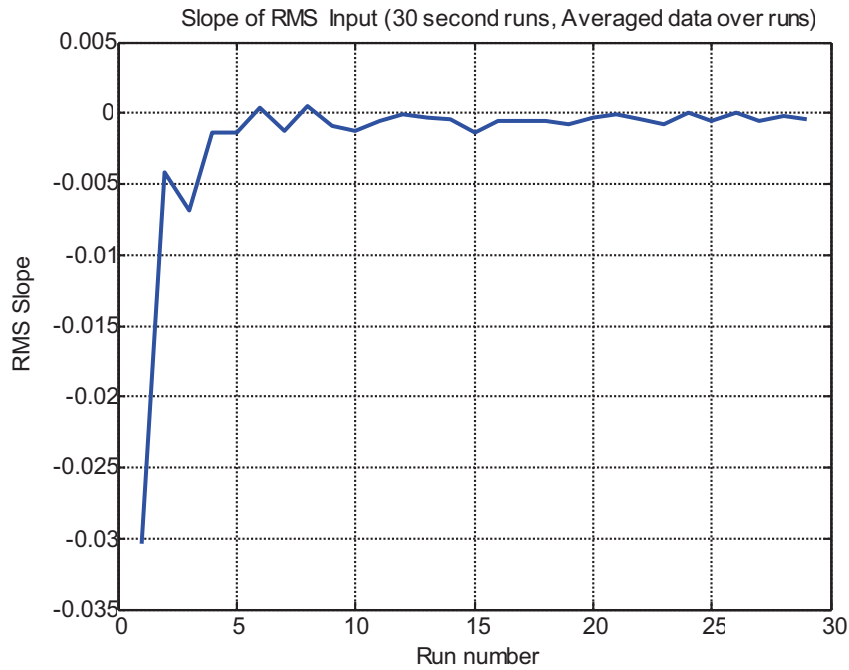


Figure 4.5.5 Slope of RMS Control Inceptor Deflection Obtained from Test within MMS Laboratory

Chapter 5 - Experimental Setup

5.1 Introduction

Experiments are conducted on a high fidelity or low fidelity control inceptor in a manner to effectively test the performance of each test subject. The importance of maintaining the proper force feedback to the test subject is not known, and these experiments will illuminate the effects of force feedback. The task performed by each test subject is a roll disturbance compensatory task. The plant dynamics used in the experiments are $1/s$ and $1/s^2$. Plant dynamics $1/s$ represents a simple control task while $1/s^2$ plant dynamics represent a more difficult task. Each test subject will complete the roll disturbance compensatory task for both the $1/s$ and $1/s^2$ dynamics. The test subjects will complete a run lasting for 30 seconds. They will conduct as many runs as necessary to reach a performance asymptote that is described within this chapter. The following chapter will present a background of the experiment performed, an experimental setup, and a protocol.

5.2 Background

The experiments within this study were conducted in the Cockpit Motion Facility (CMF) at the NASA Langley Research Center. Shown in Figure 5.2.1 is an artist conception of the Cockpit Motion Facility. The motion platform is located in the center of the facility. The motion platform has six degrees of freedom and has six 76 inch hydraulic actuators. Within this facility, there exists the ability to use each one of the three flight cockpits with motion or as a fixed base simulation. The flight cockpits used in a fixed based simulation are located on either side of the Cockpit Motion Facility. The three flight cockpits include the Research Flight Deck Simulator (RFD), the Integration

Flight Deck Simulator (IFD), and the Generic Flight Deck Simulator (GFD). Within this study the GFD was chosen because of the flexibility of changing the characteristics of the control loader system. In this experiment the GFD was used as a fixed based simulator.

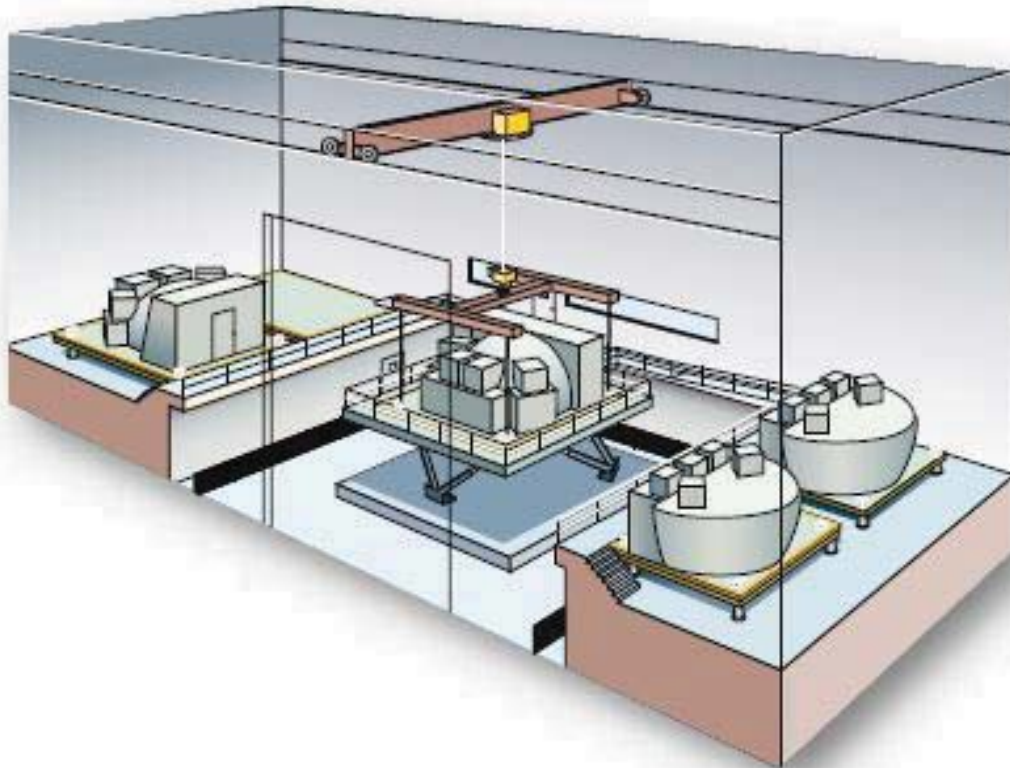


Figure 5.2.1 Cockpit Motion Facility (NASA LaRC)

The GFD cockpit uses four CRT monitors to present an out-the-window display image. The image is passed through a beam splitter and then collimated to provide the out-the-window image. These particular displays are referred to as WAC window displays which stands for wide angle collimated displays.

5.3 Implementation of Transfer of Training Study

A description on the experimental setup and protocol is discussed within this section. A quasi-transfer of training experiment is conducted where test subjects with no prior flight experience will train on a roll disturbance compensatory task. A control

inceptor representing high fidelity force feedback dynamics and a control inceptor with very minimal force feedback will be interchanged. This experiment is conducted on a fixed base simulator with an out-the-window display.

This experiment focuses on feedback cues that arise solely from the neuromuscular and visual systems. This experiment will ascertain important information on the effect of training on two different control inceptor dynamics. The simple setup allows the experiments to be repeated with other simulators.

5.3.1 Protocol

A quasi-transfer of training study consists of training test subjects to null a roll disturbance maintaining level flight using a high and low fidelity control inceptor simulation. After the test subjects are trained, they will then transfer to the high fidelity control inceptor simulation. The test subjects will be drawn from the general population in which they have no formal flight training experience. The simulation will be fixed base and will have a simple horizon out-the-window display. Implementation of the experiment will be described in the following paragraphs as well as a procedure for training the test subjects on each of the simulations. A step by step experimental protocol is located in Appendix A.

Before running tests with test subjects, a simple check on the equipment should be conducted. The display should show the target clearly. The display should also react accordingly to test subject input with the roll rate of the bank angle on the display increasing with increased control inceptor deflection. Also, the recorded force output and control inceptor deflection should have very little signal noise. The disturbance should be applied without any test subject input and the output bank angle should be recorded. This

should be compared with the disturbance generated in a computer simulation. The control inceptor should be calibrated properly making sure that at the neutral position the position being sensed is a value of zero inches. Also the force should be zero pounds when the control inceptor is at rest.

To conduct the transfer of training task, two separate groups each consisting of 10 test subjects will be used. The two groups represent the high fidelity control inceptor transfer group and the low fidelity control inceptor transfer group. One group termed the high fidelity control inceptor transfer group will train on the high fidelity control inceptor simulation. The other group termed the low fidelity control inceptor transfer group will train on the low fidelity control inceptor simulation. The test subjects will each conduct a 30 second run. The RMS tracking error and RMS control inceptor deflection will be recorded for each run. The RMS cumulative running average will be computed for both the tracking error and control inceptor deflection.

When each test subject reaches an asymptotic running cumulative average RMS tracking error, the training task will be completed for each test subject. To assist in determining if the test subject has reached an asymptote, the slope of the running cumulative average RMS tracking error between every two points is calculated. When the slope reaches a consistent value for three consecutive runs of 0.1 or less, asymptote has been reached. At the conclusion of the training session a break is administered. After each test subject trains, they will then be transferred to the high fidelity control loader simulation. The test subjects will again complete 30 second runs until they reach an asymptotic running cumulative average (RMS) tracking error. A description for the measured and the calculated parameters is described in section 5.3.2.

Each test subject is given a label HF# and LF# for the high fidelity and low fidelity transfer group respectively. Each test subject will be given a certain time slot in which they will conduct both the $1/s$ and $1/s^2$ plant dynamics experiments. The test subjects will each be briefed on the task they are to perform with a briefing statement that is located in the Experimental Protocol in Appendix A. The test subject will perform four phases of the experiment that include the familiarization phase, evaluation phase, training phase, and transfer phase. A break of 5 minutes is administered between the training and transfer phase. The test subject will then transfer to the high fidelity control loader simulation. After they have completed the task for $1/s$ plant dynamics, the test subjects will get another break of 5 minutes. After the break they will return to complete all four phases for $1/s^2$ plant dynamics. An experiment run time that gives an estimated experiment completion time is located in Appendix C.

5.3.2 Test Setup

Two different transfer of training configurations exist for the $1/s$ and $1/s^2$ plant dynamics. Experiment pseudo code is created to run these two tasks within the experiment. Much of the code implements the disturbance, Euler integration techniques, roll angle that is displayed, as well as a way to measure data associated with test subject performance. The experimental pseudo code is located in Appendix E. Figure 5.3.1 describes the general configuration for both the $1/s$ and $1/s^2$ plant dynamics.

The main difference is that the roll command is represented by a roll rate command and a roll acceleration command for $1/s$ and $1/s^2$ dynamics respectively. In Figure 5.3.1 a forcing function described in Table 4.5.1 in Section 4.5 is first generated

and then summed with the output roll angle of the plant that is commanded by the test subject.

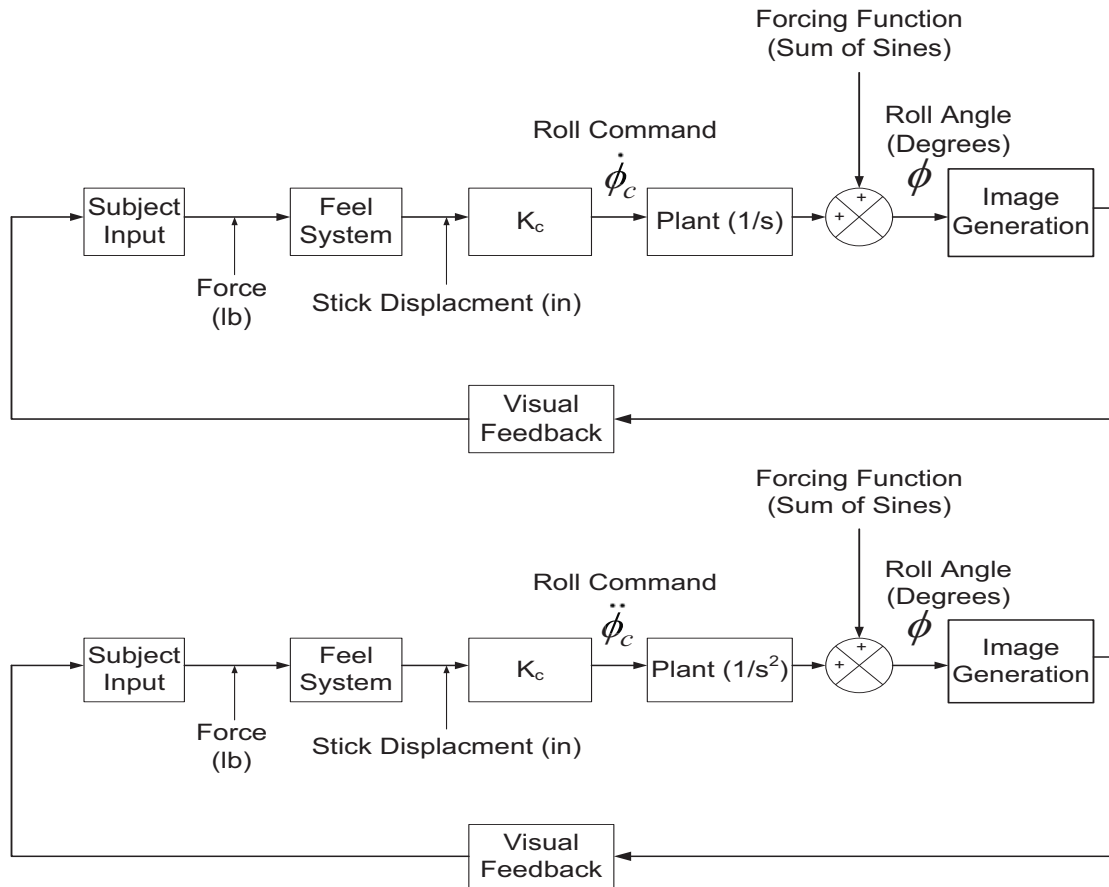


Figure 5.3.1 Quasi Transfer of Training Experimental Configuration

When the experiment starts, the forcing function will disturb a bank angle line located on the display. The test subject will view the disturbed roll angle and apply a command to the control inceptor to return the bank angle back to zero degrees. In the implementation of the experiment code, the feel system parameters are modified through the control loader software within the GFD simulator. The control inceptor deflection is measured in real time and then multiplied by the roll command gain (K_c). For $1/s$ and $1/s^2$ dynamics the roll command gain (K_c) converts the inceptor deflection into a roll rate and roll acceleration respectively. The initial value of the roll command gain (K_c) is set to 40

deg/in•sec and 40 deg/in•sec² for 1/s and 1/s² dynamics respectively. To simulate the plant dynamics of 1/s and 1/s², Euler integration is applied once or twice to the roll plant command respectively. The integration technique produces the commanded roll angle that is summed with the forcing function to produce the output bank angle displayed on an out-the-window display. A general flow chart of the experiment is shown in Appendix F.

For this experiment, a variety of parameters will be measured that will be further analyzed offline. Some of the parameters to be measured include test subject horizontal control inceptor deflection, horizontal control inceptor force, and tracking error. Some of the calculated parameters include the running cumulative average RMS tracking error, the slope of the average RMS tracking error, RMS control inceptor deflection, and PSD of the control inceptor deflection. A list of parameters along with the frequency of measurement is shown in Appendix B. One of the most important parameters is the RMS tracking error, which is used to tell if the test subject has reached a performance asymptote. To calculate the RMS tracking error, the bank angle is recorded. Each data point is squared and summed together then divided by the total number of data points. This is represented in Equation 5.3.1.

$$x_{rms} = \sqrt{\frac{x_1^2 + x_2^2 + x_3^2 + \dots + x_n^2}{n}} \quad \text{Equation 5.3.1}$$

The term (x_{rms}) represents the RMS of any data that is recorded. The symbol “n” represents the total number of data points. The term (x_n) represents each data point recorded at a discrete time interval. To calculate the running cumulative average of the RMS tracking error, Equation 5.3.2 can be used.

$$\bar{x}_{rms}(j) = \frac{(j-1) \cdot \bar{x}_{rms}(j-1) + x_{rms}(j)}{j} \quad \text{Equation 5.3.2}$$

The term j represents the run number. The term $\bar{x}_{rms}(j)$ and $\bar{x}_{rms}(j-1)$ represents the current RMS running cumulative average and the previous RMS running cumulative average respectively. The term $x_{rms}(j)$ represents the current run RMS tracking error. The RMS running cumulative average has to be initialized to the RMS of the first run. The averaging technique in Equation 5.3.1 will take place on the second run, when two RMS data points are obtained. The running cumulative average of the RMS tracking error for the first run is just the RMS tracking error of the first run.

To determine if the RMS running cumulative average has reached an asymptote, the slope between every two runs will be calculated. As the slope between two runs reaches 0.1 for 3 consecutive runs, asymptote has been reached. The formula for the slope between two runs is listed in Equation 5.3.3.

$$\Delta\bar{x}_{rms}(j) = \bar{x}_{rms}(j) - \bar{x}_{rms}(j-1) \quad \text{Equation 5.3.3}$$

The term $\Delta\bar{x}_{rms}(j)$ represents the slope of the running cumulative average RMS between two runs. The terms $\bar{x}_{rms}(j)$ and $\bar{x}_{rms}(j-1)$ represent the current and previous run RMS tracking error respectively.

5.3.3 Display Setup

The display consists of a horizon line and a bank angle reference line that will displace at an angle from the horizon reference line. The image will be displayed on an out-the-window display. A simple example of this is shown in Figure 5.3.2. The

background is black and the horizon reference line is white. The roll reference line is green in color to distinguish from the horizon reference line. To obtain the dimensions of the visual scene, a computation of the viewing dimensions for the test subject at a distance away from the display is conducted. To compute the horizontal viewing dimension H_v , Equation 5.3.4 is applied.

$$H_v = 2 \cdot \tan(\text{HFOV}/2) \cdot D_{EP} \quad \text{Equation 5.3.4}$$

The term HFOV represents the horizontal field of view angle, and D_{EP} equals the distance from the display screen that the eye of the test subject is located. To determine the vertical viewing dimension V_v , the following Equation 5.3.5 is applied.

$$V_v = 2 \cdot \tan(\text{VFOV}/2) \cdot D_{EP} \quad \text{Equation 5.3.5}$$

The term VFOV represents the vertical field of view angle, and D_{EP} again represents the distance from the display screen that the eye of the test subject is located. The length of the horizon reference line should be approximately 80% of the horizontal viewing dimension. The length of the roll reference line should be 80% of the vertical viewing dimension. The dimensions of the target on the display are shown in Figure 5.3.2. These dimensions are calculated using a vertical FOV of 27° , a horizontal FOV of 44° , and an eye point distance from the collimator of 50 inches.

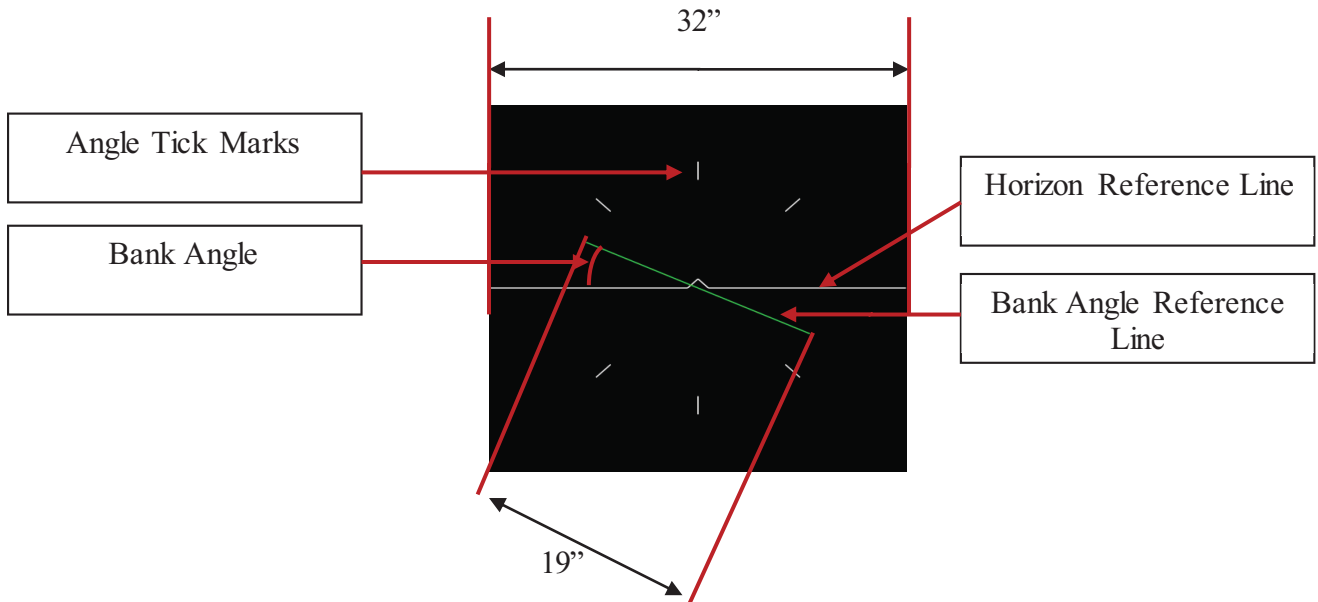


Figure 5.3.2 Out-the-Window Display Setup

5.3.4 Force Feel Parameters Implementation

In Chapter 3, the force feel parameters for the high and low fidelity control inceptors were implemented on the McFadden control loader system that is located within the GFD simulator and verified. The McFadden control loader software allows one to input certain parameters. A list of some of the parameters available for the McFadden control loader is shown in Table 5.3.1.

Parameter Name:	Units:
Inertia	(lbf/in/sec ²)
Minus Stop	inches
Plus Stop	inches
Dead Band	inches
Breakout Level	lbf
Breakout Slope	lbf/inch
Damping	lbf/inch/sec
Friction	lbf
Plus Grad Slope	lbf/inch
Minus Grad Slope	lbf/inch

Table 5.3.1 McFadden Control Loader Parameter Table

A parameter, such as inertia, is considered to be added to the inertia of the system. This parameter does not define the actual inertia of the system. The minus and plus stop are hard stops and limit the motion of the control inceptor to a negative and positive motion range in inches. The dead band creates a portion of the deflection where force feedback is not felt. The breakout level is the force required for the control inceptor to begin deflecting. Corresponding to the breakout level is the breakout slope which is usually set to a high value typically around 100 lb/in so that very little deflection occurs before the breakout force level is met.

The damping parameter is in terms of damping coefficient and not the damping ratio. This should be considered carefully when implementing the characteristics of the control inceptor. The friction parameter gives added friction force to the system. The plus grad slope and minus grad slope refer to the force gradient in lb/in. This allows the user to set the force gradient differently when pushing the control inceptor as opposed to pulling the control inceptor. Also, the McFadden control loader is able to apply different force gradients over different intervals of the deflection of the inceptor. This allows the user to create a nonlinear force gradient. Within this study only a linear force gradient is implemented and is equal in the push and pull directions.

The force feel parameters implemented on the McFadden control loader are shown below in Table 5.3.2. These parameters are shown for the test subject control inceptor which is a sidestick manipulator. The damping ratio that is defined for both the high fidelity and low fidelity control loader was converted to the damping coefficient using Equation 5.3.6. Since there still exists nonlinearities in the system due to Coulomb

friction; the apparent mass of 0.0119 lb•s²/in is used. This apparent mass was determined in Chapter 3.

$$\beta = 2 \cdot m \cdot \zeta \cdot \omega_n \quad \text{Equation 5.3.6}$$

Although the apparent mass is consistent for large deflection of the control inceptor from the neutral position, there exists greater damping when the control inceptor is close to neutral. This is due to a Coulomb friction force. The friction force near neutral causes the system to have a higher damping ratio. The calculated damping coefficient for the high fidelity control inceptor is equal to 0.3 lb•s²/in using the apparent mass. With this implemented damping coefficient, the system exhibited a higher damping ratio in the time response. The damping coefficient was then lowered to obtain a value closer to the defined damping coefficient of 0.7. The low fidelity damping coefficient was not tuned to obtain the exact damping ratio of 0.135. As long as the measured damping ratio is below 0.3, it can be considered a low fidelity control inceptor. The damping coefficient will have to be changed depending on the mass of the control inceptor being used.

The control loader should be tuned so that the time response and frequency response verifies the force gradient, damping ratio, and breakout force proposed in Table 5.3.2. It is very important to verify the control loader characteristics before conducting the quasi transfer of training study.

McFadden Control Loader					
Control Inceptor Fidelity:	Effective Mass (Roll Axis) (lb•s ² /in)	Force Gradient:	Damping Ratio ζ	Damping Coefficient β :	Breakout Force:
High Fidelity	0.0119	4 lb/in	0.7	0.25 lb•s ² /in	1.5 lb
Low Fidelity	0.025	0.7 lb/in	0.135	0.0243 lb•s ² /in	0 lb

Table 5.3.2 Implemented Control Inceptor Characteristics

Chapter 6 - Results and Discussion

6.1 Introduction

The results for the quasi-transfer of training study are presented within this section. Only quantitative results were obtained during the experiments. Subjective results were not recorded because of the inexperience of the test subjects and their ability to rate the control task accurately. First, average tracking error performance for the test subjects is presented. The tracking error was obtained by calculating the root mean square (RMS) tracking error for the duration of each run for each test subject and for both $1/s$ and $1/s^2$ plant dynamics. A cumulative average over the number of runs completed is shown. This removes any small fluctuation in a test subject's tracking error and gives a general trend for the data. Second, power spectral density (PSD) analysis and coherence analysis is presented.

A very important concept when measuring human performance is the workload used to perform each task. To measure the test subject's workload, power spectral density (PSD) analysis was employed. This technique shows the frequencies and power that each test subject uses when performing the task. Generally, a test subject will use more power and operate at a higher frequency when the task workload is greater. The power spectral density (PSD) analysis only gives insight on test subject workload and it does not give us direct insight on the test subject's performance level. This analysis is conducted to evaluate if either group has a higher workload when completing the roll disturbance compensatory tracking task.

The results presented in this section are used to evaluate the differences or similarities between training on a high fidelity or a low fidelity control loader.

6.2 Performance Metrics

Shown in Figure 6.2.1 is the average root mean square (RMS) tracking error for the high fidelity training group for the $1/s$ plant dynamics. The RMS tracking error is obtained by recording the roll angle that is shown on the display at each sampling interval, squaring the data points, dividing by the total number of data points and taking its square root.

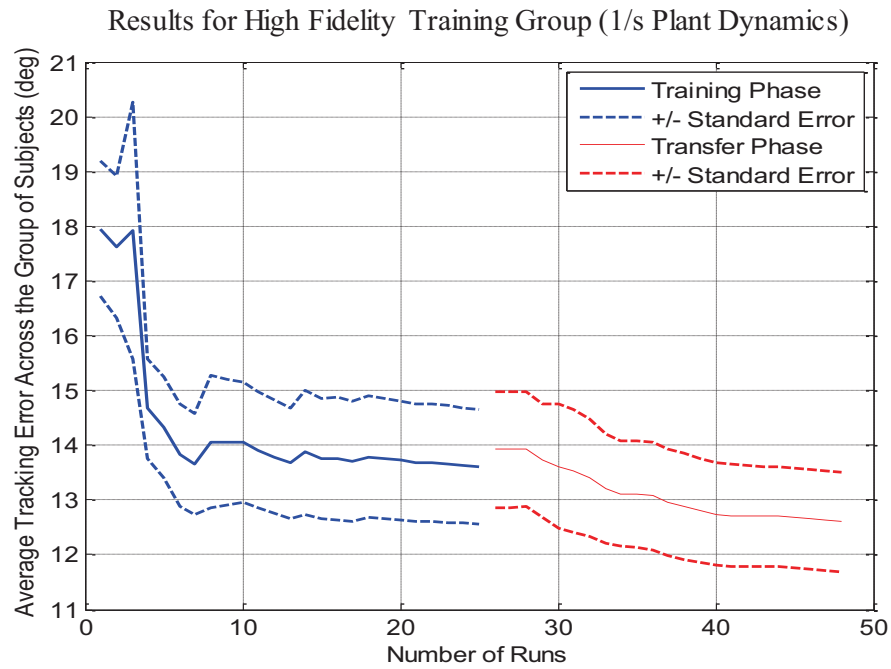


Figure 6.2.1 Average Tracking Error for High Fidelity Training Group ($1/s$ Plant Dynamics)

The subjects reach an asymptotic performance level in the training phase. The asymptotic performance level is determined if the slope of the tracking error reaches a value of 0.01 or less for three consecutive runs. The asymptotic performance level that they reach is equal to 13.61 deg. The improvement rate is equal to 0.1736 degrees per run. The standard error of the tracking error for test subjects is also shown. The standard error is equal to the standard deviation divided by the square root of the sample size. Through both the training phase and transfer phase the spread of data is consistent. When the test

subjects transfer, the tracking error remains close to the average asymptote achieved in the training phase. The difference between the asymptotic tracking error in the training phase and the initial tracking error in the transfer phase is equal to 0.31 degrees. The test subjects continue to improve slightly in the transfer phase with an improvement rate of 0.06 degrees per run. The final average tracking error is 12.6 degrees. The average number of runs to reach asymptote in the training phase is 18 runs. The average number of runs to reach asymptote in the transfer phase is 16 runs.

Shown in Figure 6.2.2 are the tracking error results for the low fidelity training group for 1/s plant dynamics.

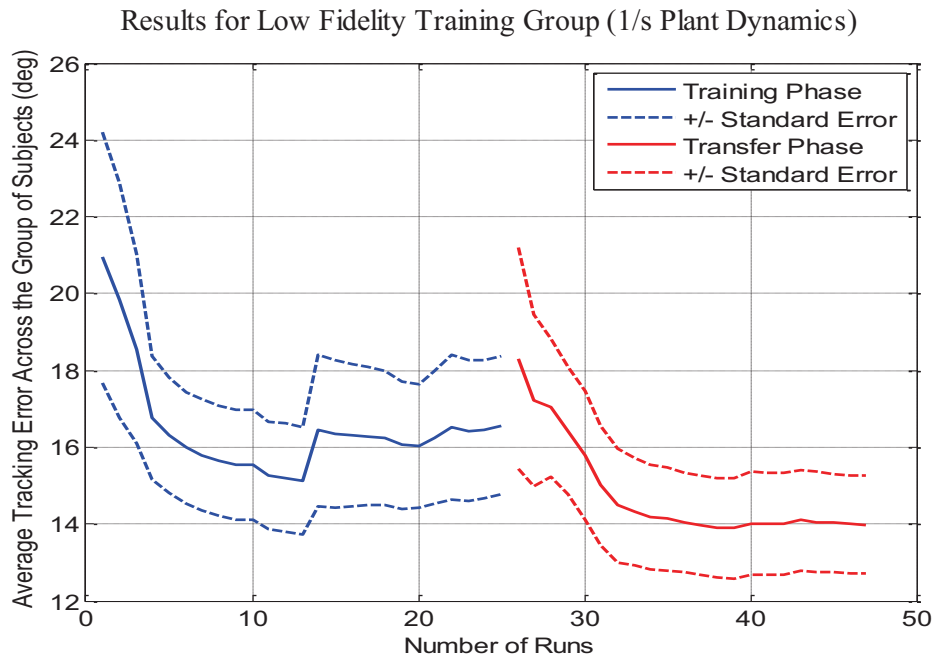


Figure 6.2.2 Average Tracking Error for Low Fidelity Training Group (1/s Plant Dynamics)

The low fidelity training group starts off with an average tracking error of 20.94 degrees. The low fidelity group is able to train to a tracking error of 16.57 degrees. The improvement rate is 0.1748 degrees per run. When this group transferred to the high fidelity control loader simulation, the tracking error initially increased. The difference

between the initial tracking error in the transfer phase and the asymptotic tracking error in the training phase is 1.74 degrees. Although the low fidelity group has an increased initial tracking error when they transfer, they are able to adapt and improve their performance. Their final asymptotic tracking error is 13.99 degrees and the improvement rate for the transfer phase is 0.196 degrees per run. With approximately 13 runs completed, there is a 54% increase in tracking error due to one subject within the group causing the sudden increase in tracking error. The average number of runs to reach asymptotic in the training phase and transfer phase is 20 and 16 runs respectively.

To compare the tracking error performance for both groups, the results are plotted together in Figure 6.2.3. The two best and two worst test subjects were removed from each group consisting of 10 test subjects to obtain a group closer in tracking performance with a smaller variance in data.

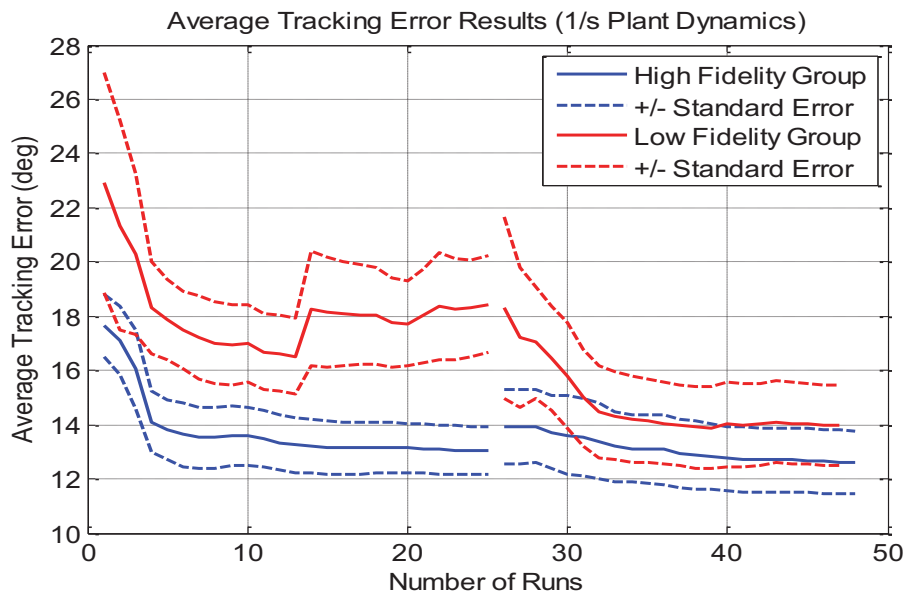


Figure 6.2.3 Average Tracking Error Results for Both Training Groups (1/s Plant Dynamics)

The two groups reach a final tracking error within one standard error of each other. This shows that some of the test subject data for the high fidelity group lies in the vicinity of

the low fidelity group. This usually suggests no significant difference between the final mean tracking errors. A t-test is performed between the groups for each run to determine if the average tracking error for each run is significantly different for each group. Using a confidence level of 95%, the t-value required for a significant difference is equal to 1.812. The t-value for the last run between the high and low fidelity group is equal to 1.54. This suggests that there is not a significant difference between the two test subject groups. In the training phase, the high fidelity and low fidelity group take 18 and 20 runs respectively to train. In the transfer phase, the high fidelity and low fidelity group take 16 runs to train.

The average tracking error results for the high fidelity training group for $1/s^2$ plant dynamics are shown in Figure 6.2.4.

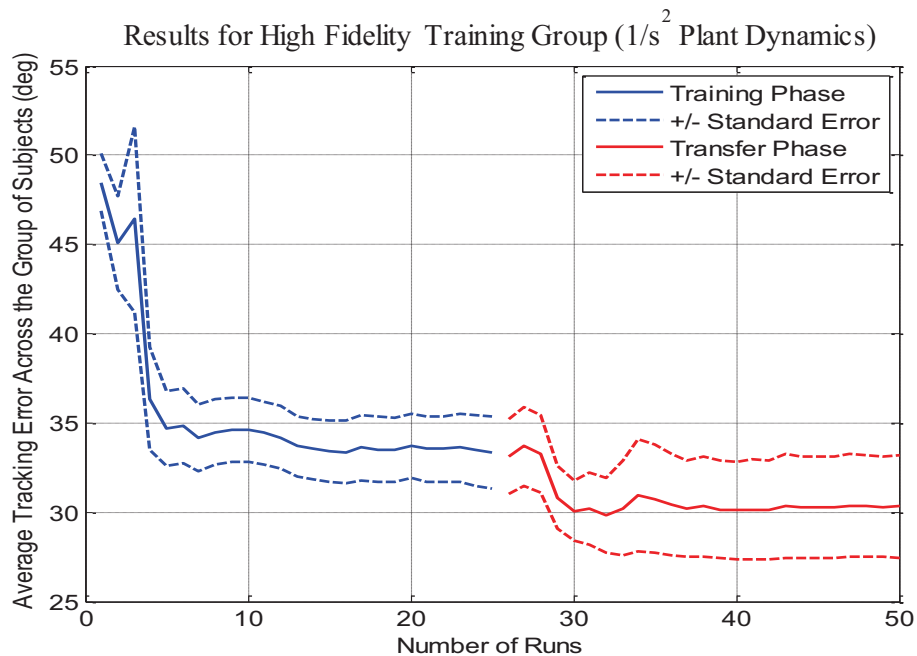


Figure 6.2.4 Average Tracking Error Results for High Fidelity Training Group ($1/s^2$ Plant Dynamics)

The results plotted in Figure 6.2.4 illustrate that the tracking error is greater for $1/s^2$ plant dynamics. The initial average tracking error is 48.49 degrees. The asymptotic tracking error is 33.32 degrees which is equal to an improvement rate of 0.6 degrees per run. The tracking error directly after the high group transfers is equal to 33.11 degrees which is 0.21 degrees different than the asymptotic tracking error in the training phase. In the transfer phase the improvement rate is equal to 0.112 degrees per run. The high fidelity group reaches their final asymptotic tracking error of 30.31 degrees in 40 runs. The average number of runs to reach asymptote in the training and transfer phase is equal to 24 and 22 runs respectively.

The low fidelity tracking error performance is plotted in Figure 6.2.5. The low fidelity group maintains a higher tracking error than the high fidelity group. The low fidelity group started with an average tracking error performance of 62.63 degrees and then trained to an average tracking error of 43.78 degrees. This is an improvement rate of 0.754 degrees per run. As shown for $1/s$ plant dynamics, the low fidelity group again has a sudden increase in their tracking error for $1/s^2$ plant dynamics right when they transfer. They are able to adapt their control and reduce the tracking to a value lower than their asymptotic tracking error in the training phase. The low fidelity training group increased their tracking error to 67.3 degrees when they transferred, which is 4.67 degrees larger than their initial tracking error. The group reaches a final asymptotic tracking error of 39.7 degrees which is an improvement rate of 1.104 degrees per run. The final asymptotic tracking error is 4.11 degrees less than the asymptotic tracking error in the training phase. The average number of runs to reach asymptote in the training and transfer phases is 25 and 23 runs respectively.

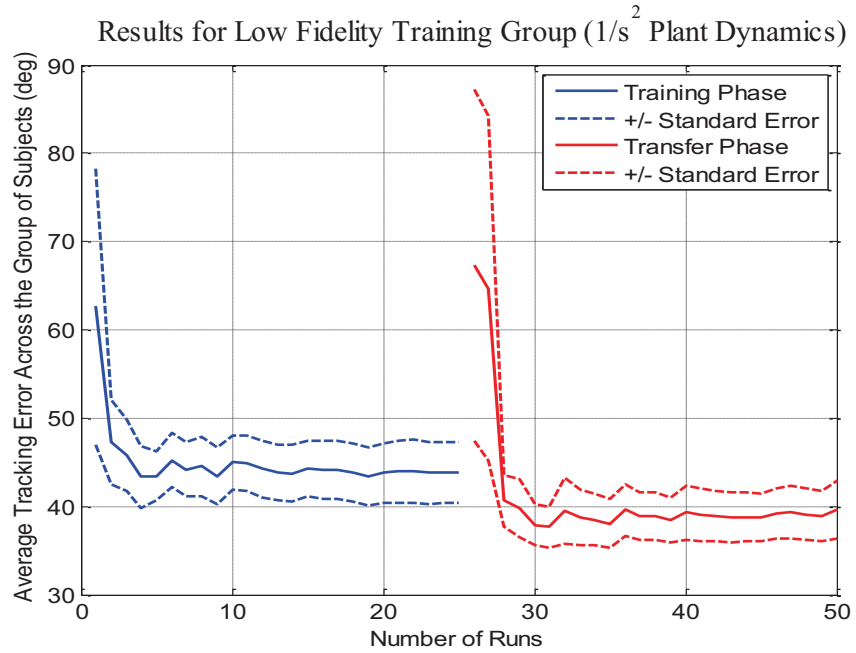


Figure 6.2.5 Average Tracking Error for Low Fidelity Training Group ($1/s^2$ Plant Dynamics)

Figure 6.2.6 compares the high fidelity tracking error to the low fidelity tracking error data. Four test subjects including the two best and two worst were again removed from the population in each group.

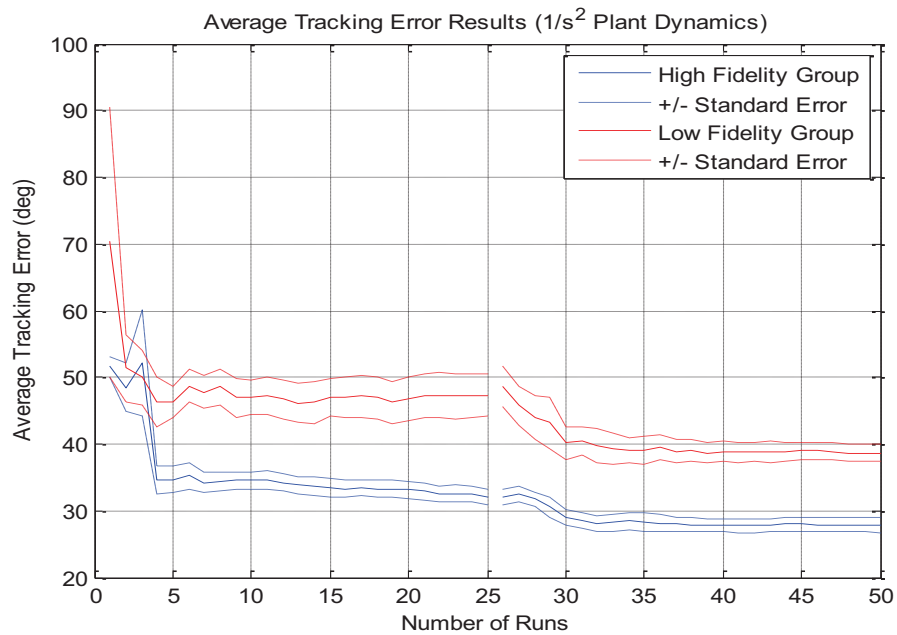


Figure 6.2.6 Average Tracking Error Results for Both Training Groups ($1/s^2$ Plant Dynamics)

A positive standard error for the high fidelity does not overlap the average tracking error for the low fidelity group. To determine if there is a significant difference between the average tracking errors for the high and low fidelity group, a t-test was performed. The two worst test subjects were removed from analysis of the data since they could not maintain adequate performance. These two test subjects obtained a tracking error beyond 180 degrees for more than one run and were not able to reach a tracking error performance asymptote. A t-value above 1.812 using a 95% confidence level suggests a significant difference between the mean of the two groups. A t-value of 2.62 is calculated for the final run of the experiment. This suggests that for $1/s^2$ plant dynamics, there is a significant difference between the final tracking error scores for the high and low fidelity training groups.

Some of the test subjects did not reach a true asymptote and therefore continued to improve their tracking error after transfer. These test subjects were re-tested with experiments consisting of 80 runs and 40 runs in the training and transfer phase. Two test subjects were chosen from each group. Both test subjects did not reach asymptote with one having better tracking error performance. Shown in Figure 6.2.7 is test subject HF001 with $1/s$ plant dynamics.

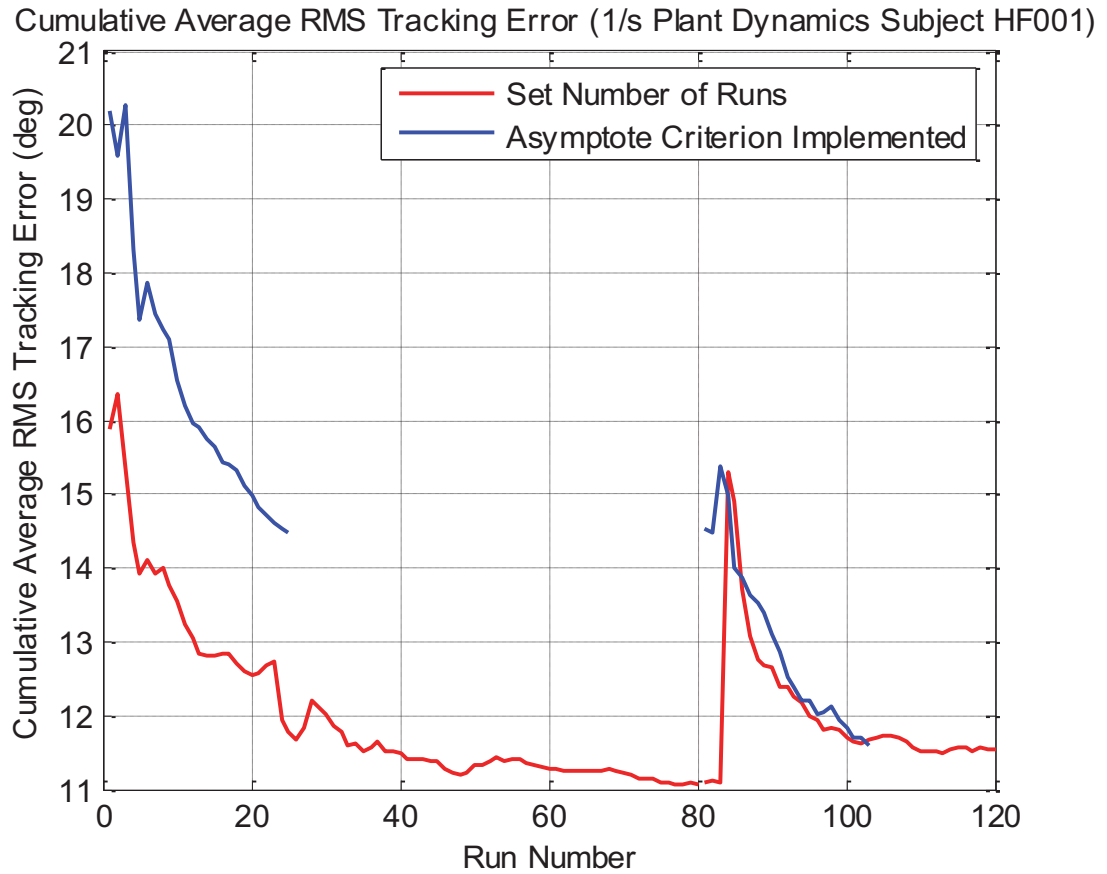


Figure 6.2.7 Average Tracking Error with Greater Amount of Runs (Test Subject HF001 1/s Plant Dynamics)

This plot shows the training data for the original experiments and the new experiments with more runs implemented. As shown, the longer runs allow the test subject to reach a performance asymptote while the original experiments show continued improvement in both the training and transfer phase. The tracking error for test subject LF009 with 1/s plant dynamics is shown in Figure 6.2.8 Average Tracking Error with Greater Amount of Runs (Test Subject LF009 1/s Plant Dynamics)

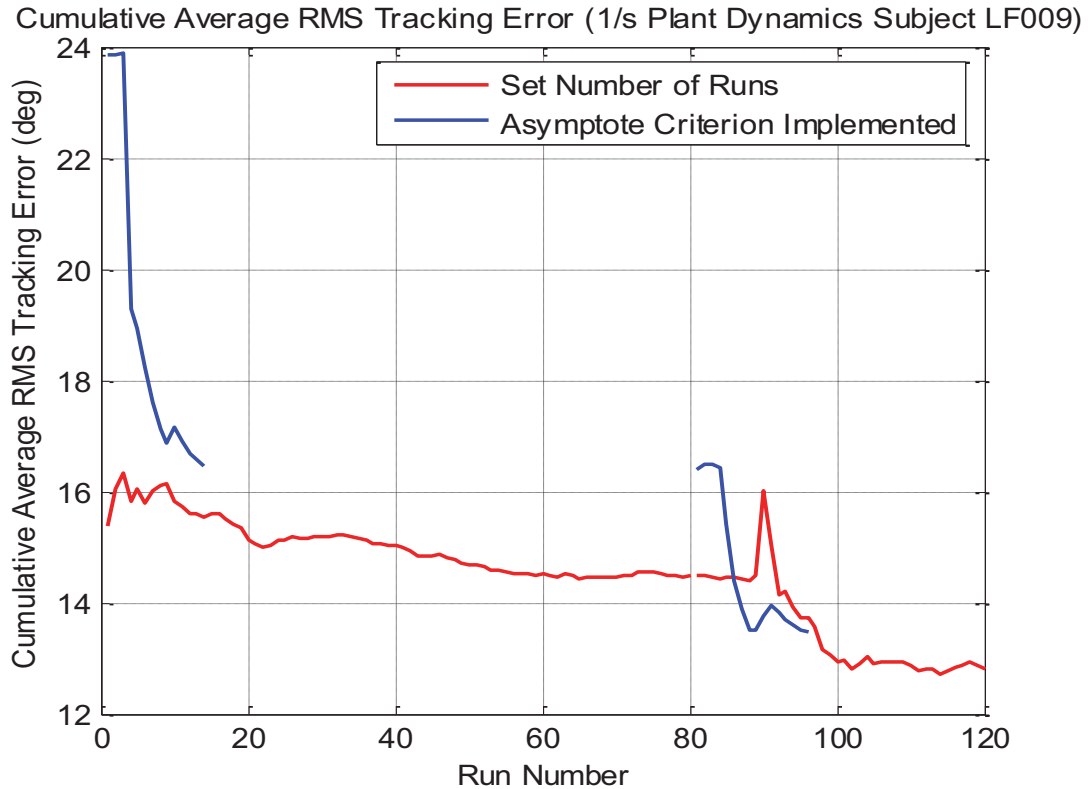


Figure 6.2.8 Average Tracking Error with Greater Amount of Runs (Test Subject LF009 1/s Plant Dynamics)

Test subject LF009 reaches an asymptote when given more runs to train. The other results using a greater number of runs to train are shown in Appendix I.

In conclusion, for the 1/s plant dynamics the high fidelity and low fidelity training groups have a similar final tracking error. The final tracking error of either group is within one standard error of each other. Both groups maintain their tracking performance as they transfer. The low fidelity group shows more improvement than the high fidelity group when they transfer and eventually reach a similar tracking performance. The low fidelity group has an improvement rate of 0.196 degrees per run while the high fidelity group has an improvement rate of 0.06 degrees per run in the transfer phase. The low fidelity group improves more drastically when they transfer suggesting that that the high fidelity control loader allows the test subject to perform better. Table 6.2.1 shows the

average number of runs for each group to reach asymptote. Both groups train within the same number of runs. The performance results for $1/s$ plant dynamics shows that there is no distinct advantage in training on the high fidelity control loader. For $1/s^2$ plant dynamics there is a greater difference in final tracking performance between the two groups. The two groups do not train to the same tracking error performance in the training phase and transfer phase. The tracking error for the two groups is not within one standard error of each other. For more difficult tasks, it is important to train on the high fidelity control loader. There is no significant difference in how many runs each group takes to reach asymptote for $1/s^2$ plant dynamics. Figure 6.2.9 and Figure 6.2.10 show the average tracking error for the first and last run in the training and transfer phase for $1/s$ and $1/s^2$ plant dynamics respectively.

Average Number of Runs to Reach Asymptote Criterion		
Group:	Training:	Transfer:
$1/s$ Plant Dynamics		
High Fidelity	18	16
Low Fidelity	20	16
$1/s^2$ Plant Dynamics		
High Fidelity	24	22
Low Fidelity	25	23

Table 6.2.1 Average Number of Runs to Reach Asymptote

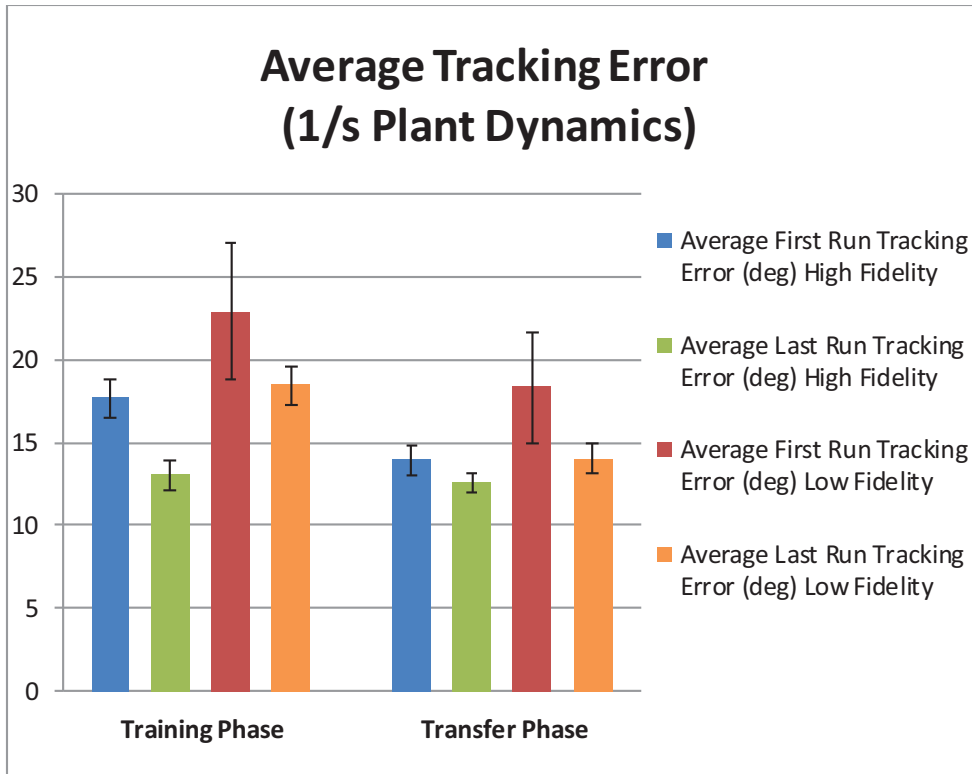


Figure 6.2.9 Average Tracking Error (1/s Plant Dynamics)

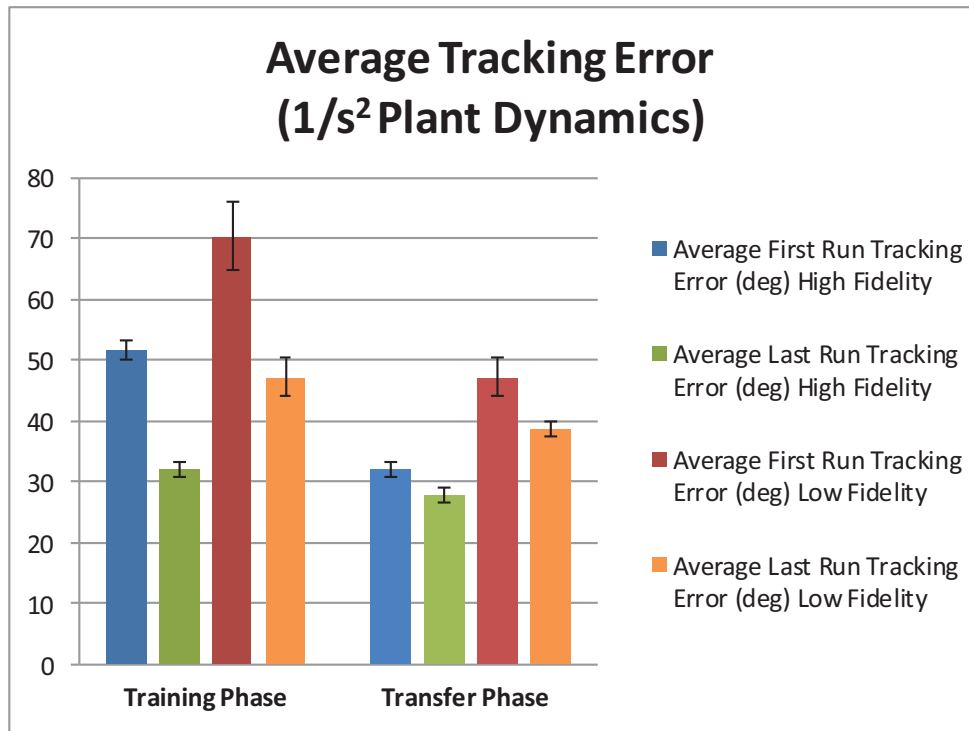


Figure 6.2.10 Average Tracking Error (1/s² Plant Dynamics)

6.3 PSD Analysis

To conduct Power Spectral Density analysis on the test subjects, the control inceptor deflection throughout each run is used. The units of power for the control inceptor deflection are in^2/Hz . To assess if the control inceptor deflection data meets the requirement of stationarity, the variance and mean square were computed for each data set. The recorded data were sampled at 50 Hz and every 4th data point was saved, therefore the effective sampling interval was 0.08 sec or 12.65 Hz. The highest frequency expected in the control inceptor deflection is 3 Hz because the disturbance input does not have frequencies beyond this. The sampling rate satisfies the Nyquist criterion. To improve the PSD, the data were re-sampled to 100 Hz to obtain more data points. When calculating the variance, the data were split into 48 windows consisting of 65 data points for a total of 3120 data points. The variance of the control inceptor deflection for every test subject in the high fidelity and low fidelity groups using 1/s plant dynamics is presented in Figure 6.3.1 and Figure 6.3.2 respectively. The variance does not grow in amplitude as a function of time. A wide sense stationary signal has a constant variance and mean at any time. There is a small fluctuation in the variance from segment to segment. Although the data are not the most stationary data, the portion of the data that had the smallest mean square and variance was chosen when analyzing the PSD to ensure credible frequency analysis. The variance and mean square for 1/s² plant dynamics and the other runs that were analyzed are presented in Appendix G.

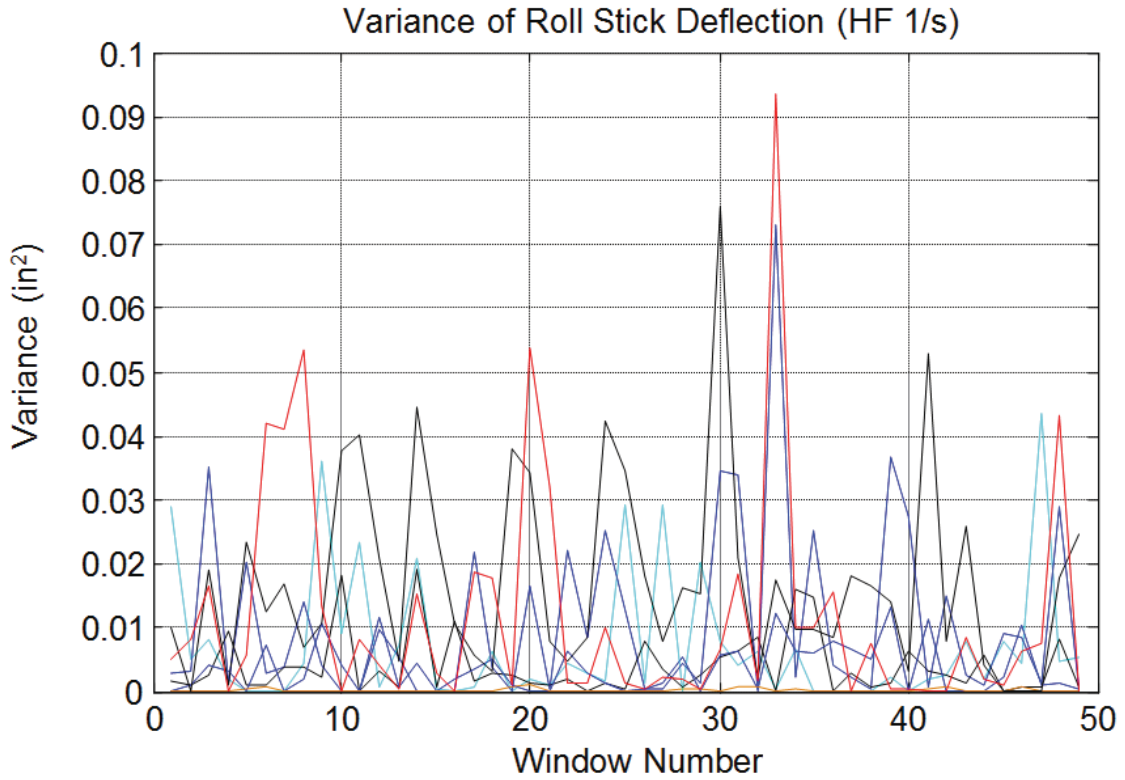


Figure 6.3.1 Variance of Roll Stick Deflection 1st Run (High Fidelity Group 1/s Plant Dynamics)

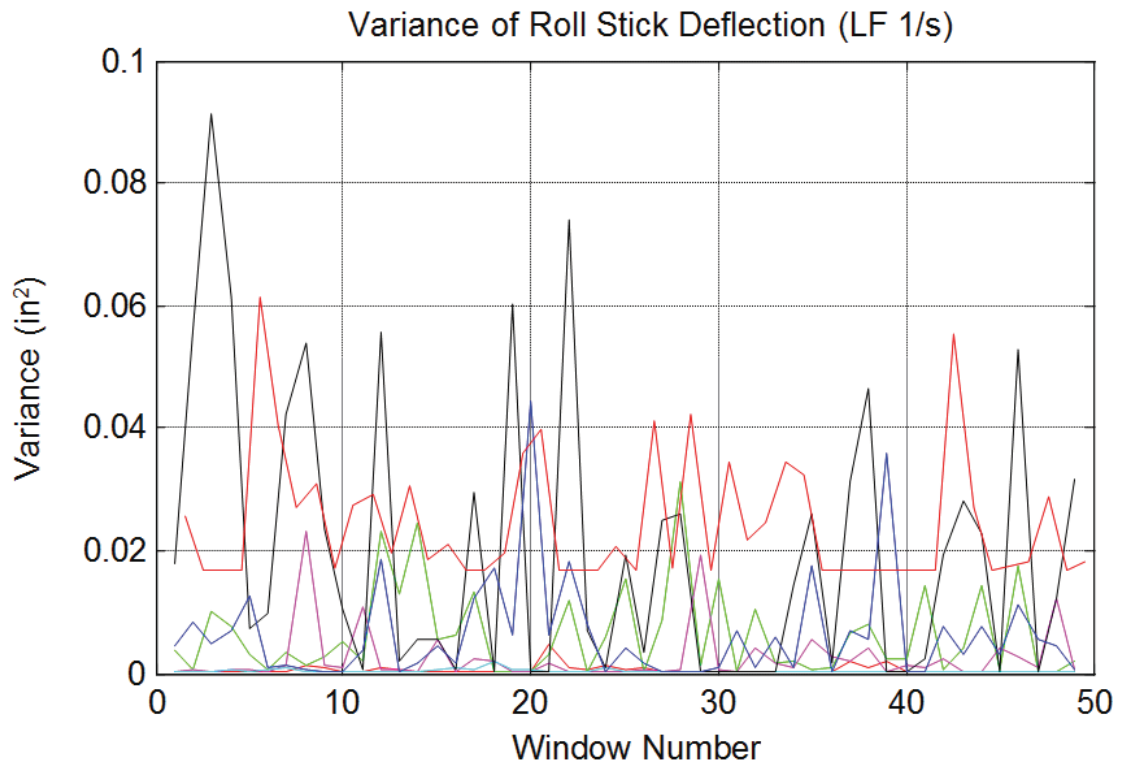


Figure 6.3.2 Variance of Roll Stick Deflection 1st Run (Low Fidelity Group 1/s Plant Dynamics)

Since 20 test subjects were used with multiple runs, only the peak power and peak frequency for each test subject were calculated for the first and last runs in the training and transfer phases. The peak power for 1/s plant dynamics is presented in Figure 6.3.3.

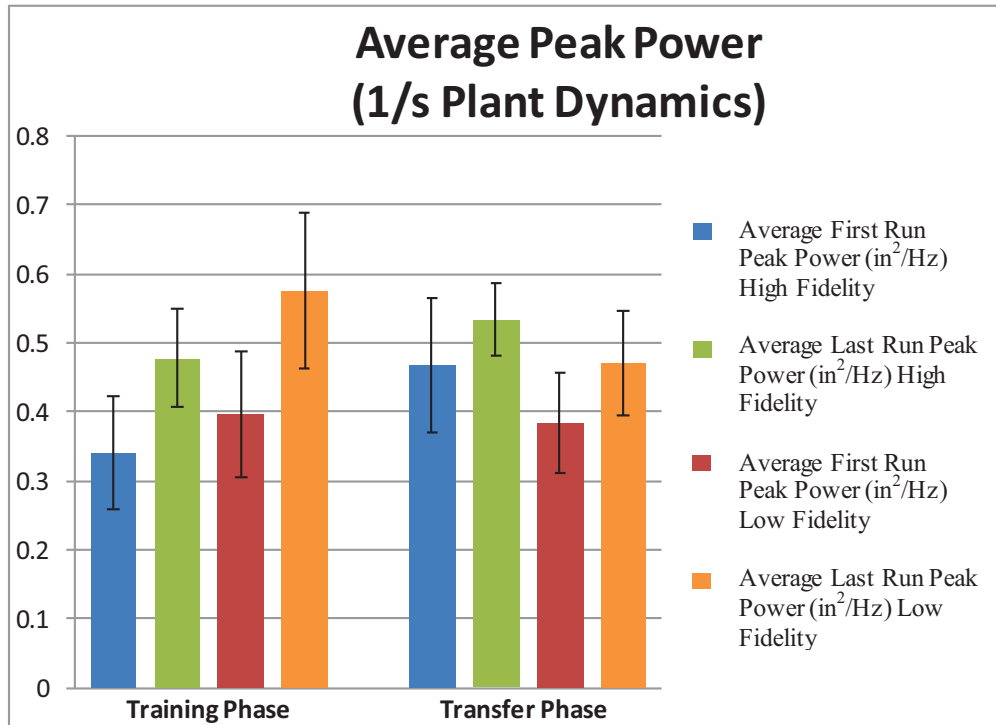


Figure 6.3.3 Average Peak Power (1/s Plant Dynamics)

Shown in Figure 6.3.3 above, there is an overlap in data for the high and low fidelity training group in the training session. There is no significant difference in the power in the training phase. There is an increase in the power from the first to the last run in the training session for both groups. This would suggest that the test subjects increase their workload as they train. This does not necessarily suggest that, because their workload is higher, they will decrease their performance. The task presented to the test subjects could cause the test subjects to become more involved in their control behavior further reducing their tracking error.

In the transfer phase, the low fidelity group has reduced their power while the high fidelity group maintains their peak power. Using a t-test to determine if there is a significant difference in the average power between the two groups, t-values of 0.0844 and 0.939 were calculated for the first and last runs of the transfer phase. Using a 95% confidence level, a t-value above 1.812 suggests a significant difference. Both values suggest there is no significant difference in the power used for either the high or low fidelity group. The reduction in power of the low fidelity group from the last run of the training phase to the first run of the transfer phase suggests that their control inceptor deflection is reduced, that their peak frequency increases, or that both the control inceptor deflection reduces and their peak frequency increases. The low fidelity group adapts and continues to increase their power within the average of the high fidelity group.

The peak frequencies for the high and low fidelity training groups using 1/s plant dynamics are presented in Figure 6.3.4.

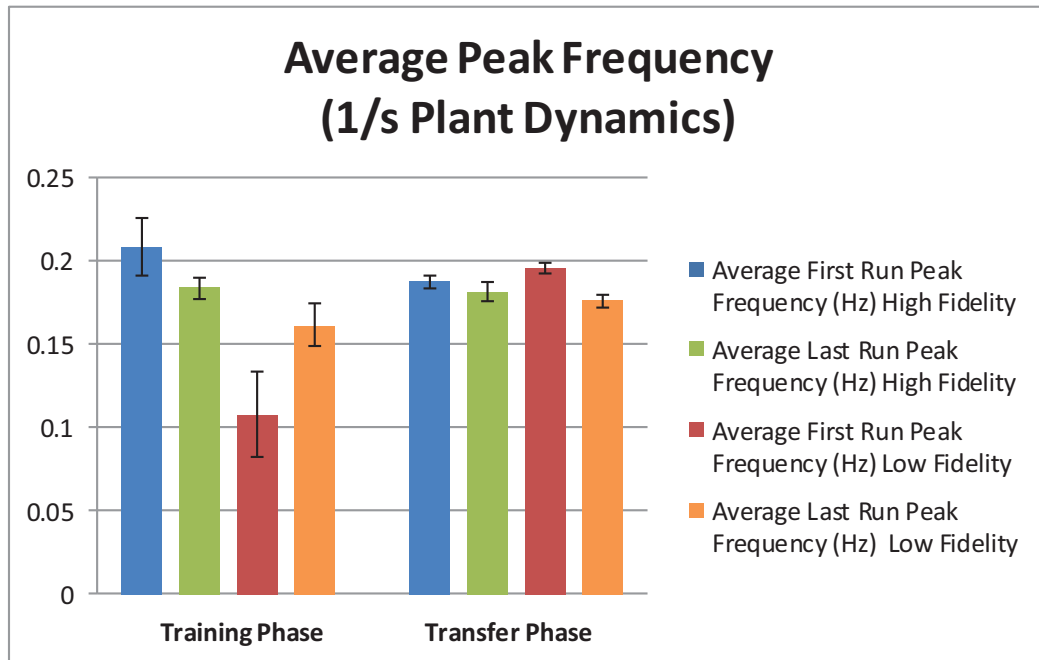


Figure 6.3.4 Average Peak Frequency (1/s Plant Dynamics)

During the training phase, the peak frequency of the low fidelity group is lower than the high fidelity training group. The t-value between the two groups for their first run in the training phase is equal to 2.992, which is greater than the significant t-value of 1.812 suggesting these peak frequencies are different for the two groups. Eventually, after both groups train they reach approximately the same peak frequency between 0.18 and 0.2 Hz. One of the higher amplitude sinusoids in the disturbance has a frequency of 0.1868 Hz. When the high fidelity transfer group transfers they maintain their peak frequency but when the low fidelity group transfers there is an increase in the peak frequency. The t-value between the first run peak frequency in the transfer phase for the high fidelity and low fidelity group is 1.055 suggesting no significant difference. Eventually, the low fidelity group reaches an average peak frequency closer in value to the high fidelity training group around 0.173 Hz.

The peak power for $1/s^2$ plant dynamics is shown in Figure 6.3.5. The peak power used for the test subjects is around 10 times the amount used for $1/s$ plant dynamics. This shows that a higher workload is necessary for this task. The $1/s^2$ plant dynamics is a much harder task since it creates a higher sensitivity and adds delay for the test subjects. When the test subjects apply a control inceptor deflection, it is multiplied by a roll command gain which creates roll acceleration command. The test subjects are trying to control the bank angle with roll acceleration. This gives more sensitivity to control inceptor inputs and also makes it harder to predict the commanded bank angle based on control inceptor deflection input.

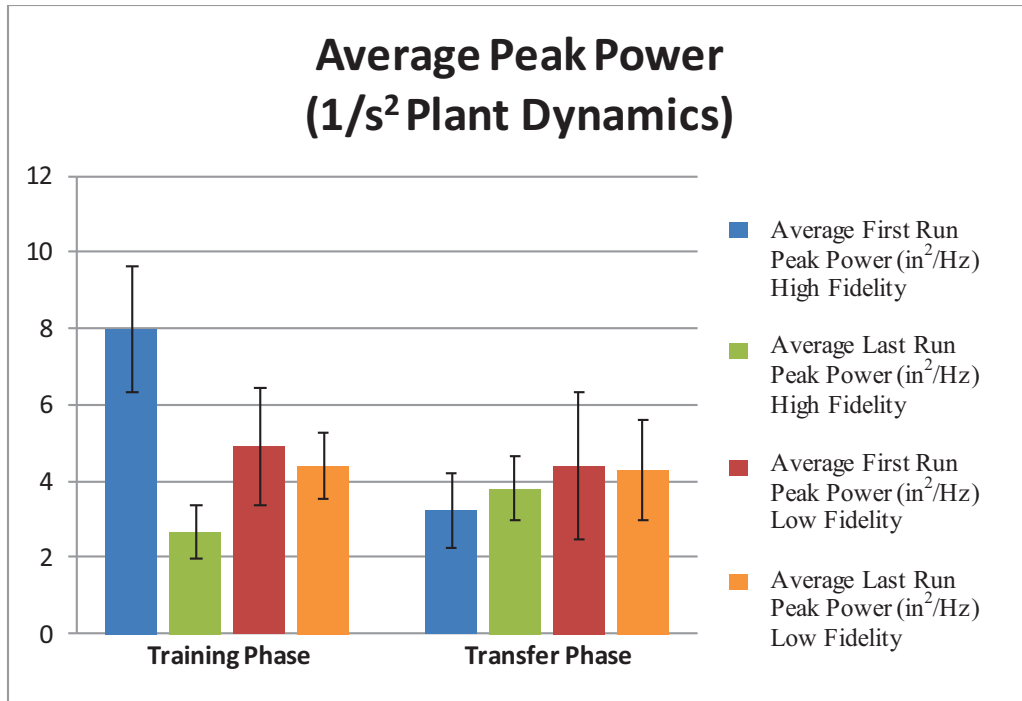


Figure 6.3.5 Average Peak Power (1/s² Plant Dynamics)

For both training groups, the peak power is similar and within one standard error of each other. Generally, the high fidelity group reduces their power from the first run to the last run in the training phase. The transition from training phase to transfer phase is important in determining if training on one control inceptor has a training advantage. The low fidelity group does not drastically increase or reduce their power when they transfer. This is also shown in their tracking error performance in which the two groups tend to maintain their tracking error when they transfer. The power level between groups is not significantly different.

Presented in Figure 6.3.6 is the peak frequency for the 1/s² plant dynamics. The low fidelity group initially has a lower peak frequency than the high fidelity training group. As they train, the low fidelity training group increases their peak frequency. As the high fidelity group transfers, the average peak frequency increases 25%. The majority of high fidelity test subjects increase their peak frequency with one test subject increasing

his/her peak frequency from 0.293 Hz to 0.5615 Hz. The high fidelity test subjects are maintaining a higher peak frequency than the low fidelity group. There is a greater difference in the peak frequency than for 1/s plant dynamics. The peak frequencies and peak power for each test subject is shown in Appendix H.

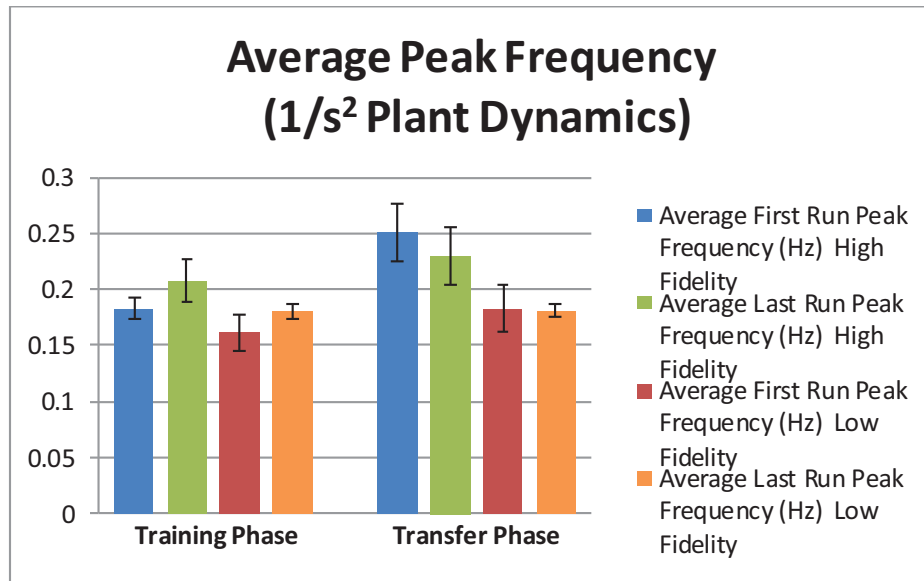


Figure 6.3.6 Average Peak Frequency (1/s² Plant Dynamics)

The average peak power and peak frequency gives us a general sense of where test subjects are using most of their power. The peak power used by most test subjects is between 0.18 and 0.2 Hz. One of the frequencies contained in the disturbance is 0.1862 Hz. The peak power and frequency gives an observation of the test subject's workload at one peak frequency that is not always equal between test subjects. To determine the difference between the two groups, the average Power Spectral Density (PSD) for 1/s is plotted in Figures 6.3.8 through 6.3.10. The PSD is averaged by adding up the power at each frequency and dividing by the total number of test subjects and plotting this against the frequency vector that is common to all test subjects. There is a plot for the last run training phase, the first run transfer phase and last run transfer phase for both 1/s and 1/s²

plant dynamics. As a comparison to the test subject's Power Spectral Density, the PSD of the disturbance forcing function is shown below in Figure 6.3.7.

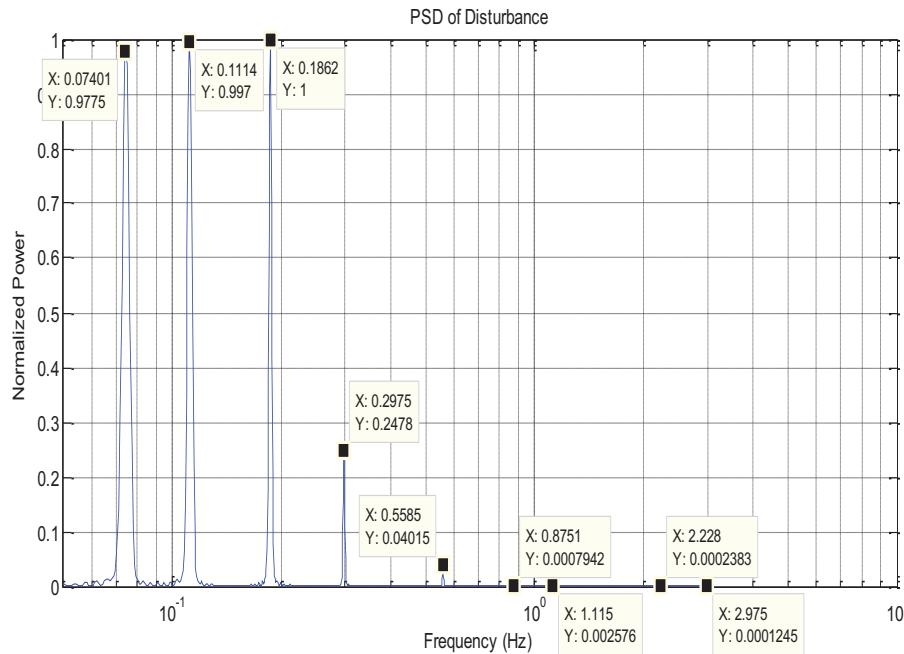


Figure 6.3.7 PSD of Disturbance Forcing Function

The peak frequencies within the PSD of the disturbance correspond with the frequencies of the nine sinusoids used to develop the sum of sinusoids disturbance. The power at higher frequencies is in the vicinity of 10^4 times smaller than the highest power.

The average PSD for the high fidelity and low fidelity training groups in the last run of the training phase is very similar. They have the same peak power around 0.45 in^2/Hz and peak frequency around 0.1953 Hz. The three other peak frequencies include 0.293 Hz, 0.5615 Hz, and 1.11 Hz. These peak frequencies are around the frequencies of the sum of sinusoids disturbance. When the high fidelity training group transfers they maintain a similar peak frequency and peak power in the transfer phase. The low fidelity group reduces their peak power and maintains the same peak frequencies as the high fidelity group. The low fidelity group increases their peak power and maintains a similar

power spectral density as the high fidelity training group in the last run transfer phase. The similarity in peak frequencies and peak powers for both groups suggest very similar control strategy. The similar control strategy results in similar tracking error performance.

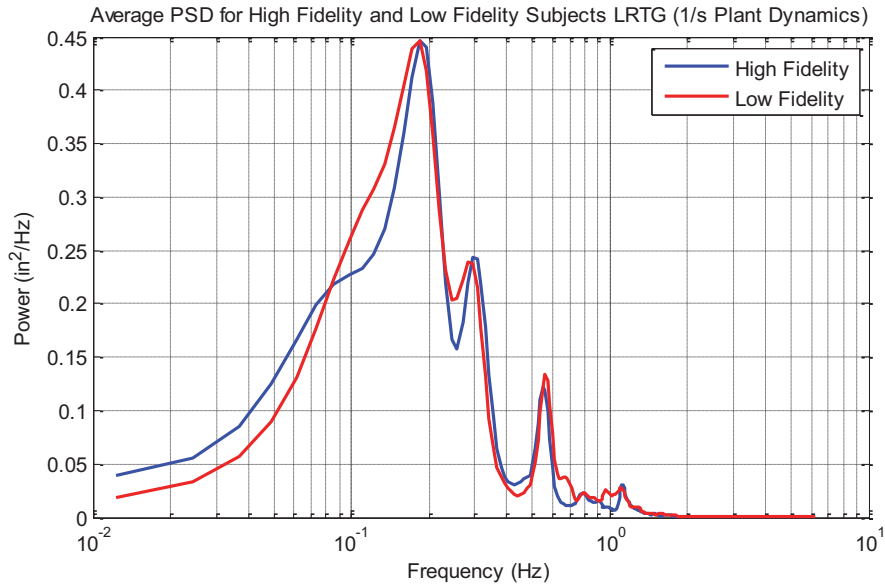


Figure 6.3.8 Average PSD for High Fidelity and Low Fidelity Training Test Subjects Last Run Training (1/s Plant Dynamics)

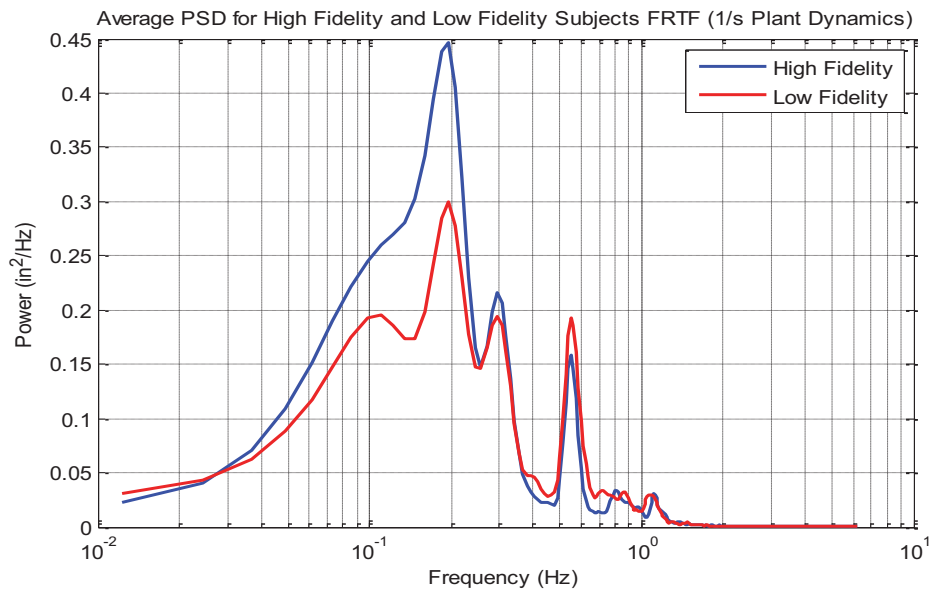


Figure 6.3.9 Average PSD for High Fidelity and Low Fidelity Training Test Subjects First Run Transfer (1/s Plant Dynamics)

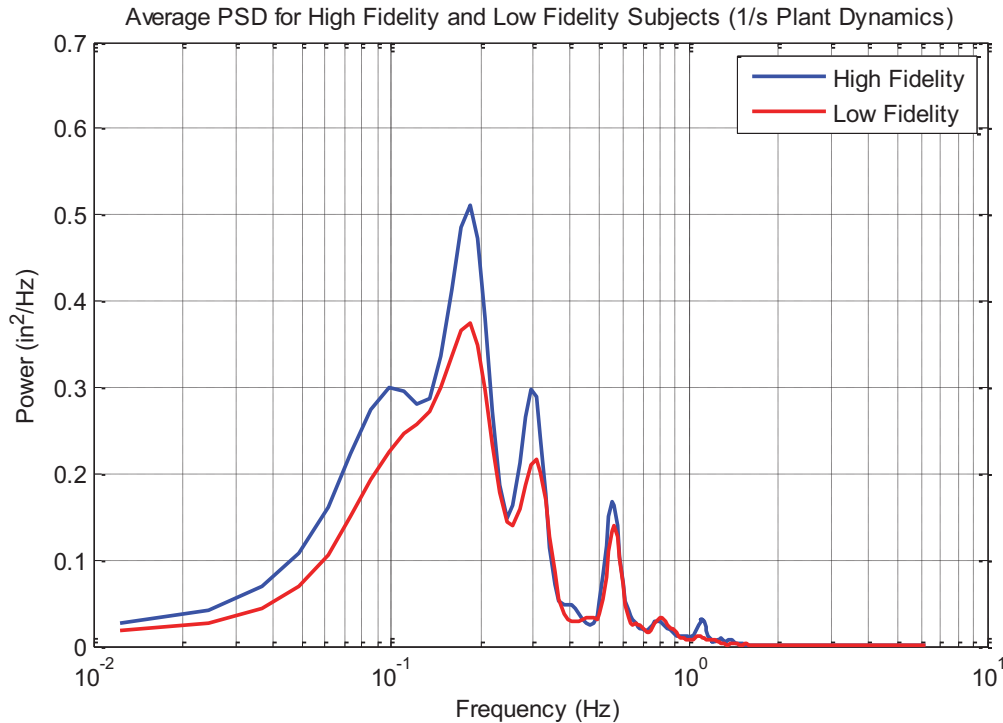


Figure 6.3.10 Average PSD for High Fidelity and Low Fidelity Training Test Subjects Last Run Transfer (1/s Plant Dynamics)

For $1/s^2$ plant dynamics there is a difference in peak power. The average power spectral density (PSD) for $1/s^2$ is plotted in Figures 6.3.11 through 6.3.13. In this case, the low fidelity group maintains a higher peak power and fewer peak frequencies than the high fidelity group. The high fidelity group maintains greater power at the higher frequencies and has less power at frequencies below 0.1 Hz. As both groups transfer they increase their power with the low fidelity group containing a higher peak power. The high fidelity group has increased their power at 0.293 Hz. Still, the high fidelity group is able to operate in more than one frequency and at the higher frequencies. In the final run of the transfer phase, the low fidelity group adapts and operates at the extra frequencies that the high fidelity group initially operated at. The high fidelity group increases their peak frequency while the low fidelity group reduces their peak power adopting a similar control strategy with the same power and frequency peaks. The dissimilar power

spectrum in the training phase gives insight into the significant difference in tracking performance.

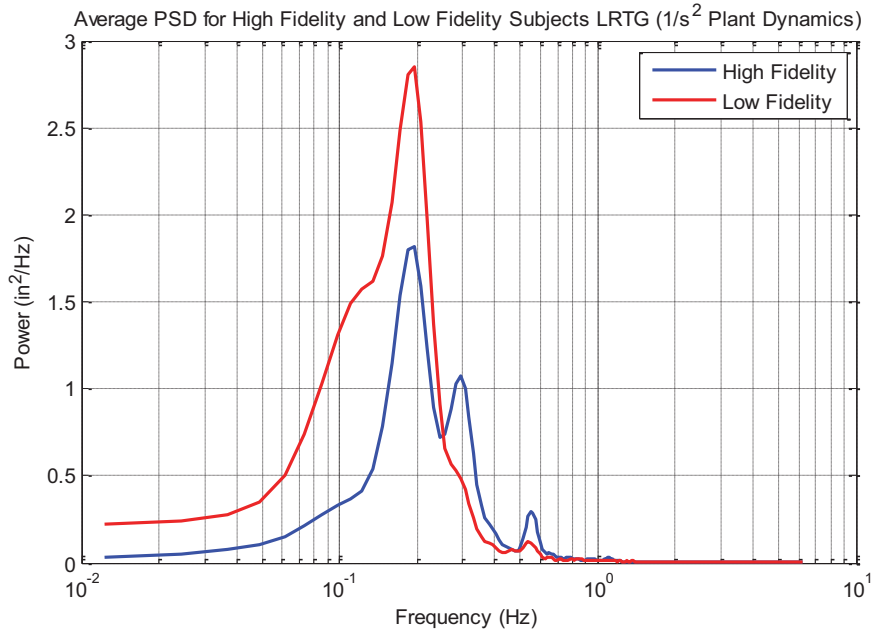


Figure 6.3.11 Average PSD for High Fidelity and Low Fidelity Training Test Subjects Last Run Training ($1/s^2$ Plant Dynamics)

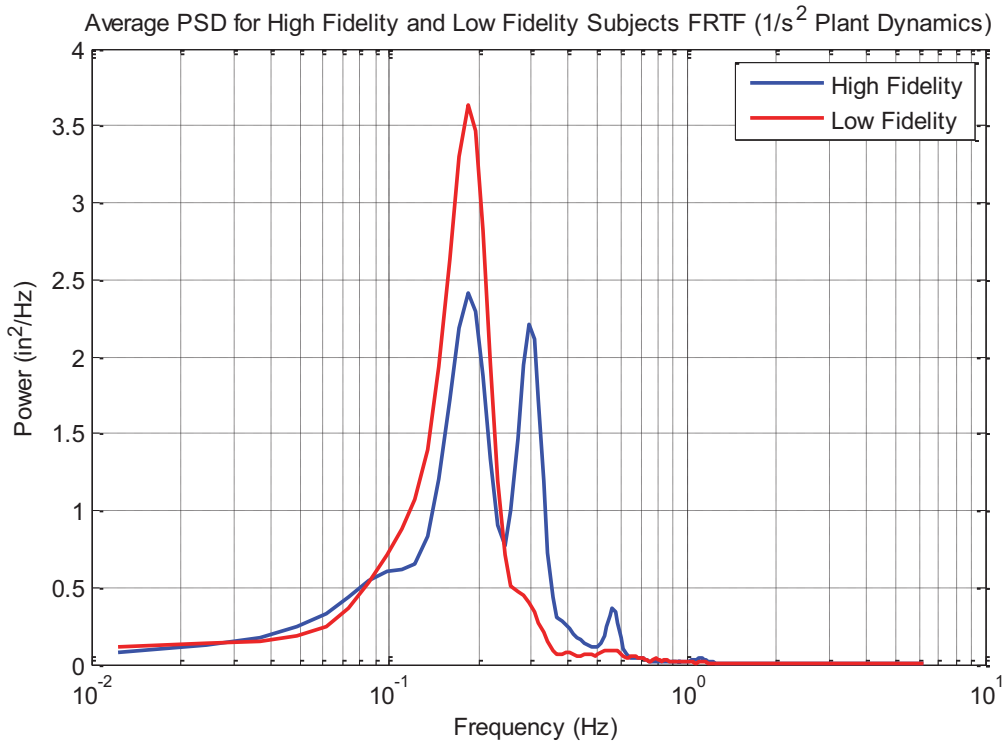


Figure 6.3.12 Average PSD for High Fidelity and Low Fidelity Training Test Subjects First Run Transfer ($1/s^2$ Plant Dynamics)

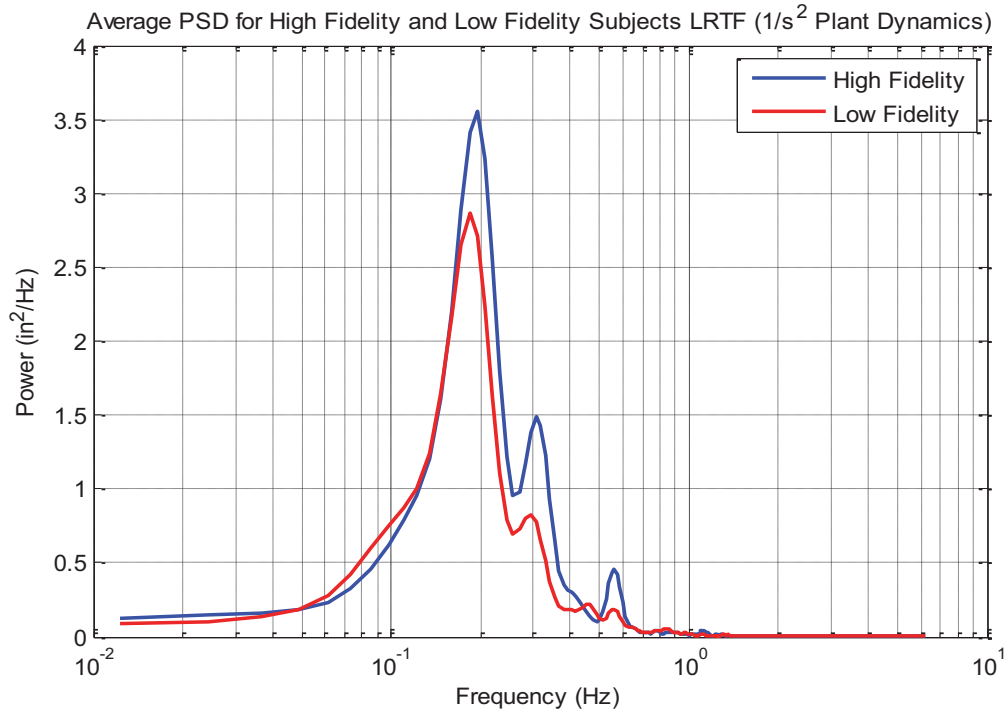


Figure 6.3.13 Average PSD for High Fidelity and Low Fidelity Training Test Subjects Last Run Transfer ($1/s^2$ Plant Dynamics)

To understand how each test subject's power is related to performance, the PSD of the two best and two worst test subjects, based on their tracking error performance, is utilized. Shown in Figure 6.3.14 and Figure 6.3.15 is the PSD for the two worst and two best performing test subjects for the high fidelity and low fidelity group using $1/s$ plant dynamics respectively. Shown in Figure 6.3.16 and Figure 6.3.17 is the PSD for the two worst and two best performing test subjects for the high fidelity and low fidelity group using $1/s^2$ plant dynamics respectively. The test subjects that have the best performance have the two largest power amplitudes and are operating with more power in the upper frequencies. Reduced power at the same frequencies between two test subjects suggests less workload. Less workload does not necessarily indicate that the test subject is performing better. Increased power at the specific peak frequencies implies that the test subjects are using higher control inputs. A higher control input correlated well with the

disturbance gives the test subject greater control authority. A small control input is not enough to null the difference while too much control input overcompensates for the disturbance.

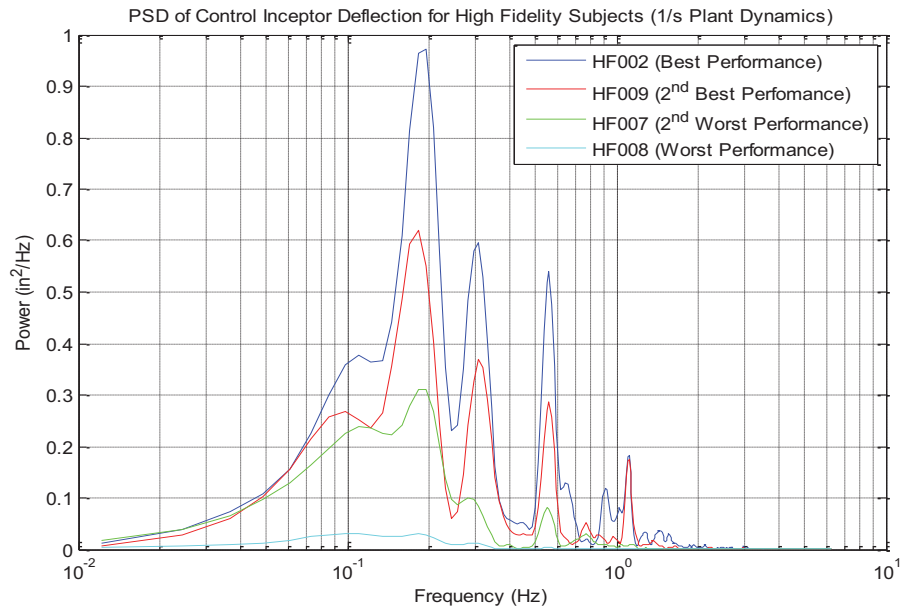


Figure 6.3.14 PSD of Control Inceptor Deflection for Best and Worst Test Subjects (High Fidelity 1/s Plant Dynamics)

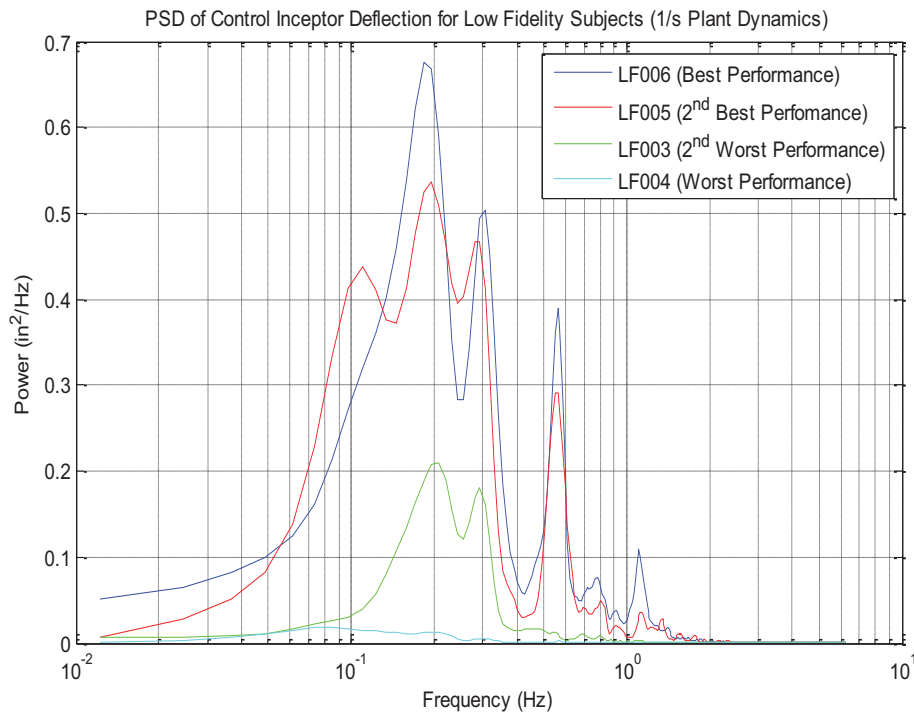


Figure 6.3.15 PSD of Control Inceptor Deflection for Best and Worst Test Subjects (Low Fidelity 1/s Plant Dynamics)

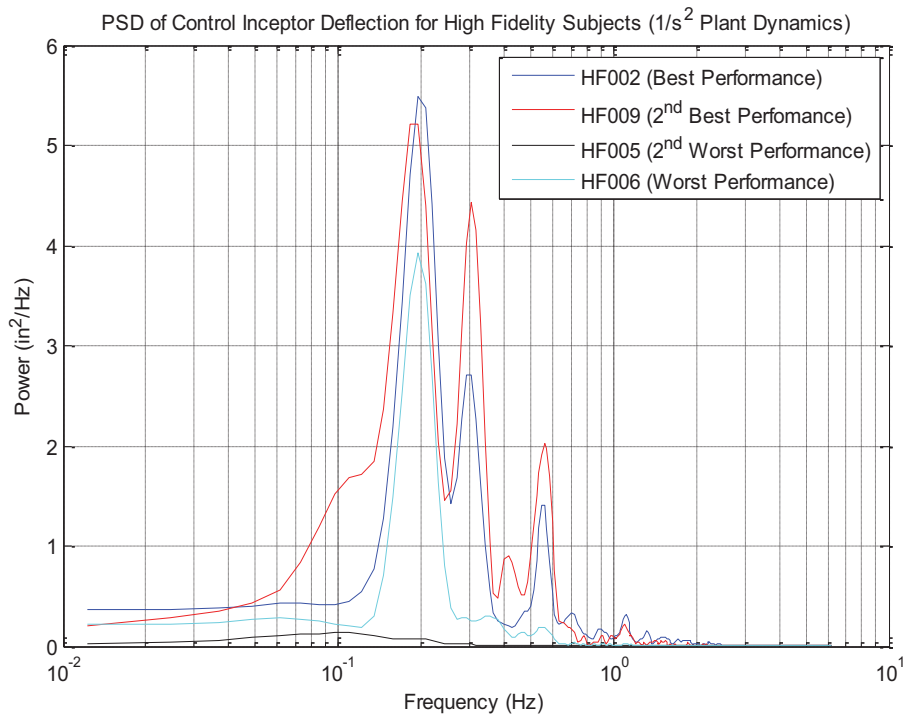


Figure 6.3.16 PSD of Control Inceptor Deflection for Best and Worst Test Subjects (High Fidelity $1/s^2$ Plant Dynamics)

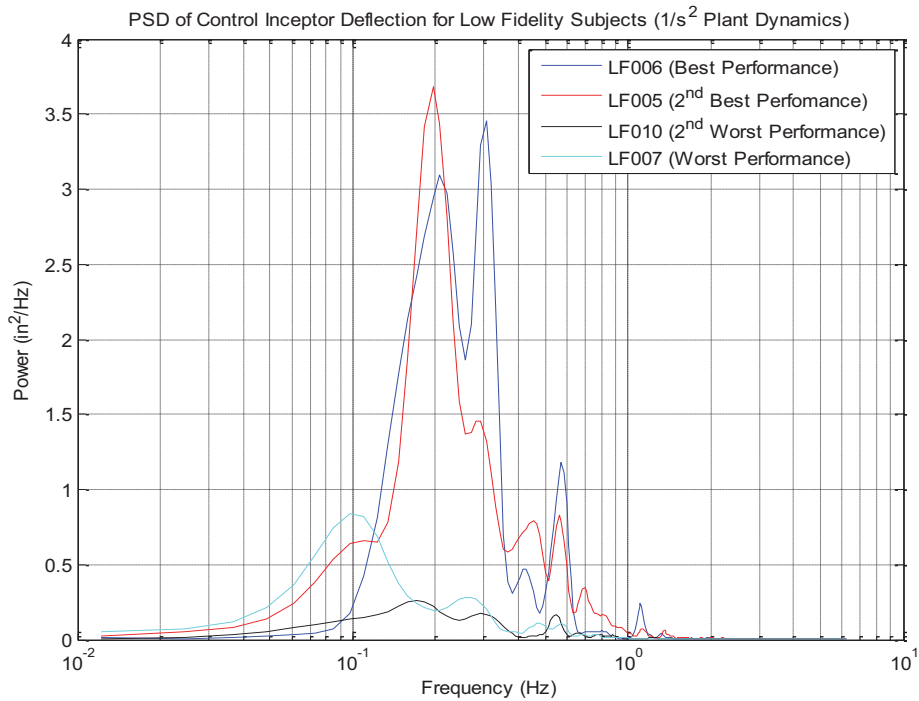


Figure 6.3.17 PSD of Control Inceptor Deflection for Best and Worst Test Subjects (Low Fidelity $1/s^2$ Plant Dynamics)

6.4 Coherence Analysis

The next analysis involves the coherence of each test subject's control inceptor deflection to the disturbance. Coherence analysis shows the correlation between two signals. The two best and two worst test subjects were removed from both the high fidelity and low fidelity training groups. This leaves us with six test subjects in each group. Since it is difficult to interpret the data from all 12 test subjects from both groups at one time, only three test subjects from each group are presented in each coherence figure.

Shown in Figure 6.4.1 is the coherence for test subjects using $1/s$ plant dynamics. The two groups typically have the highest coherence between 0.18 and 0.2 Hz. There is also a peak in the coherence at 0.5371 Hz and 1.123 Hz. These values correspond to the frequencies contained within the disturbance. At the upper frequencies the test subjects are less correlated with the disturbance. There is a lot of noise beyond 1.2 Hz which is due to the sparse frequency information from the disturbance input and control inceptor deflection. This portion is disregarded for analysis.

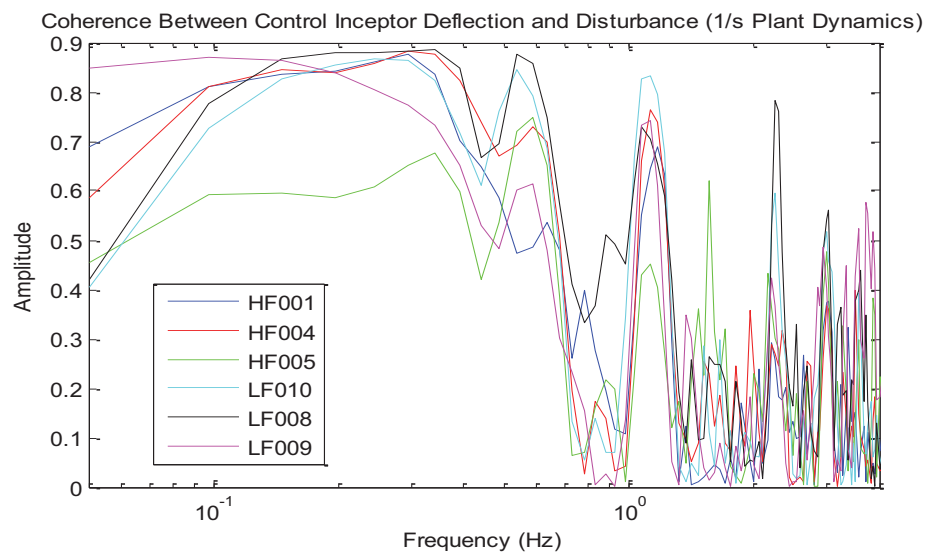


Figure 6.4.1 Coherence between Control Inceptor Deflection and Disturbance Forcing Function (1/s Plant Dynamics)

Shown in Figure 6.4.2 is the coherence for $1/s^2$ plant dynamics. For $1/s^2$ plant dynamics there seems to be less coherence across all frequencies. Also, the test subject's coherence between 0.05 and 0.3 Hz is much lower for $1/s^2$ plant dynamics. The frequencies in this range are very important since most of the power in the disturbance signal is dedicated to the lower frequency range. The lower coherence at the lower frequencies has an adverse effect on the test subject's control strategy. The test subjects tend to adapt to a low frequency high amplitude motion in which most of the test subjects reach the maximum deflection of the control inceptor in both directions. The coherence for $1/s^2$ is much more diversified between test subjects than the coherence for $1/s$ plant dynamics. The harder task causes test subjects to be highly uncorrelated with the disturbance. Test subjects need to be highly correlated with the disturbance across its nine frequencies to perform with a minimum tracking error.

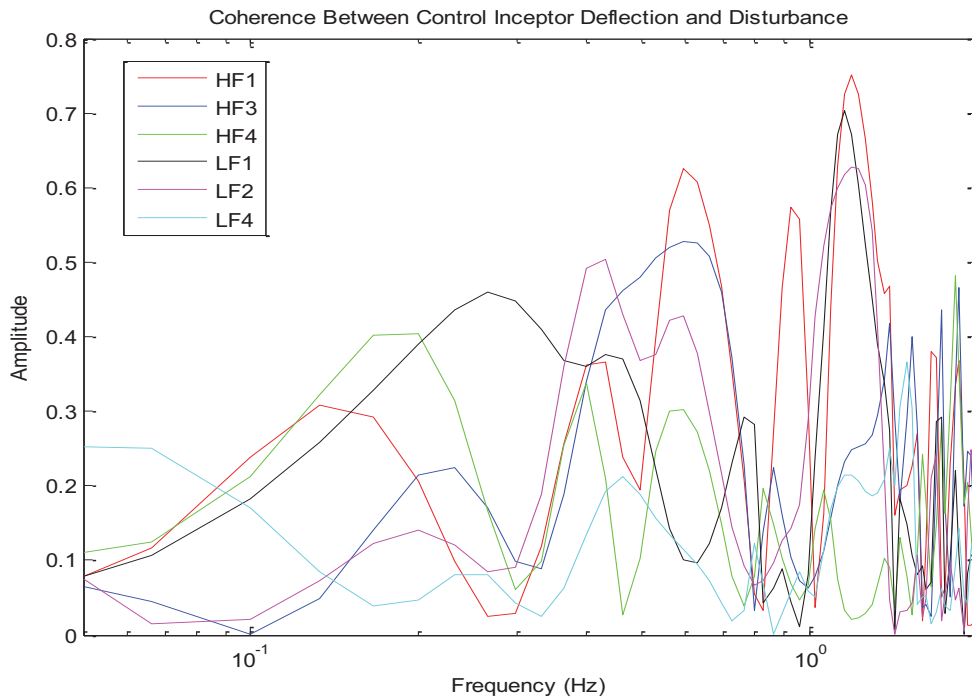


Figure 6.4.2 Coherence between Control Inceptor Deflection and Disturbance Forcing Function ($1/s^2$ Plant Dynamics)

6.5 Frequency Responses of Test Subjects

In pursuing an investigation of human control strategy, the frequency response relating the input roll error as seen by the test subject and the output control inceptor deflection was sought. The frequency response function is related to PSD by means of a Fast Fourier transform (FFT) which is a faster algorithm to calculate the Discrete Fourier transform (DFT). The periodogram method was used to calculate the PSD and is equal to the Discrete Fourier Transform (DFT) of the autocorrelation. Equation 6.5.1 corresponds to the PSD calculation using the periodogram method.

$$PSD = \frac{1}{N} \sum_{m=-M}^M \sum_{i=0}^{N-1-|m|} x[i]x[i+|m|] w[m] e^{-j2\pi \frac{k}{N}n} \quad \text{Equation 6.5.1}$$

To implement this method, the input signal was first zero-padded which is conducted by adding zeros to the end of the signal and making the signal length equal to a power of two. Next, a Hamming window function is applied to the zero-padded signal equal to the length of the signal. Next the autocorrelation is found by obtaining the convolution of the signal with the signal at a different time. The signal vector was flipped making its first value a value at the end of the signal so that the signal is being convolved with future values of itself. The absolute value is taken to calculate the magnitude of the complex number obtained when computing the Discrete Fourier Transform (DFT). The code to obtain the PSD is shown in Appendix J.

The frequency response of a linear system relates the amplitude and phase of the output to the input. There are many ways to measure the frequency response of a system. A frequency sweep, a sum of sinusoids, band-limited white noise, and an impulse can be injected into a system to be measured. Obtaining the frequency response converts the time-domain signal into the frequency domain representation. This is conducted using the

Fourier transform which represents a time domain signal as a sum of sinusoids with different amplitudes, phases and frequencies. When a sinusoid is passed through a linear time invariant (LTI) system, only the amplitude and phase change for the sinusoid. By measuring the difference of the amplitude and phase between the output and input at each frequency, a frequency response can be obtained.

Traditional methods include exciting the system by applying a frequency sweep consisting of sinusoids of different frequencies and constant amplitude to the input. The output response is measured and the amplitudes and phases of each sinusoid at each frequency are individually calculated. New techniques exist which allow the user to excite the system with a frequency sweep, sum of sinusoids, or an impulse and use the quotient of the Fast Fourier Transform (FFT) of the output and the input. The frequency response analysis has been discussed previously in Chapter 4 in Section 4.4. This technique was used to obtain the frequency response of the control inceptor used in the quasi-transfer of training experiment.

To better understand the behavior of the test subjects, the frequency response was attempted for each test subject. However, testing multiple test subjects is time consuming when implementing a frequency sweep. The roll disturbance compensatory experiment was designed with a sum of sinusoids disturbance. The sum of sinusoids method has been used in the past by Johnston and Aponso (1988) [10] to obtain frequency response functions for test subjects. The system to be measured in this case is the human control strategy. The input to the human is the roll error shown on the display and the output used is the control inceptor deflection. The FFT technique shown in Chapter 4, Section 4.4 was employed.

The FFT is an efficient way to compute the Discrete Fourier Transform (DFT) of a signal. The Fourier transform is a way of converting the time domain into the frequency domain. The Fourier transform is similar to the Fourier series. The Fourier series represents any periodic signal as a sum of sinusoids in the complex form $\sum_{k=-\infty}^{\infty} c_k e^{jk\omega_0 t}$.

To estimate the Fourier coefficients c_k , Equation 6.5.2 is used.

$$c_k = \frac{1}{T} \int_{t_0}^{t_0+T} x(t) e^{-jk\omega_0 t} dt \quad \text{Equation 6.5.2}$$

The term c_k is a complex number which represents both the amplitude and phase of a periodic sinusoid. The Fourier coefficients c_k can only be analyzed at a multiple of the periodic signal frequency. The Fourier transform is similar to the Fourier coefficients in that it builds the signal out of a sum of sinusoids of different frequencies. The difference is that the Fourier transform can be used for non-periodic signals. The formula for the Fourier transform is shown in Equation 6.5.3.

$$X(\omega) = \int_{-\infty}^{\infty} x(t) e^{-j\omega t} dt \quad \text{Equation 6.5.3}$$

The Fourier transform has a very similar structure to the Fourier coefficients except that the Fourier transform can be calculated at any frequency of importance when dealing with a signal that is not composed of harmonic frequencies. As shown, the Fourier transform is applied over an infinite time scale. This can only be solved analytically and cannot be analyzed with discrete data points over a finite time signal. The Discrete Time Fourier Transform (DTFT) is used for discrete data sets. The DTFT is shown in Equation 6.5.4.

$$X(\Omega) = \sum_{n=-\infty}^{\infty} x[n]e^{-j\Omega n} \quad \text{Equation 6.5.4}$$

The structure again is very similar to the continuous time Fourier transform shown in Equation 6.5.3 except that it is a summation of discrete data points. Again, this requires an infinite number of data points. To deal with a finite number of data points, the Discrete Fourier Transform (DFT) shown in Equation 6.5.5 is used.

$$X(k) = \sum_{n=0}^{N-1} x[n]e^{-j2\pi kn/N} \quad \text{Equation 6.5.5}$$

The DFT represents the DTFT sampled at integer intervals. By having a limited number of data points, it limits the accuracy of the computed DFT. The number of data points limits the spacing of frequencies that the DFT is calculated at. The frequency interval is limited by Equation 6.5.6.

$$\omega_k = \frac{2\pi kF_s}{N} \quad \text{Equation 6.5.6}$$

This formula shows that the sampling rate and number of data points has an effect of how closely spaced the samples of the DTFT are. Increasing the number of points without increasing the sampling frequency can be done two ways. The length of the signal collected has to be sufficiently long for a specific sampling rate to get more frequency points. The higher the sampling rate, the longer the signal has to be to produce a finer DFT frequency vector. Increasing the sampling rate of a data set that is time-limited, does not improve the number of frequency points for the DFT. One way to increase the number of points is to run the signal for a longer time period. The problem with this is

that it can only be done when collecting data. If you already have data for a certain time period, the method of zero-padding can improve the DFT calculation.

Since the data collected from each test subject was run for only 30 seconds, the method of zero-padding was used. To also remove the effect of spectral leakage a Hamming window function was applied to each signal. To show the effect of zero-padding and lengthening the time signal, the single sided amplitude spectrum of the sum of sines disturbance is plotted in Figure 6.5.1.

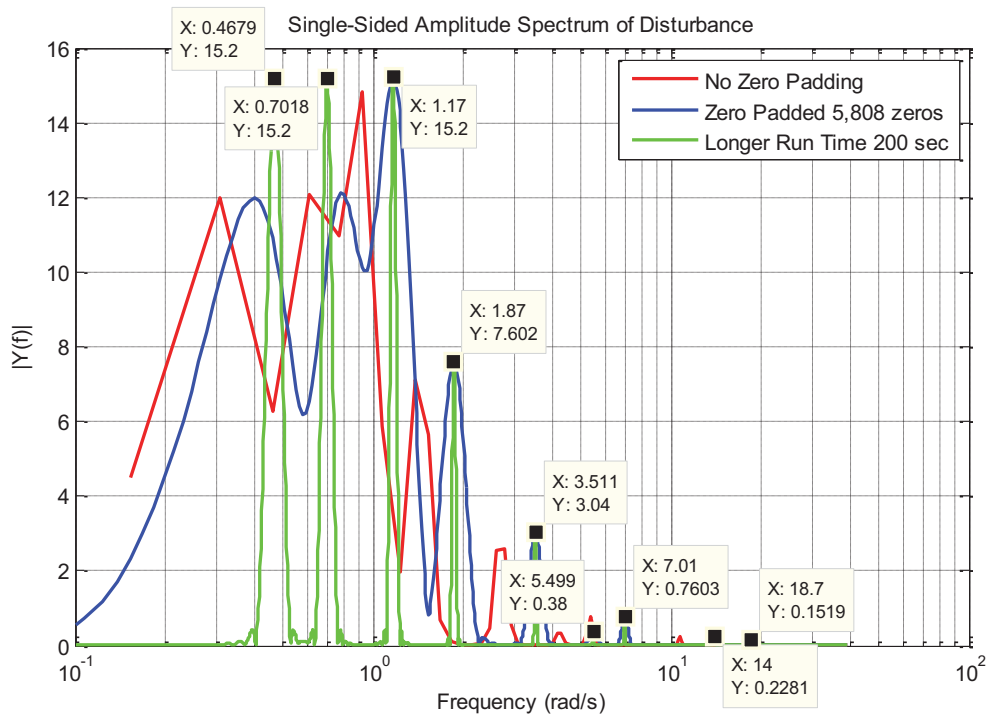


Figure 6.5.1 Single Sided Amplitude Spectrum of Disturbance

The corresponding amplitudes and frequencies of the sinusoids present in the disturbance are shown in Table 6.5.1.

Sine Wave	1	2	3	4	5	6	7	8	9
Frequency (ω_i rad/s)	0.467	0.701	1.17	1.87	3.51	7.01	11/2	14	18.7
Amplitude (A_i)	15.2	15.2	15.2	7.6	3.04	0.76	0.38	0.228	0.152

Table 6.5.1 Disturbance Sum of Sinusoids Parameters

The FFT of the disturbance signal with a 31.28 second length and a 12.5 Hz sampling rate does not correspond well with the frequencies contained in the disturbance. Zero-padding the signal improves the location of the peaks. The zero-padded signal still does not match the amplitudes and frequencies of the sum of sinusoids accurately. Increasing the length of the signal from 31.28 seconds to 200 seconds has the best improvement. When zero-padding, the added zeros create a higher frequency resolution, but do not add any more information to the DFT. By collecting longer data samples, it is adding more information to process the DFT. The only thing that can be concluded is that for the sample data that was taken in the experiments; zero-padding and the use of a window function other than a rectangular window can improve the DFT calculation. The frequency response results with zero-padding and windowing are shown in Figure 6.5.2.

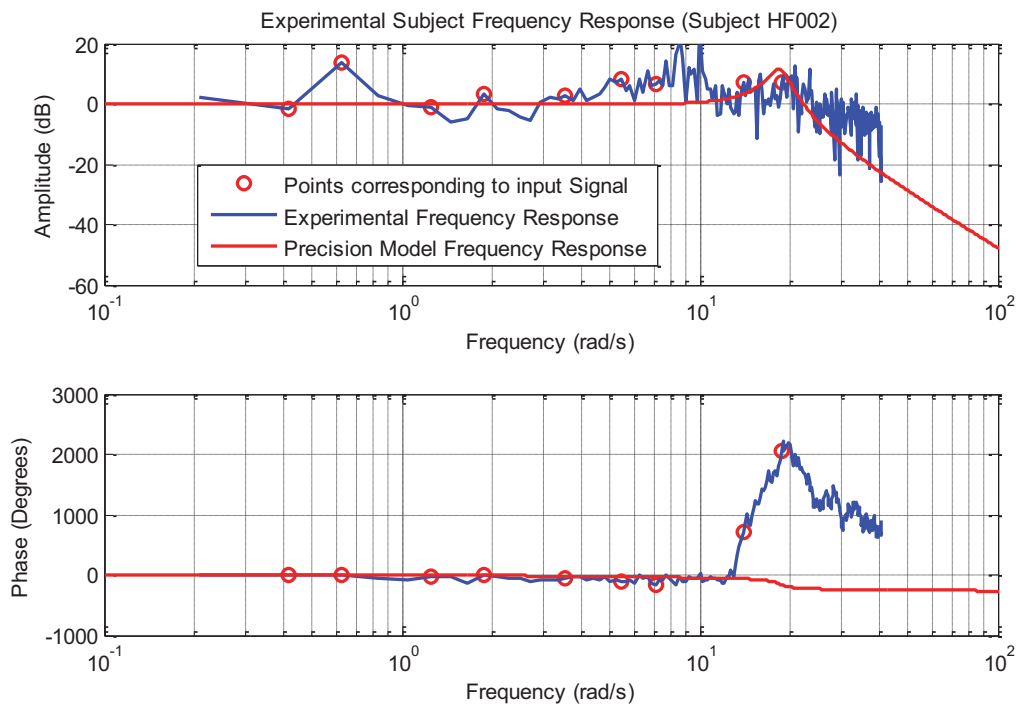


Figure 6.5.2 Test Subject HF002 Experimental Frequency Response

In this plot, the frequency response of the test subject along with a precision model adopted from Magdaleno & McRuer (1986) [11] are plotted. The precision model used is shown in Equation 6.5.7.

$$Y_p = \frac{4082.328}{(s+11.8)(s^2 + 2(.138)(18.6)s + (18.6)^2)} \quad \text{Equation 6.5.7}$$

The response does not correspond well with the precision subject model. Also the phase representation diverges at above 10 rad/s. The frequency response was going to be used to determine bandwidth, crossover frequency, gain margin, and phase margin calculations. From this frequency response the bandwidth cannot be clearly determined. This response represents only one run completed by test subject HF002. To improve the frequency response, four runs at the end of training were combined and the frequency response was averaged across the four runs. The response is shown in Figure 6.5.3.

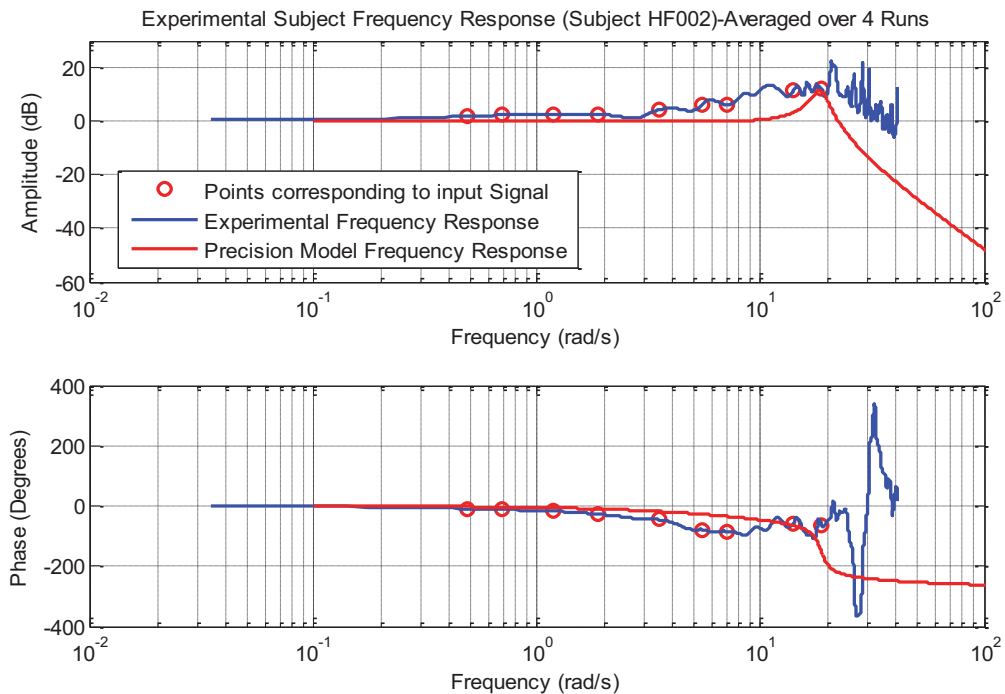


Figure 6.5.3 Test Subject HF002 Experimental Frequency Response Averaged Over Four Runs

In this figure, there seems to be a better frequency response but it is limited by the number of input frequencies that stimulated the system. Above 18.7 rad/s, the highest frequency in the input disturbance, there is noise and the phase is not reliable. Looking at the coherence (Figure 6.5.4 & Figure 6.5.5) between the input signal represented by the roll error and the output control inceptor deflection, the coherence drops off drastically after 10 rad/s. Because the coherence between signals is small after 10 rad/s, our frequency response will be unreliable above this frequency.

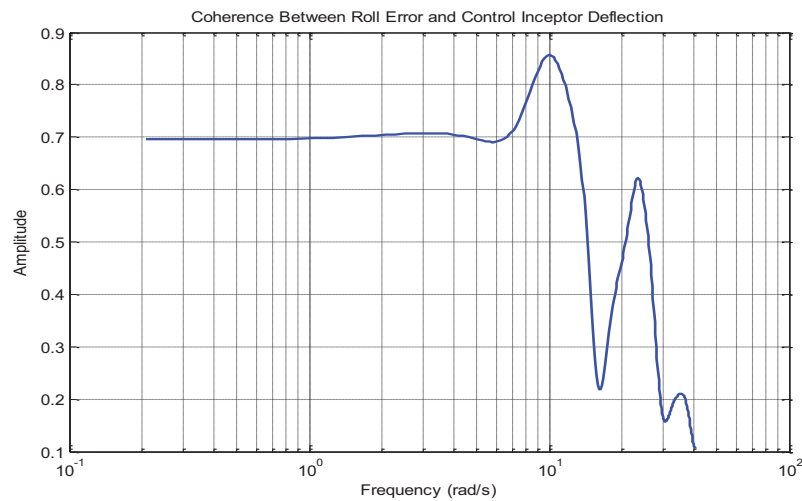


Figure 6.5.4 Coherence Between Roll Error and Control Inceptor Deflection for One Run (Test Subject HF002)

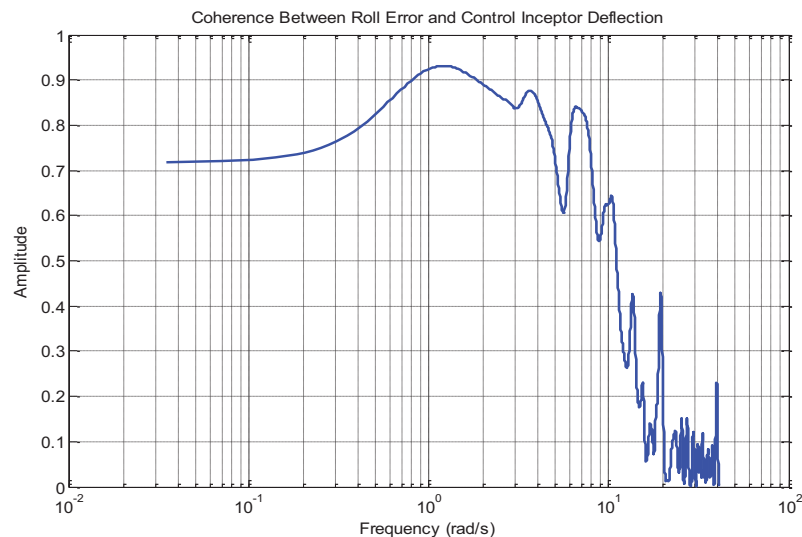


Figure 6.5.5 Coherence Between Roll Error and Control Inceptor Deflection Average over Four Runs (Test Subject HF002)

To test the frequency response method using a sum of sinusoids input disturbance function on a linear time invariant (LTI) system, the disturbance was passed through a second order transfer function in Matlab [21]. The second order transfer used is shown in Equation 6.5.8. The frequency response was found using the Matlab [21] program in Appendix D.

$$H(s) = \frac{(6)^2}{s^2 + 2(0.135)(6)s + (6)^2} \quad \text{Equation 6.5.8}$$

Shown in Figure 6.5.6 is the frequency response with input disturbance as defined by Table 6.5.1. This was the disturbance used within the compensatory tracking task. The frequency response is only reliable at the points corresponding to the frequencies in the input disturbance signal. These points are represented by circles on the plot. This is because the frequency response is a comparison of output amplitude and phase to input amplitude and phase. For a linear system, the experimenter will only have outputs at the same frequency as the input signal. If output information exists at different frequencies than the input, the experimenter has a non-linear system, and frequency response methods are unreliable.

The same frequency response with more frequency points included in the input disturbance signal is shown in Figure 6.5.7. Also, the frequency was extended up to 25 rad/s. As shown, the points corresponding to the input frequencies line up better with the true frequency response. After 25 rad/s, no comparison can be made between the output and input, so the results are not consistent with the true response. This behavior is shown in the experimental response, where the lack of frequency points causes unwanted noisy behavior between successive frequency points. This shows how increasing the number of

frequencies and extending the frequency to a higher frequency in the input disturbance can improve results.

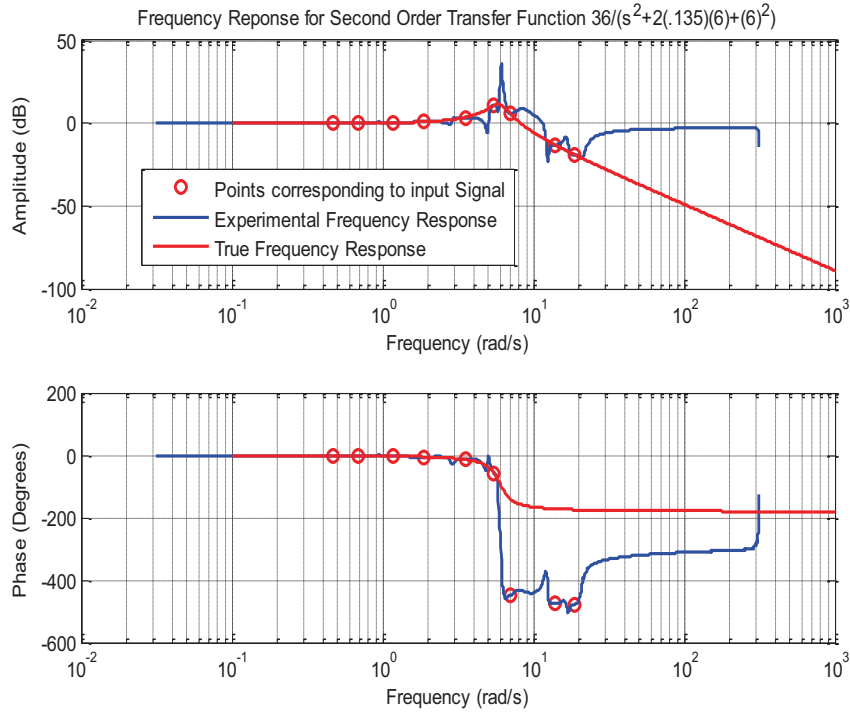


Figure 6.5.6 Frequency Response for LTI System (Original Disturbance Forcing Function)

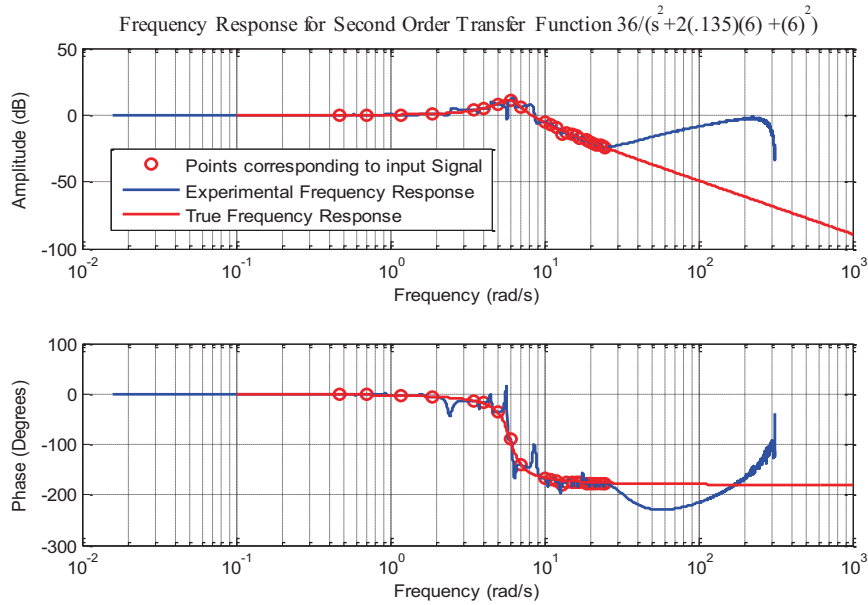


Figure 6.5.7 Frequency Response for LTI System (Finer Frequency Vector Input)

The frequency response (Figure 6.5.8) using a chirp signal with closely spaced frequencies was input into the transfer function. The response matches the true response very well. The input forcing function presented to the test subjects needs higher frequencies and finer spaced frequencies. Since a sum of sinusoids is presented to the test subject, including higher frequencies may cause the test subject to have a more difficult time responding with the same frequency motion.

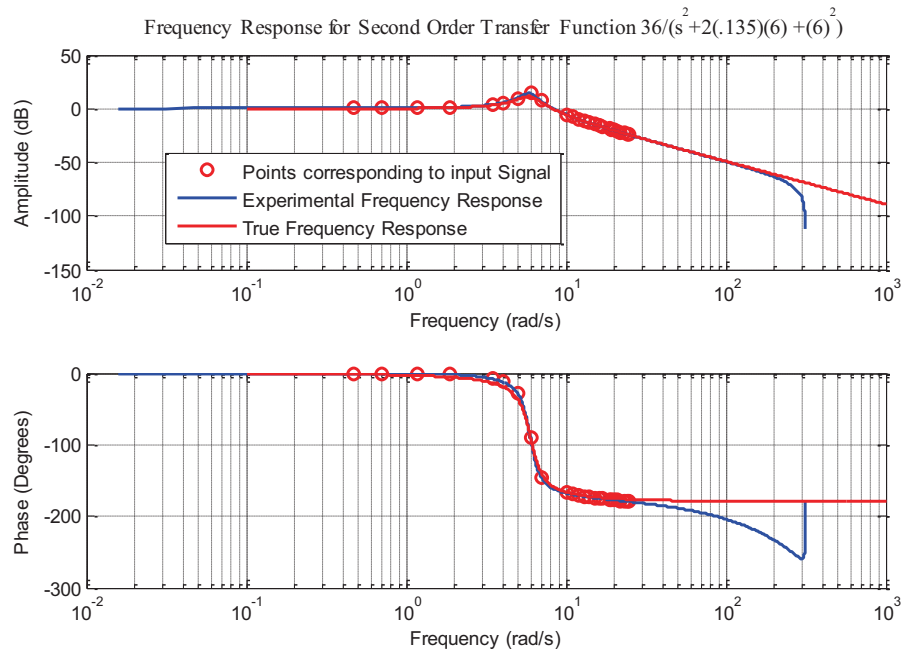


Figure 6.5.8 Frequency Response for LTI System (Chirp Input Signal)

In conclusion, the frequency response results were not sufficient to accurately determine bandwidth and other control strategy differences between test subjects. To get a better frequency response function for each test subject, the input forcing function has to be investigated. The forcing function as is has to include more in-between frequencies and the amplitude for each frequency has to be set accordingly so test subjects are able to respond to those frequencies. Longer runs of 2 to 4 minutes will also aid in better FFT

results. The sampling rate should also be increased to at least 100 Hz when recording data.

6.6 Remnant

Remnant is defined as the portion of the operator's output that is not related to the system input. The remnant is the result of the non-linear behavior of the test subjects. This gives rise to the quasi-linear model of the human. The describing function is represented by the linear correlated input and output of the test subject. The remnant describes the remaining non-linear behavior of the test subject. Shown in Figure 6.6.1 and Figure 6.6.2 are the PSDs of test subject HF002 and test subject HF005.

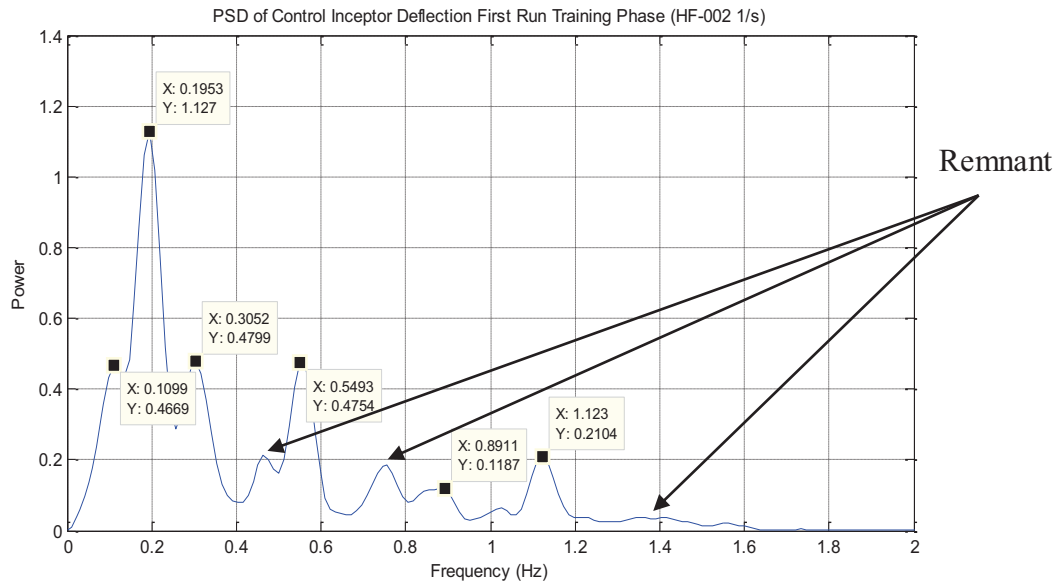


Figure 6.6.1 PSD of Control Inceptor Deflection for Test Subject HF002

Examples of remnants are labeled in these figures. The points labeled in this figure are the frequencies that are near the frequencies of the input disturbance. These frequencies are very close to the disturbance input frequencies but not the exact frequencies. From test subject to test subject, the peak powers occur near the disturbance input frequencies. The power not corresponding to the spikes in the power spectral density is considered the

remnant. Most of the test subjects do not contain a significant remnant suggesting they maintain a mostly linear behavior.

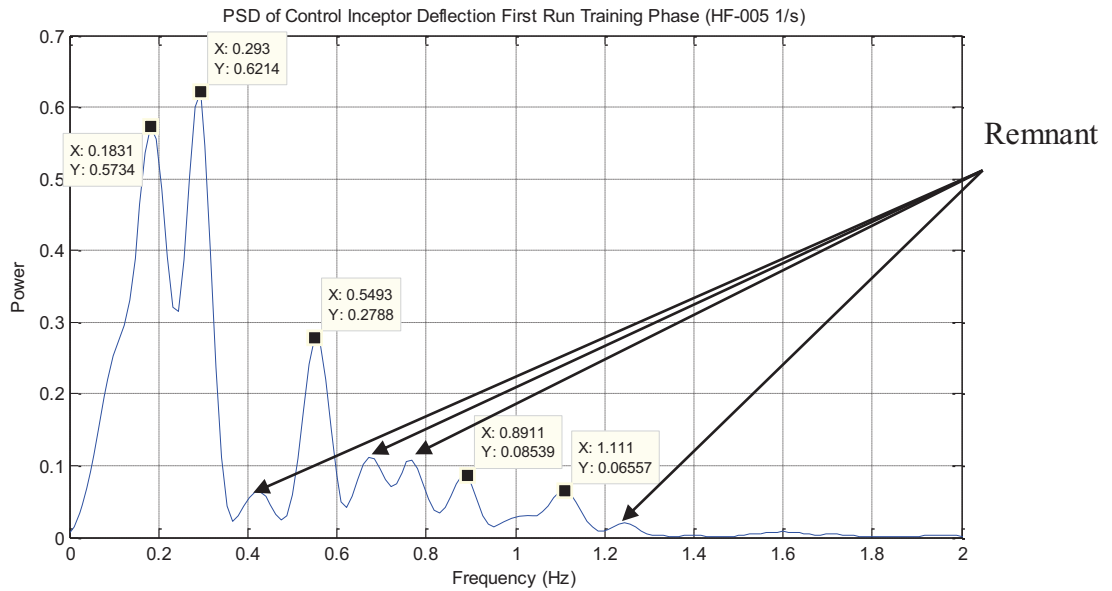


Figure 6.6.2 PSD of Control Inceptor Deflection for Test Subject HF005

Chapter 7 – Conclusions and Future Recommendations

7.1 Summary

This research was conducted in order to ascertain differences that exist when training on a high fidelity or a low fidelity control loader simulation. This will either dispute or verify the importance of maintaining a high fidelity control loader when training pilots. Along with comparing the difference between the two training groups, it provides examples of frequency domain methods to analyze test subject control strategy. These experiments can be modified to better characterize the human control strategy. Techniques using power spectral density (PSD) to characterize human control behavior is a fairly new concept and this has to be further analyzed to understand how the PSD is related to human control.

The first step in this research was to review the neuromuscular system and the many experiments conducted to understand how to effectively test two different control loader dynamics and the effect it has on the test subject performing the task. This literature review together with knowledge about control systems was the basis for developing an experiment to test subjects.

The second step was to develop the experimental task. The experiment consisted of a roll disturbance compensatory task. This is a typical task used to test human performance in a simulator because of easy implementation and transportability to other simulators. The two tasks used were a simpler task consisting of $1/s$ plant dynamics and a harder task using $1/s^2$ plant dynamics.

The next step was to determine the proper dynamics to represent the high fidelity and low fidelity parameters. The high fidelity parameters were determined from the literature and the low fidelity from a computer joystick. The low fidelity control inceptor represents a low damped, small force gradient control inceptor. These dynamics were implemented and then verified by determining the damping ratio and force gradients from the time and frequency responses.

Finally 20 test subjects were split into two groups consisting of 10 each. One group trained on the high fidelity control inceptor and the second group trained on the low fidelity control inceptor. After training both groups were then transferred to the high fidelity control inceptor simulation.

7.2 Conclusions

The results show that for $1/s$ plant dynamics the two groups maintain a similar control strategy throughout the training and transfer phases. Their performance measured

using the root mean (RMS) tracking error for each run over the course of the experiment shows very similar performance without a significant difference. The power spectrum density for the two groups shows similar peak power and peak frequency. Typically, the test subject's peak power coincided with a portion of the 9 frequencies in the sum of sinusoids disturbance. This shows that they are responding directly to the disturbance in their control strategy.

The test subjects also have a maximum peak power at a frequency between 0.18 and 0.2 Hz which is one of the highest amplitudes in the sum of sinusoids disturbance. Two sinusoids with a frequency of 0.074 Hz and 0.112 Hz in the sum of sinusoids disturbance have the same amplitude of 15.2 degrees roll angle as the 0.2 Hz sinusoid. Test subjects maintain power below 0.2 Hz but do not peak within this region. The power also decreases beyond 0.2 Hz as does the disturbance amplitude. The disturbance shows lower frequency behavior more so than high frequency behavior. The amplitude decreases for the higher frequency sinusoids. An interesting behavior shown is that the low fidelity control loader training test subjects generally have a lower peak frequency for their first run but they train to a higher peak frequency similar to the high fidelity group even before they transfer. The high fidelity group maintains their peak power better when they transfer than the low fidelity group, but the low fidelity group adapts very quickly and soon increases their peak power. By the last run, both groups have similar peak power and peak frequencies.

For $1/s^2$ plant dynamics, the difference between the two groups is greater. The high fidelity group performs better in terms of having a smaller asymptote tracking error. Also, the power spectrum density suggests a different control strategy by either group.

The low fidelity group uses all their power at one frequency around 0.2 Hz, while the high fidelity group uses their power at higher frequencies. The power dedicated to one frequency, especially a low frequency, suggests a high amplitude oscillatory behavior at one frequency. This is a typical strategy when the test subject cannot keep up with the disturbance. Both groups use much higher power for $1/s^2$ plant dynamics suggesting high amplitude control inceptor deflection. The low fidelity training group adapts this high amplitude nature through the training phase and first run transfer phase. They eventually use their power at the higher frequencies suggesting that the high fidelity control inceptor allows them to operate in the higher frequencies. The PSD for both groups is very similar during the last run of the experiment showing that the low fidelity test subjects adapt and pick a strategy similar to the high fidelity test subjects. The results show that maintaining a high fidelity control loader system is more important for the harder task. The test subjects that performed the worst in each group for both $1/s$ and $1/s^2$ plant dynamics generally use less power and use this power at fewer frequencies than the best performing test subjects within the group.

In conclusion, there is no significant difference in the performance and power spectral density between the high fidelity group and the low fidelity group for $1/s$ plant dynamics. The similar control behavior represented by the PSD agrees with the similar tracking error achieved by both training groups. The low fidelity test subjects trained with similar peak power and peak frequencies through the training phase and transfer phase. This allows the low fidelity test subjects to adapt when they transfer to the high fidelity control dynamics. For $1/s^2$ plant dynamics there is an advantage to training on the high fidelity control loader. Both the tracking error and power spectrum density is different for

both groups using $1/s^2$ plant dynamics. The low fidelity group adapts their use of peak power and frequencies to match the high fidelity group in the last run transfer phase, but only maintain one peak frequency in the training phase and first run transfer phase. The low fidelity group has low coherence at the peak frequency they operate at. The use of one peak frequency combined with a highly uncorrelated test subject leads to degraded tracking error performance.

7.3 Future Recommendations

There are many improvements that can be implemented to further analyze the human control strategy. In the experiments only 20 test subjects were used. Although 20 test subjects are significant to test differences, some test subjects were removed. These experiments will be repeated with more test subjects and will be grouped accordingly to statistical properties.

The experiment could be improved by refining the asymptotic criterion when a test subject has trained. To determine when test subjects reached training asymptote, the slope of the tracking error between two runs was computed. A criterion was set that the slope should reach a value of 0.1 or less for three consecutive runs. This value was set based on tests performed off-line. It was observed that some test subjects didn't reach an asymptote. A new definition of horizontal asymptote can be derived for new experiments or a longer number of runs can be conducted to ensure test subjects reach asymptote.

Another improvement to be made is to the disturbance forcing function. The disturbance forcing function was adopted from the literature and represents a sum of 9 sinusoids with increasing frequencies and decreasing amplitudes. The higher frequency sinusoids might not be seen by the test subjects with the diminished amplitude. It would

be beneficial to analyze the disturbance and change the amplitudes to see the effect it has on the test subject. The test subjects might adopt a different control strategy or shift their peak power. This would show the limitation of the neuromuscular system and the effect of changing vehicle dynamics.

The implementation of a non-linear force gradient for the control inceptor dynamics could enhance the study further. Only a linear force gradient was implemented in this study. The experiments could test if non-linear force gradients are better than training with a linear force gradient. This change could mimic the effects of the non-linear aerodynamics on the control surfaces.

This research is ongoing and is important to vehicle simulation. The main interface to the vehicle is the neuromuscular limb interaction and it is very important to understand the effects of poorly simulating control inceptor dynamics. Many experiments can be tested concerning different control inceptor dynamics and to develop a better understanding of human control strategy.

Appendices

Appendix A: Control Loader Quasi Transfer of Training Experimental Protocol

Pre-Experiment

Description

The purpose of the pre-experiment phase is to make sure the implementation of the roll compensatory task is ready for experimentation. The pre-experimental tests are conducted with a simulator pilot.

Initial Tests

1. Ensure that the display is showing the target clearly.
2. Ensure that the system responds properly to test subject input. Deflect the control inceptor at increasing amplitudes and hold. The roll rate of the display bank angle reference line should consistently increase with increasing control inceptor deflection.
3. Activate disturbance and ensure the output of the display responds to the disturbance. The roll reference line on the display should show a quasi random response.
4. Test data recording. Make sure output sensor measurements are within the operating range.
 - a) Deflect control inceptor one direction and then the other. In one direction, the output control inceptor position sensor should show decreasing values and increasing values in the other direction. The control inceptor position should be at a value of 0 when centered and is not deflected. Force values should increase in either direction as one deflects the control inceptor further. The force should also be calibrated to zero when no input is applied to the control inceptor.
 - b) Activate disturbance and do not apply any control inceptor input. Obtain the bank angle measurement. This should be the same as the disturbance input that has gone through the plant dynamics defined in the Control Loader Quasi Transfer of Training Experimental Plan.

Roll Command Gain Tuning

Plant Dynamics 1/s

- High Fidelity/Low Fidelity
 1. Initialize roll command gain at 40 deg/sec/in.
 2. Run roll compensatory task and note if the system is controllable
 3. Adjust gain if needed.

Plant Dynamics $1/s^2$

• High Fidelity/Low Fidelity

1. Initialize roll command gain at $40 \text{ deg/sec}^2/\text{in}$.
2. Run roll compensatory task and note if the system is controllable
3. Adjust gain if needed.

Experiment

Description

Each test subject will go through all four phases of the experiment before the next test subject conducts the experiment. A break will be administered in between the training and quasi transfer sessions for each test subject. The high fidelity transfer group will train on one day and the low fidelity group will train on another day. A break will be administered after each training session and then again before the test subjects start training on $1/s^2$ plant dynamics.

Familiarize

1. Test subjects will be briefed on the task they are to perform.
2. Allow test subjects to perform a single run of the experiment for both $1/s$ and $1/s^2$ dynamics.

Evaluation

1. 10 test subjects will be assigned to the low fidelity control loader transfer group and another 10 test subjects will be assigned to the high fidelity control loader transfer group. Test subjects will be assigned a number associating them with either group. The high fidelity group will start with HF001 and the low fidelity group will start with LF001.
2. For subsequent tasks the control inceptor deflection, bank angle, control inceptor force, and tracking error will be recorded throughout the run. The RMS & STD input will be calculated for each test subject for the one run length at a later time. Also, a PSD analysis of the control inceptor deflection and control inceptor bandwidth input will be calculated at a later time. This is the baseline performance level for each test subject.
3. Each test subject in the high fidelity control loader transfer group is to perform a 30 second run of the high fidelity control loading roll tracking compensatory task for $1/s$ and $1/s^2$ plant dynamics.
4. Test subjects will give a Modified Cooper Harper Rating (CHR) for both runs of $1/s$ and $1/s^2$ dynamics. They may also give any comments on tasks.
5. Repeat Steps 2-5 for the low fidelity control loader transfer group.

Training

1. The high fidelity control loader transfer group will train on the high fidelity control loader simulation and the low fidelity transfer group will train on the low fidelity control loader simulation.
2. The test subjects will perform the roll compensatory tracking task for $1/s$ and $1/s^2$ plant dynamics. Each run will last for 30 seconds.
3. They will conduct as many runs as necessary to reach a performance asymptote. In this case, the cumulative running average of the RMS tracking error will be used as the performance metric. As the slope of this performance metric approaches zero, asymptote has been reached.

Throughout each run, the following parameters will be recorded. These parameters along with frequency of measurement are listed in the Control Loader Quasi Transfer of Training Experiment Plan.

- a) Bank Angle
 - b) Control Inceptor Deflection
 - c) Control Inceptor Force
 - d) RMS Control Inceptor Deflection
 - e) Running Cumulative Average of RMS Tracking Error
 - f) Running Cumulative Average RMS Control Inceptor Deflection
 - g) Slope of the Running Cumulative Average of the RMS Tracking Error
4. After the training session has ended for each test subject, they will give a Modified Cooper Harper Rating (CHR) and comment on tasks performed.

Quasi-Transfer

1. Run roll compensation tasks again for $1/s$ and $1/s^2$ plant dynamics. The low fidelity control loader transfer group will transfer to the high fidelity control loader simulation for further experimentation. The high fidelity control loader transfer group will continue experimentation in the high fidelity control loader simulation.
2. The test subjects will again conduct as many runs as necessary to reach a performance asymptote.
3. The cumulative running average of the RMS tracking error is also used to measure when test subjects have reached a performance asymptote.
4. The same parameters recorded for the training sessions will also be recorded for the transfer sessions.
5. A Modified Cooper Harper Rating and test subject comments are recorded at the end of the experiment.

Data Analysis

1. Record the control inceptor deflection, bank angle of the plant, and control inceptor deflection for every run for the entire run.
2. From these recorded parameters, the RMS tracking error should be calculated. Obtain the RMS running cumulative average tracking error over the runs completed.
3. When the RMS running cumulative average tracking error reaches an asymptote the run has completed. Take the slope of every two runs for the RMS running cumulative average. When the slope reaches 0.001 for a consistent 5 runs, asymptotic performance has been reached.
4. From the recorded parameters, the standard deviation (STD) of the control inceptor deflection, the RMS control inceptor deflection, the RMS Tracking Error, the PSD of the control inceptor deflection, and the control inceptor input bandwidth will be calculated.
5. A comparison will be made between all of the calculated parameters for the low fidelity transfer group and the high fidelity transfer group. Also, each transfer group will be analyzed for variation within. The comparison will reveal any effects of training on one simulation as opposed to the other.

Experimental Briefing

The experiment that will be performed today is a roll compensatory task. A roll angle will be shown on the display as a roll reference line. There will also be a horizon reference line representing a zero roll angle. A disturbance that is somewhat random will cause the roll reference line to move with unexpected behavior. The task is to return the roll reference line to a zero roll angle. This occurs when the roll reference line overlaps the horizon reference line. You will be given one run of the task to familiarize yourself with the experiment.

Appendix B: Experimental Measured and Calculated Parameters

Experimental Parameters	Required During Training Sessions	Required During Transfer Sessions	Frequency of Measurement		Parameter Type
			Training Sessions	Transfer Sessions	
RMS Control Inceptor Deflection	Yes	Yes	Every Run	Every Run	Calculated
Running Cumulative Average of RMS Tracking Error over Runs	Yes	Yes	Every Run	Every Run	Calculated
RMS Tracking Error	Yes	Yes	Every Run	Every Run	Calculated
Slope of Running Cumulative Average of the RMS Tracking Error	Yes	Yes	Between 2 Runs	Between 2 Runs	Calculated
STD Control Inceptor Deflection	No	No	None	None	Calculated
PSD Control Inceptor Deflection	No	No	None	None	Calculated
Control Inceptor Input Bandwidth	No	No	None	None	Calculated
Roll Rate	No	No	None	None	Calculated
Bank Angle	Yes	Yes	Every Run for Entire Run	Every Run for Entire Run	Recorded
Control Inceptor Deflection	Yes	Yes	Every Run for Entire Run	Every Run for Entire Run	Recorded
Control Inceptor Force	Yes	Yes	Every Run for Entire Run	Every Run for Entire Run	Recorded
Cooper Harper Rating	Yes	Yes	After Each Trial	After Each Trial	Recorded

Appendix C: Experiment Run Time

Estimated Run Time for Each Experiment Phase (High & Low Fidelity $1/s$ & $1/s^2$ Plant Dynamics)						
Test Subject Number	Familiarize Phase	Evaluation Phase	Training Phase	Breaks	Quasi-Transfer Phase	Total Run Time
HF001	2×30 sec	2×30 sec	2×10 min	2×5 min	2×5 min	42 min
HF002	2×30 sec	2×30 sec	2×10 min	2×5 min	2×5 min	42 min
HF003	2×30 sec	2×30 sec	2×10 min	2×5 min	2×5 min	42 min
HF004	2×30 sec	2×30 sec	2×10 min	2×5 min	2×5 min	42 min
HF005	2×30 sec	2×30 sec	2×10 min	2×5 min	2×5 min	42 min
HF006	2×30 sec	2×30 sec	2×10 min	2×5 min	2×5 min	42 min
HF007	2×30 sec	2×30 sec	2×10 min	2×5 min	2×5 min	42 min
HF008	2×30 sec	2×30 sec	2×10 min	2×5 min	2×5 min	42 min
HF009	2×30 sec	2×30 sec	2×10 min	2×5 min	2×5 min	42 min
HF010	2×30 sec	2×30 sec	2×10 min	2×5 min	2×5 min	42 min
Total Experiment Time	10 min	10 min	3 hrs 20 min	1 hr 40 min	1 hr 40 min	7 hrs
LF001	2×30 sec	2×30 sec	2×10 min	2×5 min	2×5 min	42 min
LF002	2×30 sec	2×30 sec	2×10 min	2×5 min	2×5 min	42 min
LF003	2×30 sec	2×30 sec	2×10 min	2×5 min	2×5 min	42 min
LF004	2×30 sec	2×30 sec	2×10 min	2×5 min	2×5 min	42 min
LF005	2×30 sec	2×30 sec	2×10 min	2×5 min	2×5 min	42 min
LF006	2×30 sec	2×30 sec	2×10 min	2×5 min	2×5 min	42 min
LF007	2×30 sec	2×30 sec	2×10 min	2×5 min	2×5 min	42 min
LF008	2×30 sec	2×30 sec	2×10 min	2×5 min	2×5 min	42 min
LF009	2×30 sec	2×30 sec	2×10 min	2×5 min	2×5 min	42 min
LF010	2×30 sec	2×30 sec	2×10 min	2×5 min	2×5 min	42 min
Total Experiment Time	10 min	10 min	3 hrs 20 min	1 hr 40 min	1 hr 40 min	7 hrs

Appendix D: Matlab [21] Code to Calculate Frequency Response

```
%Man Machine Systems (FRF Frequency Response Function)

%Slicing the Input and Output Signals
numseg=1
lengthseg=round(length(Input)/numseg);
for i=1:numseg
M1(i)=(i-1)*lengthseg+1;
M2(i)=(i)*lengthseg;
if M2(i)>length(Input);
    M2(i)=length(Input);
end
end

%Calculating the Fourier Transform, Cross Correlation and Auto
Correlation
for n=1:length(numseg)
    win1=hamming(lengthseg);
    Ninput=Input(M1(n):M2(n));
    Noutput=Output(M1(n):M2(n));
    [y1,F,T] = spectrogram(Ninput,win1,0,[.6:.01:3.97],100);
    [y2,F,T] = spectrogram(Noutput,win1,0,[.6:.01:3.97],100);
    Tin=205;
    CCin(:,n)=conj(y1).*y2;
    ACout(:,n)=(abs(y1)).^2;
end

%Calculating Magnitude and Phase between Output and Input
AC=mean(ACout,2);
CC=mean(CCin,2);
FRF=CC./AC;
figure(4)
subplot(2,1,1)
[mag,phase,F1]=bode(tf_hf,{.1,18.95})
mag=20*log10(mag);
    semilogx(F1,mag(:,:,),'r')
    hold on
Mag=20*log10(abs(FRF));
semilogx(2*pi*F,Mag); grid on
title('Frequency Response of Low Fidelity Control Loader')
ylabel('Amplitude (dB)')
xlabel('Frequency (rad/s)')
subplot(2,1,2)
Phase=unwrap(angle(FRF))*180/pi;
semilogx(2*pi*F,Phase); grid on
hold on
    semilogx(F1,phase(:,:,),'r')
ylabel('Phase (Degrees)')
xlabel('Frequency (rad/s)')
```

Appendix E: Experiment Pseudo Code

Create output table for each test subject that includes the Control Inceptor Deflection, Control Inceptor Force, Roll Angle Output, over the entire run and for each run. The data should be stored at every sampling interval.

```
% Pseudo Code for Quasi Transfer of Training Control Loader Experiment

%Initialization
SubjectNum %Subject Number 1:10 for Both High Fidelity & Low Fidelity
Simulation. Label this differently such as SubjectNum=HF001 and
SubjectNum=LF001 to distinguish between High Fidelity and Low Fidelity
Data.
t=0; % sec
h=.001; % Sampling Time (seconds) Depends on simulation sampling time
runL=30; % Run Time (seconds)
RollA1(1)=0;
RollA2(1)=0;
RunN=0; %Run number. Initialized to the zero runs before program starts
-----

%% Code for 1/s Plant Dynamics
n=t/h; %Iteration number. The time divided by the sampling time

%Commanded Plant Input
% ContIncpPos is the Test Subject Control Inceptor Deflection in
inches. Store these values at each sampling interval throughout the
run. Also store these values for every Run.
KC=80; %Roll Command Gain (deg/lb*sec)
CPI(n)=ContIncpPos(n)*KC; %Commanded Plant Input. Store at every
sampling interval throughout the run. Also store these values for every
Run.

%Development of Disturbance
Freq=[.467,.701,1.17,1.87,3.51,7.01,11/2,14,18.7]; % Frequencies of the
9 sinusoids
Amp=[15.2,15.2,15.2,7.6,3.04,.76,.38,.228,.152]; %Amplitudes of the 9
sinusoids
%t represents Time in seconds
Dist=Amp(1)*sin(Freq(1)*t)+Amp(2)*sin(Freq(2)*t)+Amp(3)*sin(Freq(3)*t)+
Amp(4)*sin(Freq(4)*t)
+Amp(5)*sin(Freq(5)*t)+Amp(6)*sin(Freq(6)*t)+Amp(7)*sin(Freq(7)*t)+Amp(
8)*sin(Freq(8)*t)
+Amp(9)*sin(Freq(9)*t); %Disturbance
%Euler Integration to Obtain Roll Angle of the Plant Dynamics
%Commanded Plant Input Passed through One Integration.

RollA1(n+1)=RollA1(n)+CPI(n)*h; % Roll Angle when Plant Command is
Integrated Once. This is calculated at every sampling time of
simulation
RollF1(n)=RollA1(n)+Dist(n) %Output Roll Angle for 1/s dynamics. Sum of
commanded plant roll angle and disturbance. Store these values at every
iteration and for every run. This drives display
```

```

if t=30
RunN = RunN+1
end

%Tracking Error, Cumulative Running Average Tracking Error and RMS
Tracking Error (Post Processed)
%1/s Plant Dynamics

%n represents each data point. Have to record Output Roll Angle RollF1
for every sampling interval
N=length(RollF1) % Total number of data points of Output Roll Angle
for n=1:N % This for loop goes through every data point collected for
the Output Roll Angle
RollF1Sq(n)=RollF1(n)^2; %Each Data Point of Output Roll Angle Squared
end

TrackError(RunN)=sqrt(sum(RollF1Sq)/N); %RMS Tracking Error of Each Run

%Cumulative Running Average of RMS Tracking Error
if RunN >=2 % Start calculating Cumulative Running Average Tracking
Error when RunN =2
TrackErrorC(RunN)=(TrackError(RunN-1)*(RunN-1)+TrackError(RunN))/N
%Cumulative Tracking Error
end

%Slope of the Cumulative Running Average of RMS Tracking Error
if RunN >=2 %Start calculating Slope at Run # 2
diffTE(1)=0 %initialize the slope to zero.
diffTE(RunN)=(TrackErrorC(RunN)-TrackErrorC(RunN-1)); % Slope at every
two points.
end

if diffTE<=.001
end

-----
-----

%% Code for Plant Dynamics of 1/s^2

n=t/h; %Iteration number The time divided by the sampling time

% Commanded Plant Input
% ContIncpPos represents the Test Subject Control Inceptor Deflection
in inches. Store these values at each sampling interval throughout the
run. Also store these values for every Run.
KC=80; %Roll Command Gain (deg/lb*sec)
CPI(n)=ContIncpPos(n)*KC; %Commanded Plant Input. Store at every
sampling interval throughout the run. Also store these values for every
Run.

%Development of Disturbance
Freq=[.467,.701,1.17,1.87,3.51,7.01,11/2,14,18.7]; % Frequencies of the
9 sinusoids

```

```

Amp=[15.2,15.2,15.2,7.6,3.04,.76,.38,.228,.152]; %Amplitudes of the 9
sinusoids
% t represents Time in seconds
Dist=Amp(1)*sin(Freq(1)*t)+Amp(2)*sin(Freq(2)*t)+Amp(3)*sin(Freq(3)*t)+
Amp(4)*sin(Freq(4)*t)
+Amp(5)*sin(Freq(5)*t)+Amp(6)*sin(Freq(6)*t)+Amp(7)*sin(Freq(7)*t)+Amp(
8)*sin(Freq(8)*t)
+Amp(9)*sin(Freq(9)*t); % Disturbance

%Euler Integration. Conducted at each time step
%Commanded Plant Input Integrated Twice

RollA1(n+1)=RollA1(n)+CPI(n)*h; %Commanded Plant Input Integrated Once
RollA2(n+1)=RollA2(n)+RollA1(n)*h; % Roll Angle when Plant Command is
Integrated Twice
RollF2(n)=RollA2(n)+Dist(n); %Output Roll Angle for 1/s^2 dynamics. Sum
of commanded plant roll angle and disturbance. Store these values at
every iteration and for every run. This drives displays

if t=30;
RunN = RunN+1
end

%Tracking Error, Cumulative Running Average Tracking Error and RMS
Tracking Error (Post Processed)

% n represents each data point. Have to record Output Roll Angle RollF1
for every sampling interval
N=length(RollF1) Total number of data points of Output Roll Angle
for n=1:N % This for loop goes through every data point collected
for the Output Roll Angle
RollF2Sq(n)=RollF2(n)^2; %Each Data Point of Output Roll Angle Squared
end
TrackError2(RunN)=sqrt(sum(RollF2Sq)/N); %RMS Tracking Error of Each
Run

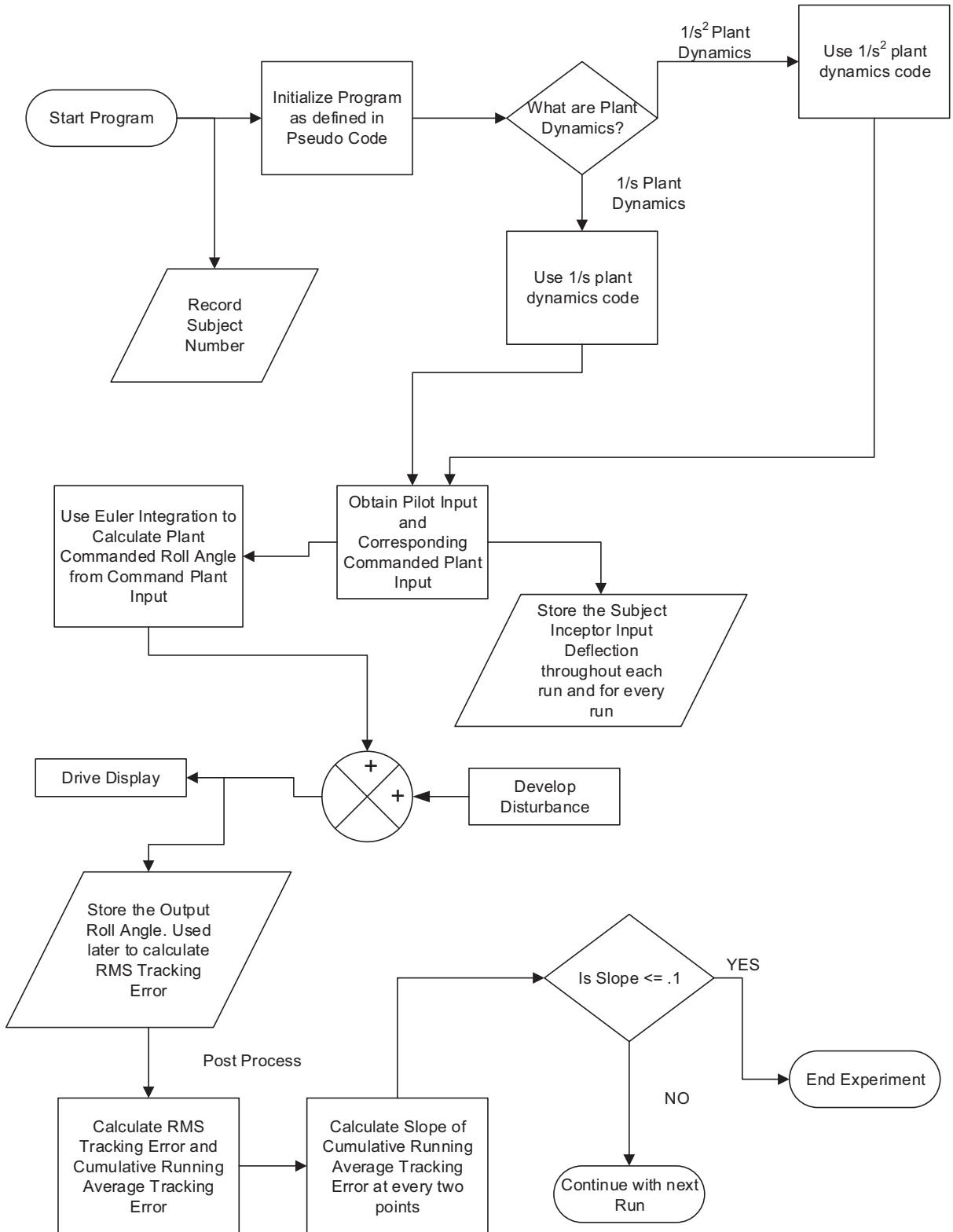
if RunN >=2 %Have to start at Run #2 Have to start calculating
Cumulative Running Average Tracking Error when RunN =2
TrackErrorC2(RunN)=(TrackError2(RunN-1)*(RunN-
1)+TrackError2(RunN))/RunN
end

%Slope of the Cumulative Running Average of RMS Tracking Error
if RunN >=2 %Start calculating Slope at Run # 2
diffTE2(1)=0 %initialize the Slope to zero.
diffTE2(RunN)=(TrackErrorC2(RunN)-TrackErrorC2(RunN-1)); % Slope at
every two points.
end

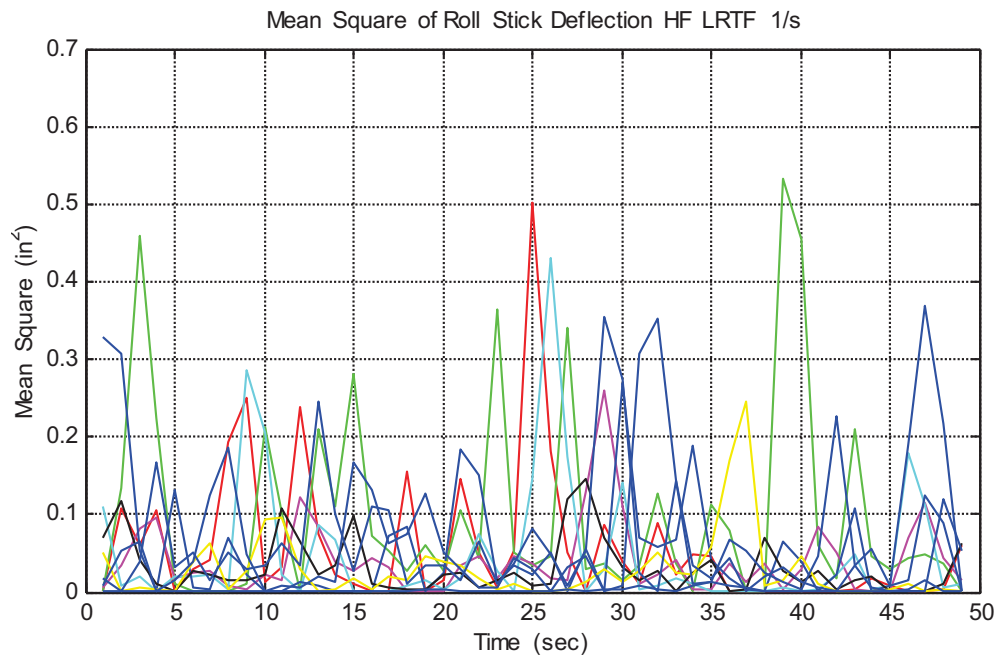
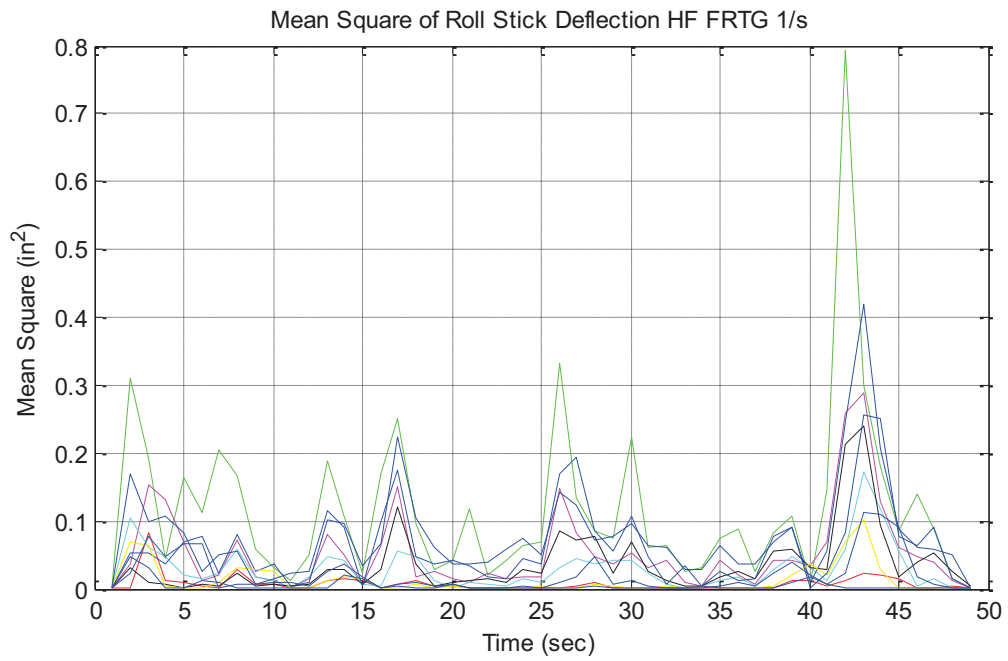
if diffTE2<=.001
end

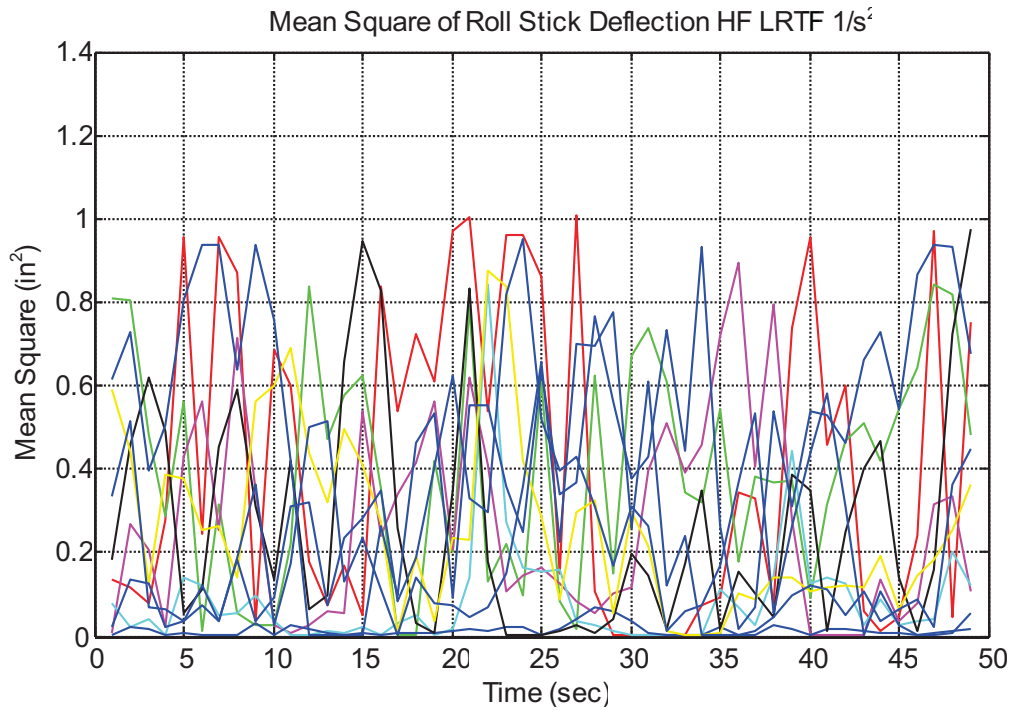
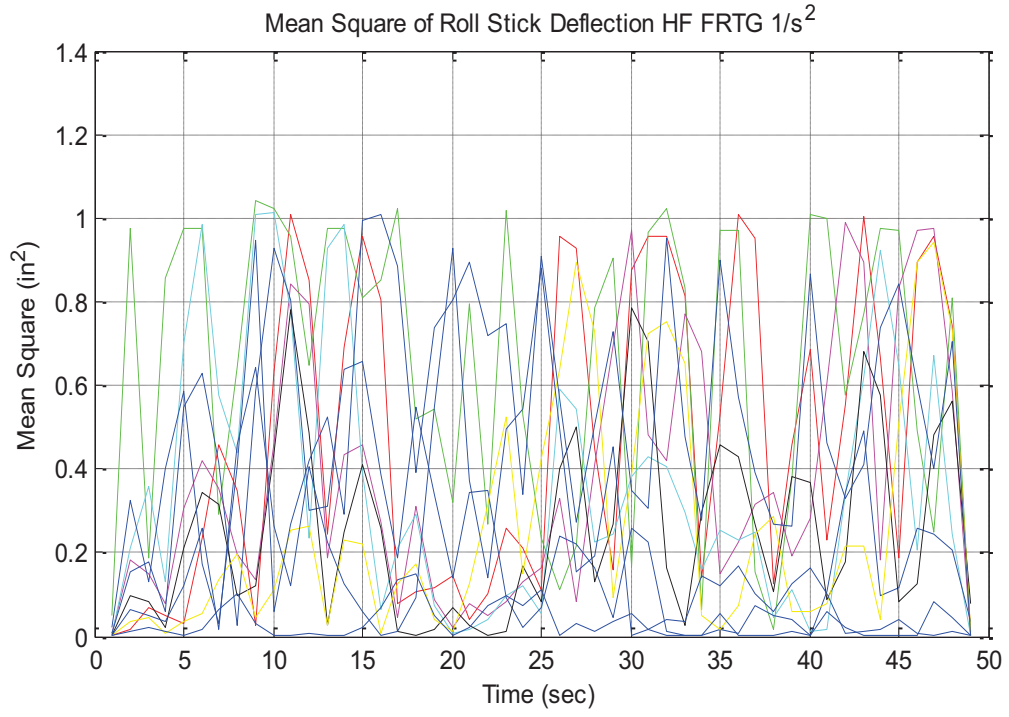
```

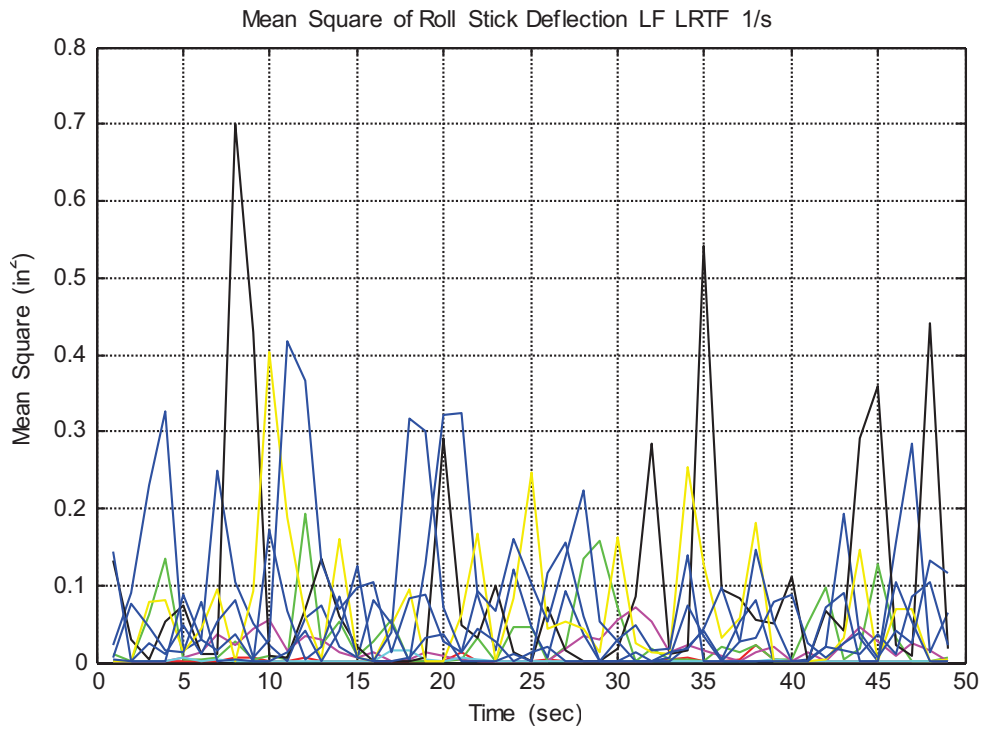
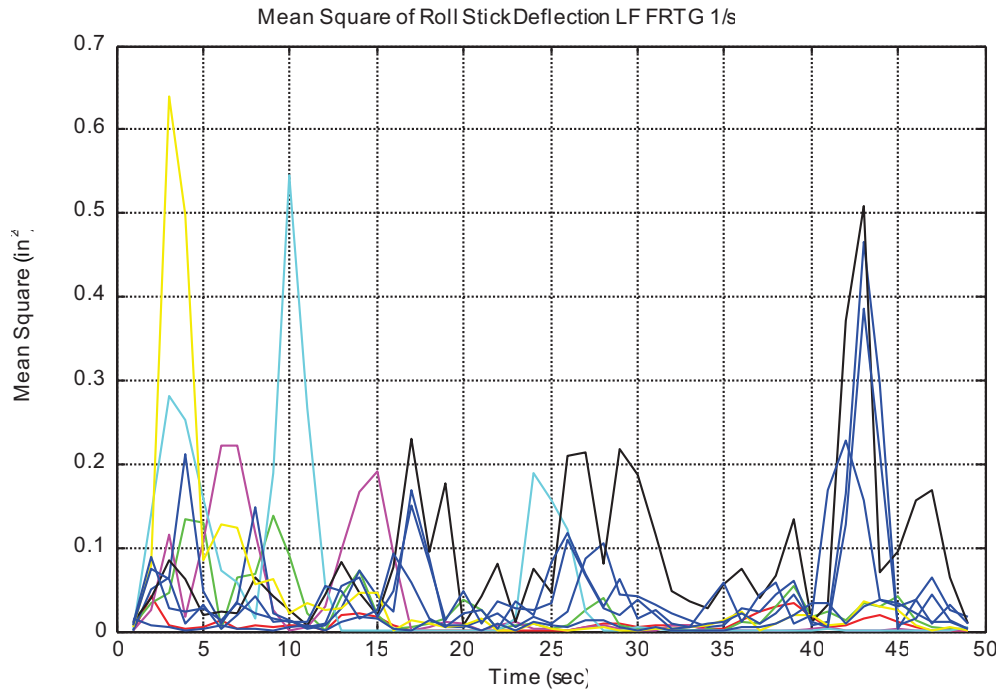
Appendix F: Experiment Flow Chart

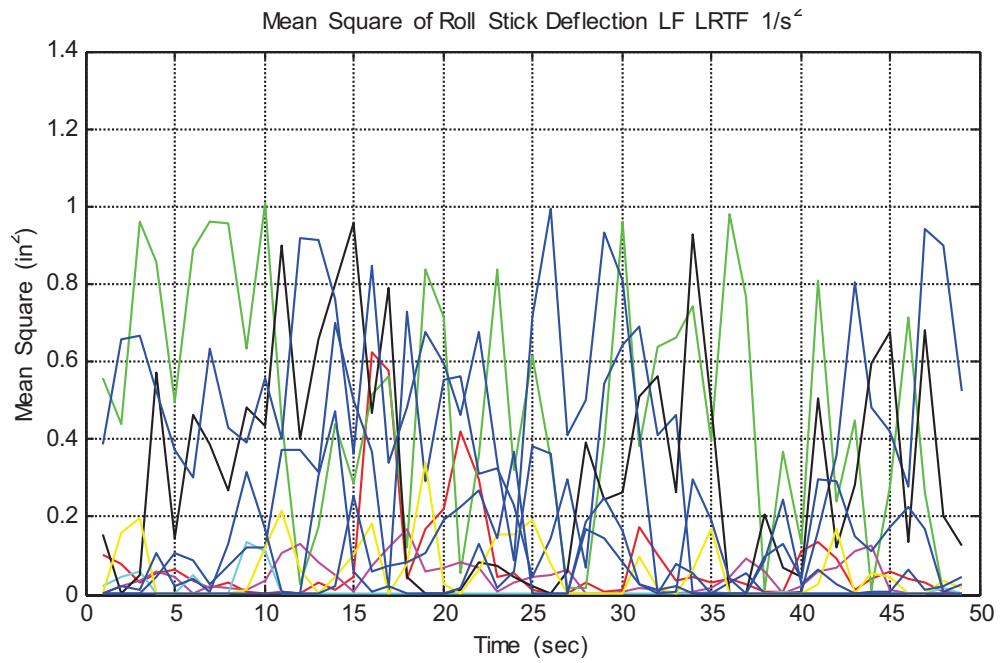
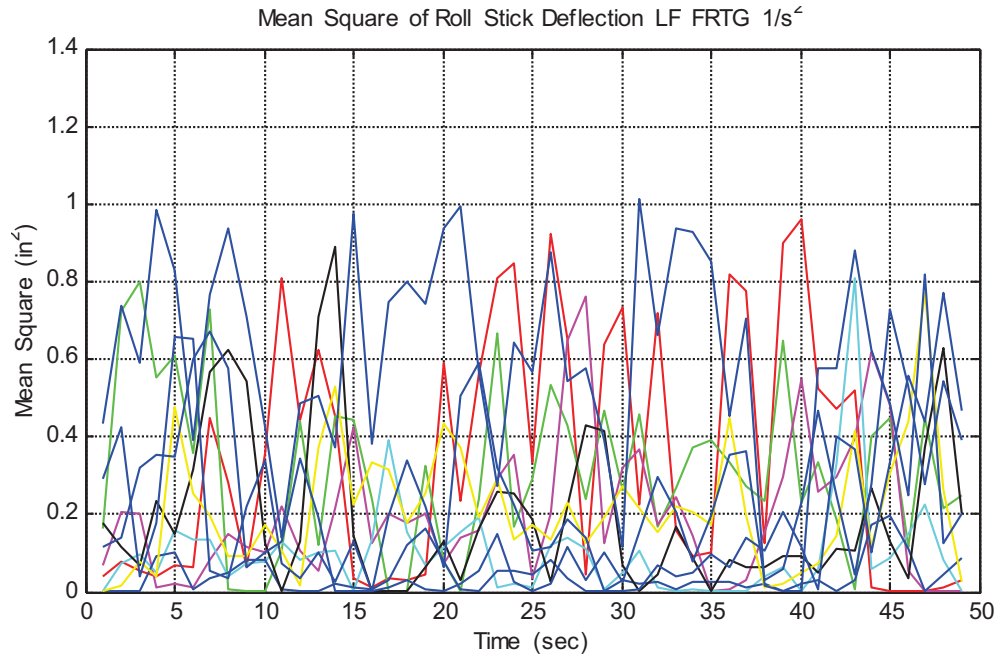


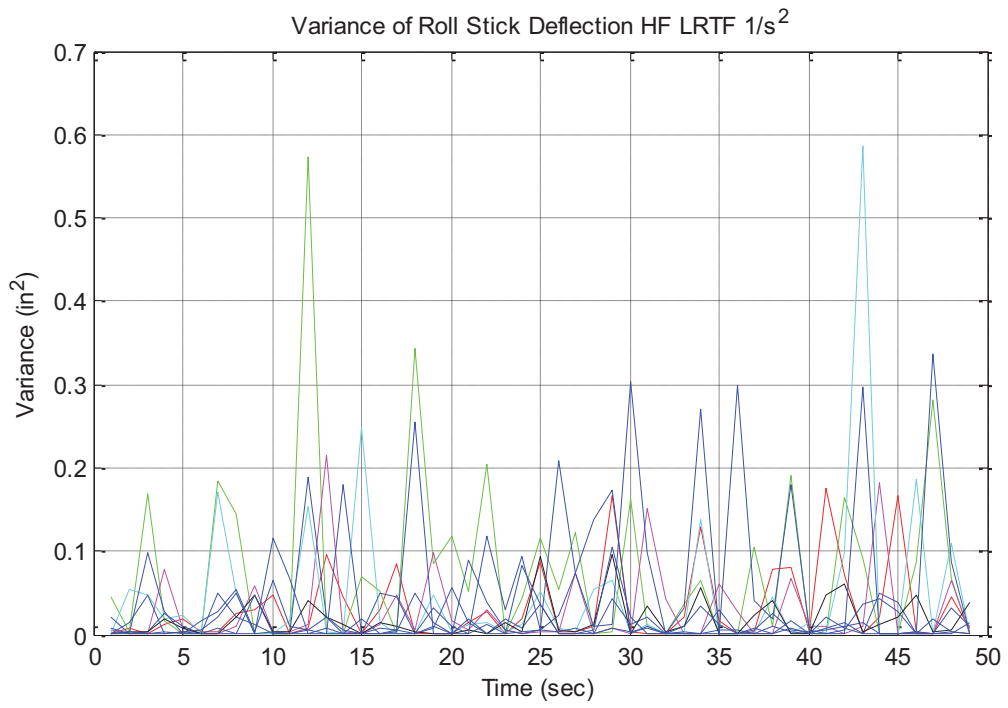
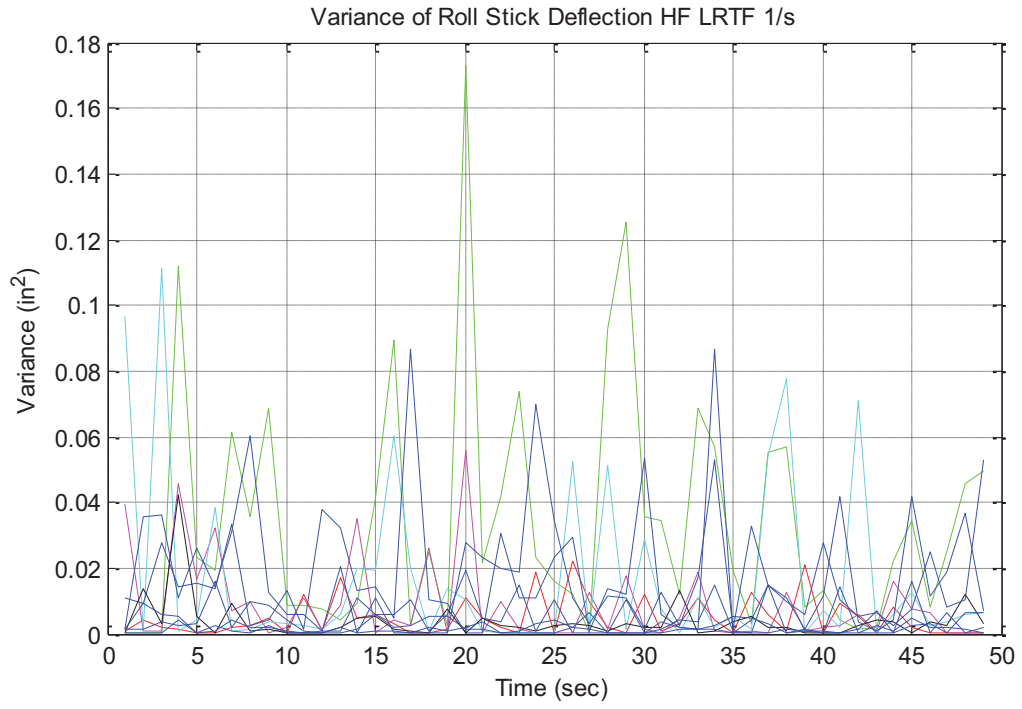
Appendix G: Mean Square and Variance for High Fidelity and Low Fidelity Training Groups

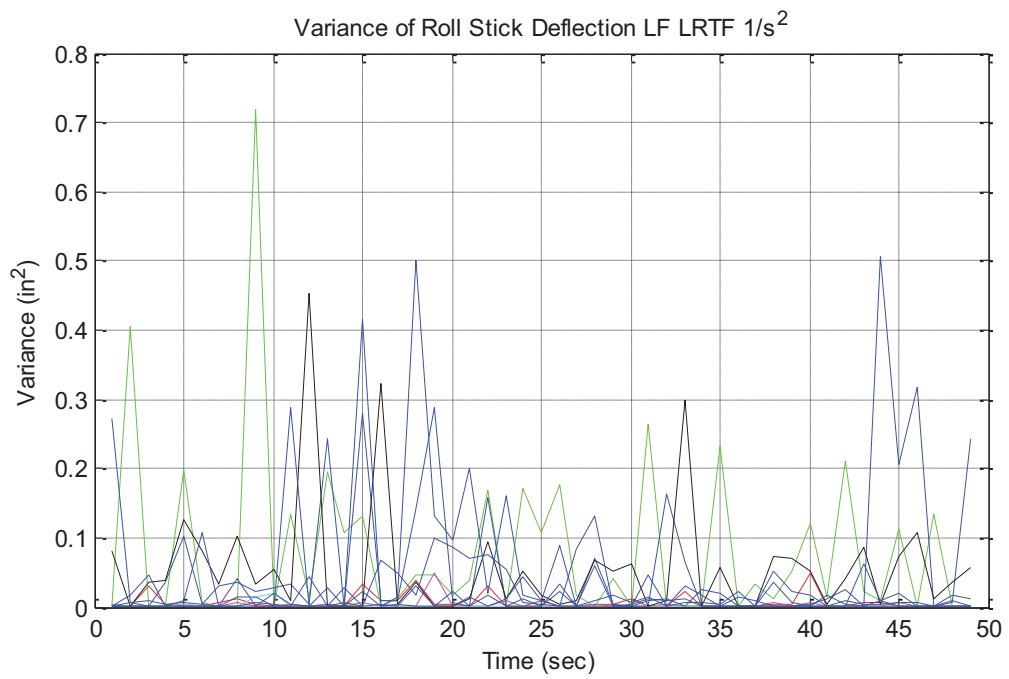
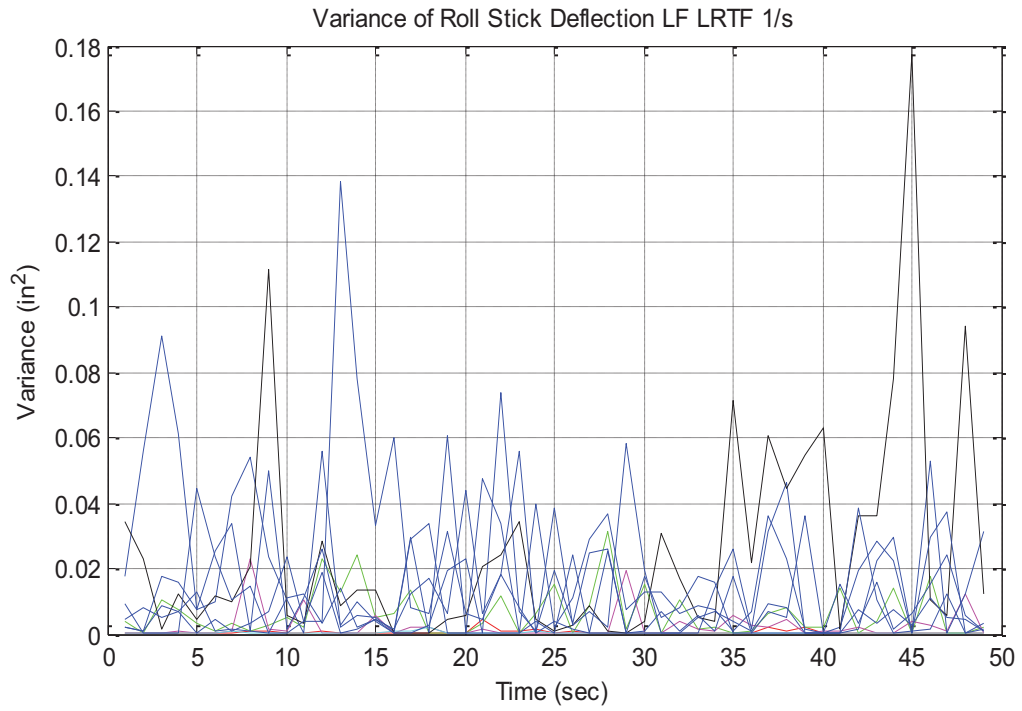




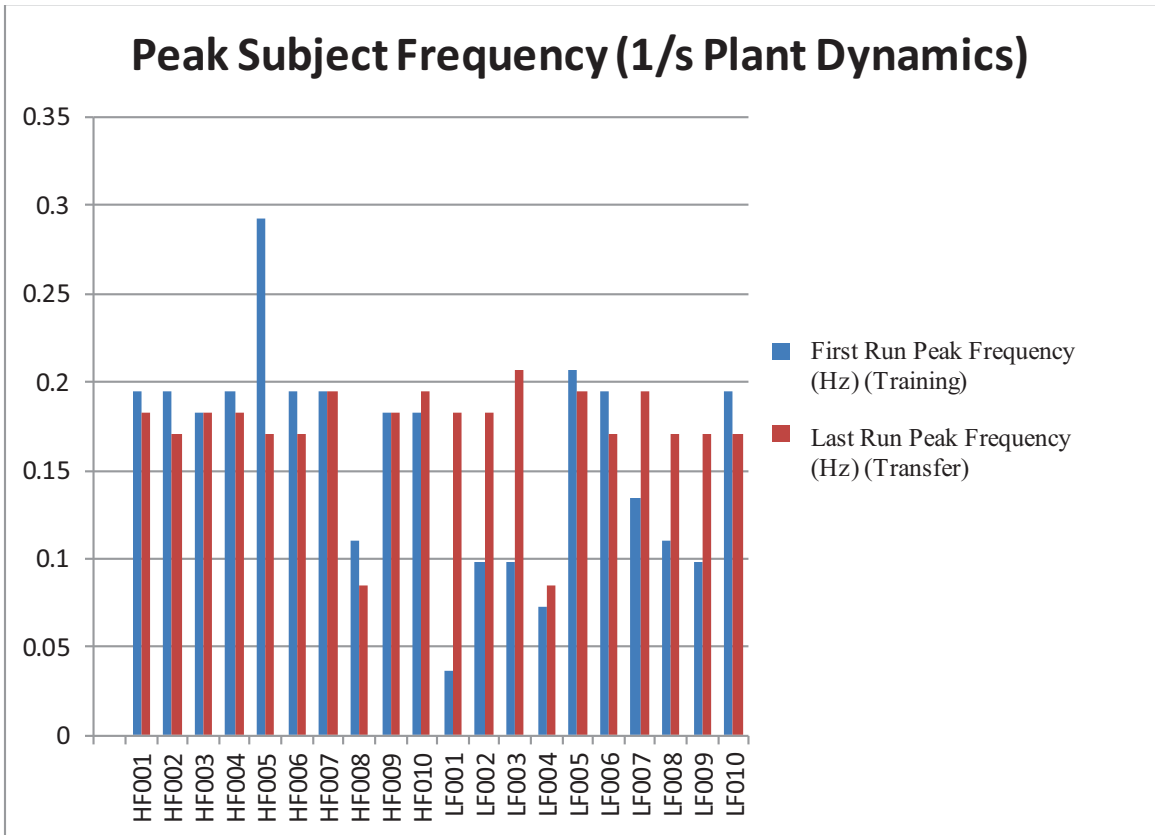
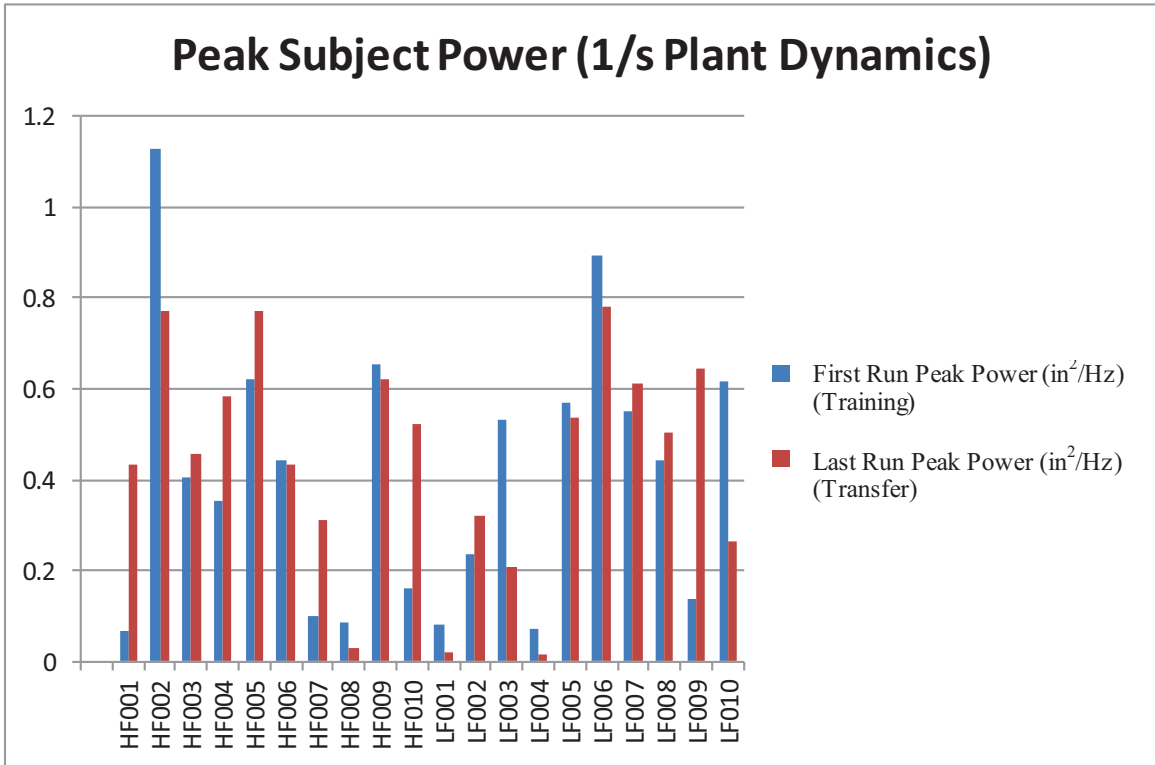


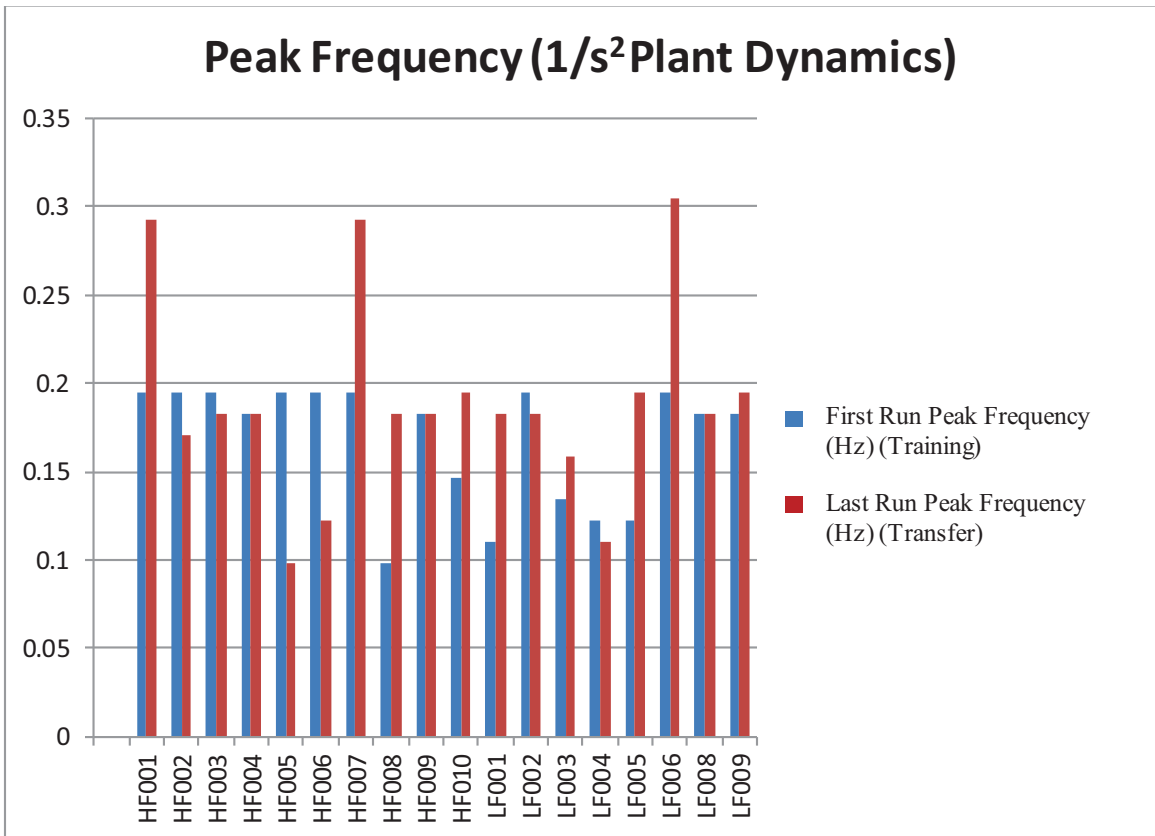
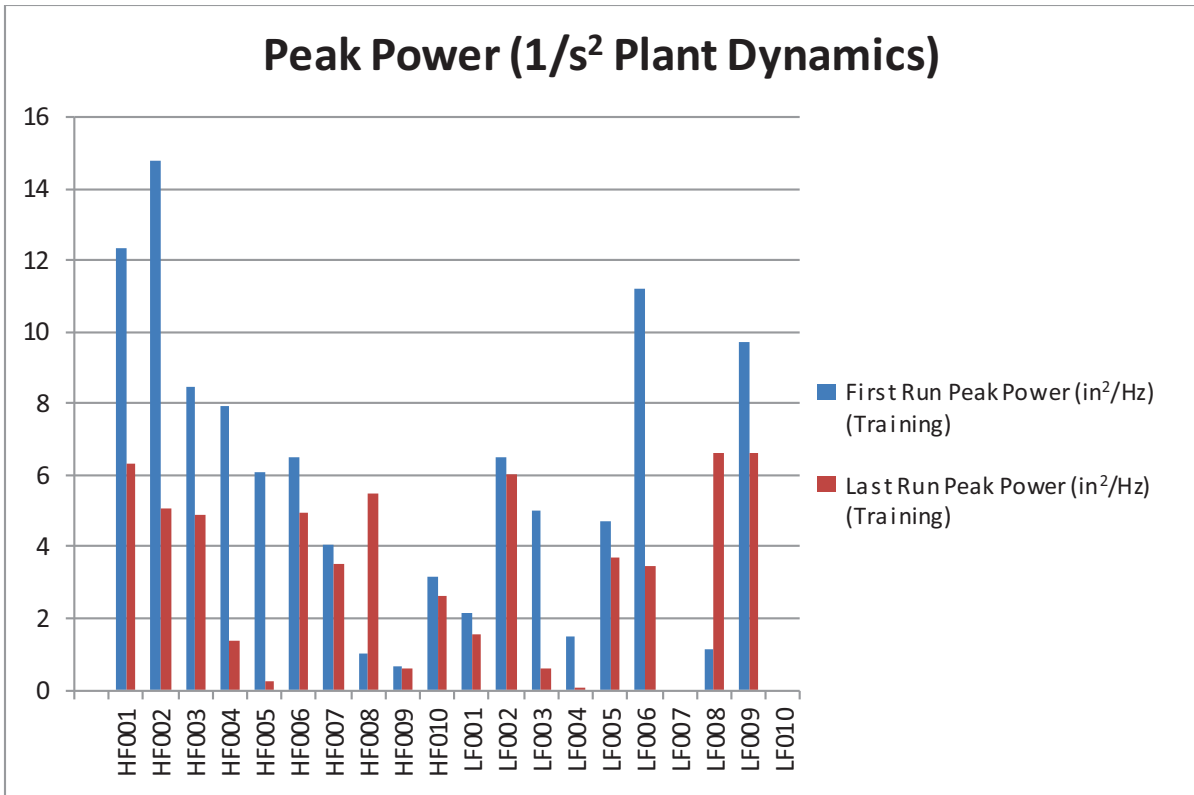




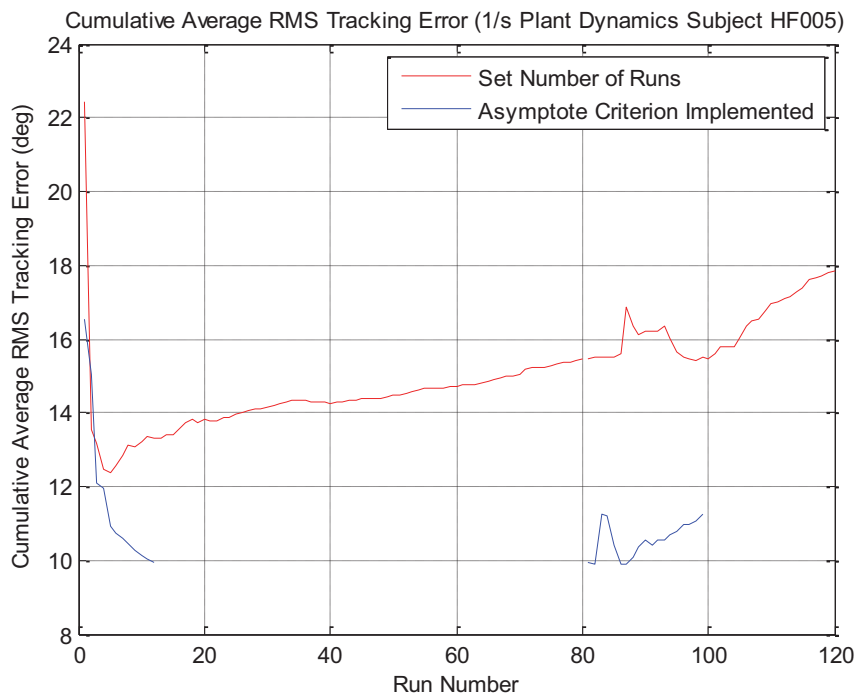
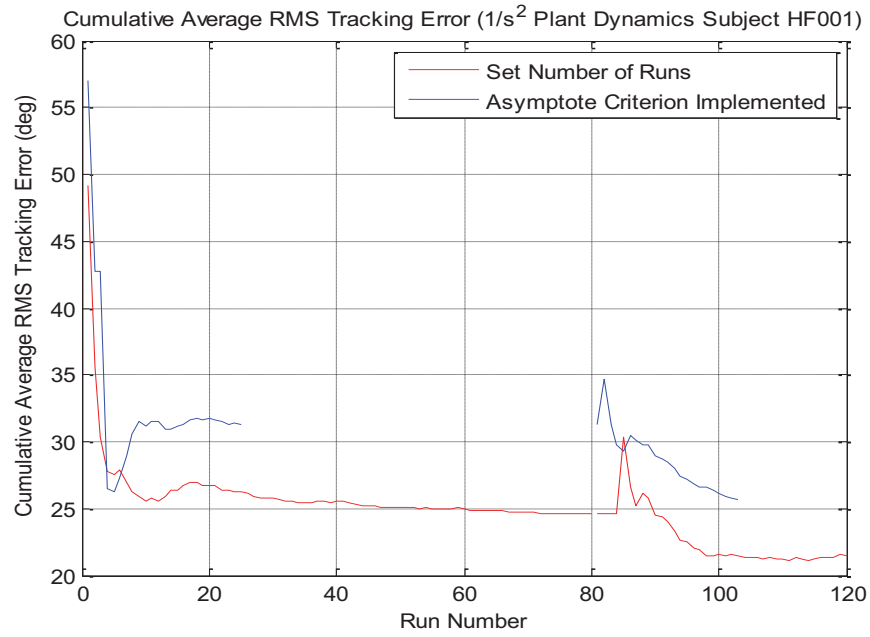


Appendix H: Peak Power and Frequency for Every Test Subject

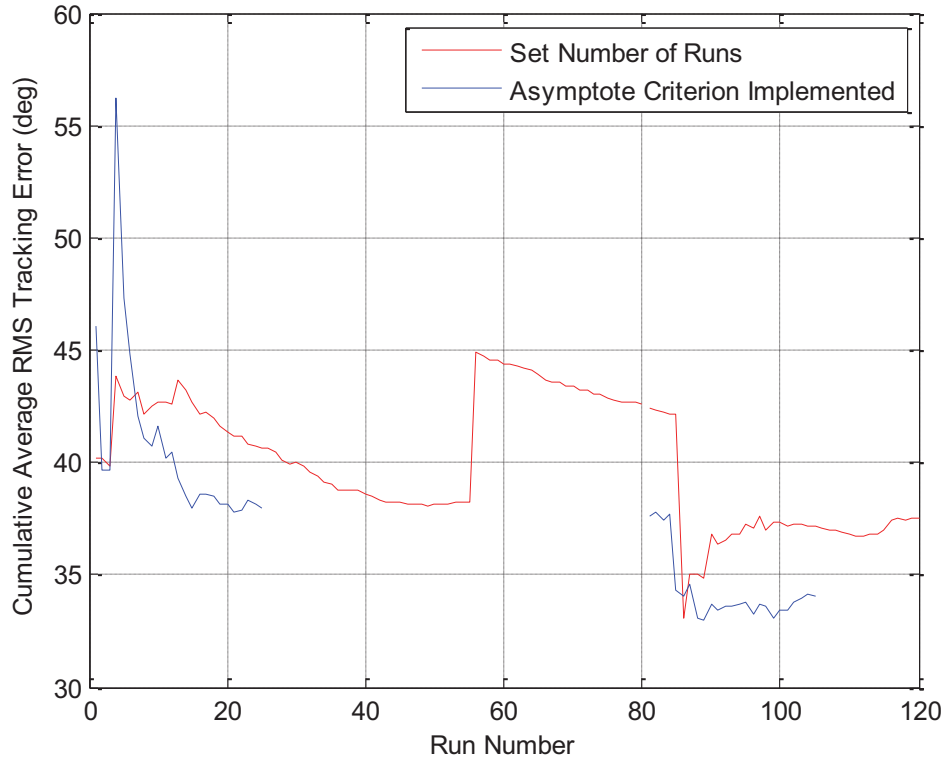




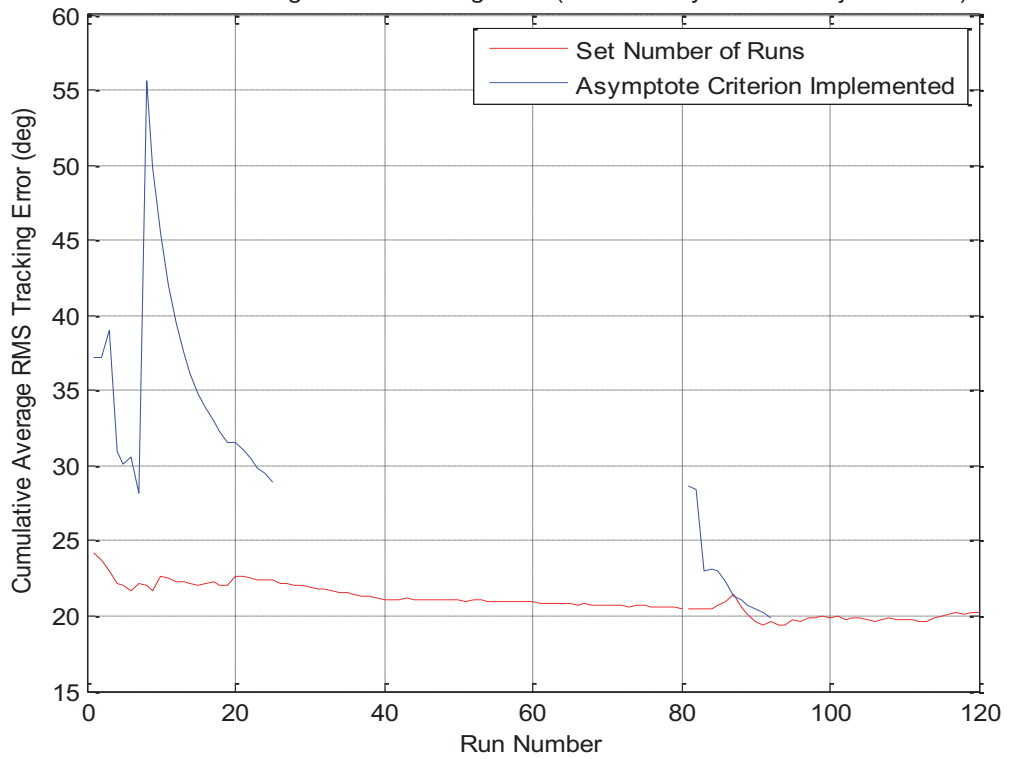
Appendix I: Average Tracking Error Using More Runs to Train

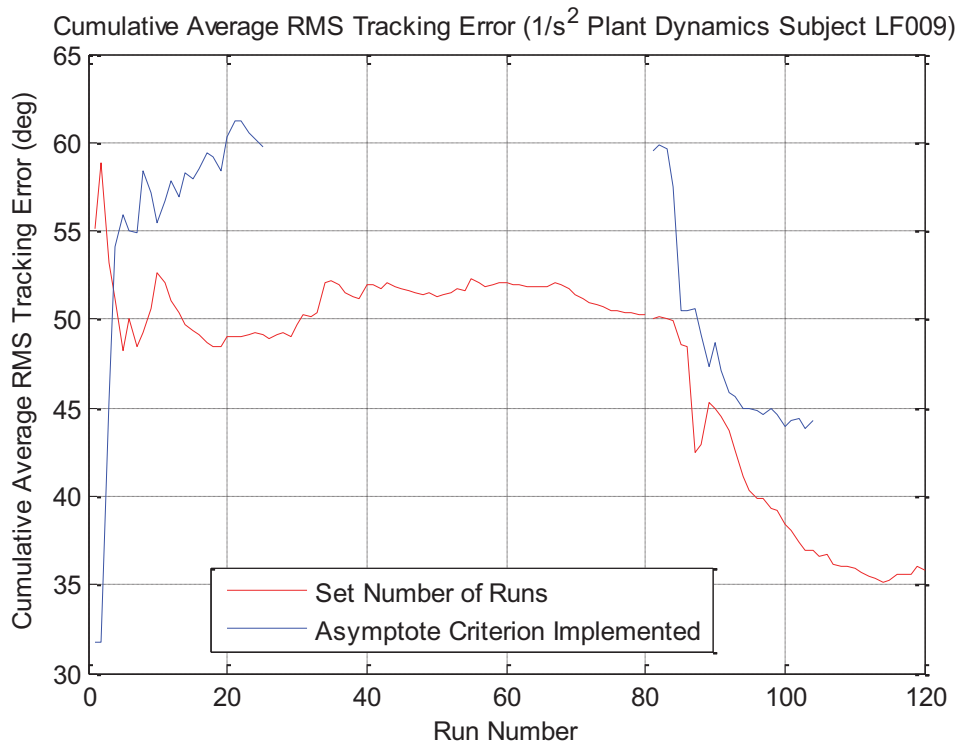
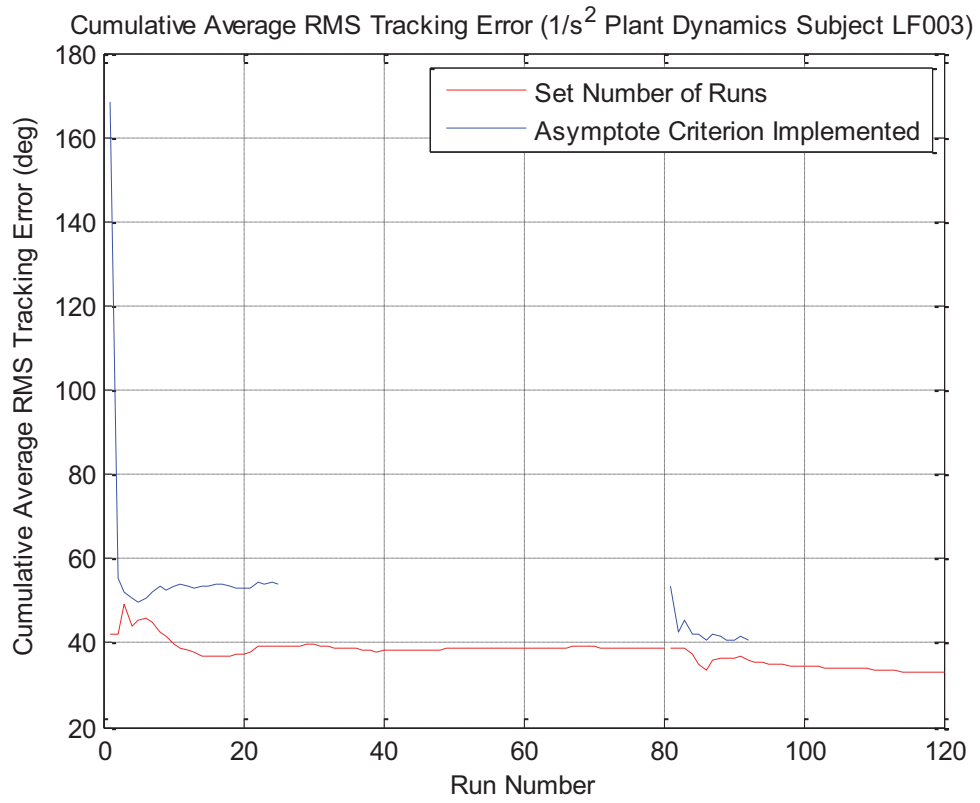


Cumulative Average RMS Tracking Error ($1/s^2$ Plant Dynamics Subject HF005)



Cumulative Average RMS Tracking Error ($1/s$ Plant Dynamics Subject LF003)





Appendix J: Smoothed Periodogram Matlab [21] Code

```
% Calculating the smoothed periodogram
function s = smoper(x,w);

% Input parameters:
% x: the data vector
% w: the window;
% Output:
% s: the smoothed periodogram, of length equal to that of x.

if (rem(length(w),2) == 0),
    error('Window in SMOOPER must have an odd length');
end
x = reshape(x,1,length(x));
%x = x - mean(x);
kappa = (1/length(x))*conv(x,flipr(x));
%kappa = conv(x,flipr(x));
n = 0.5*(length(kappa)-length(w));
s = fft([zeros(1,n),w,zeros(1,n)].*kappa);
s = abs(s(1:length(x)));

function [P, f] = smPSD(x, T, ifNorm, N, n)

% input: x--the signal
% input: T--the sampling rate of the signal
% input: ifNorm--flag for normalization (1) or not (0)
% input: N--window size
% input: n--window overlap
% output: P--the PSD
% output: f--the frequency (Hz)

% perform "slicing" of the signal
j=1;
L=0;

while L<=length(x)
    intvec(j,:)=[(j-1)*(N-n)+1, j*(N-n)+n];
    L=j*(N-n)+n;
    if intvec(j,2)>length(x)
        dta=intvec(j,2)-length(x);
        X(:,j)=[x(intvec(j,1):end); zeros((intvec(j,2)-length(x)),1)];
    end
end
```

```

else
    X(:,j)=x(intvec(j,1):intvec(j,2));
end
j=j+1;
end

% ----- proceed with PSD calculation -----
for j=1:size(X,2)

    x=X(:,j);
    len=length(x);

    % determine the length of FFT
    i=-1;
    K=0;
    while K<length(x)
        i=i+1;
        K=2^i;
    end
    % zeropad the signal to the length of FFT
    xz=[x' zeros(1, K-len)];

    if (rem(len,2) == 0), % determine the length of the window, it must be odd
        lwin=len-1;
    else
        lwin=len;
    end
    w = window(@hamming,lwin); % use hamming window. other window can also be
used
    %w = window(@hann,lwin); % use hann window. other window can also be used
    %w = window(@rectwin,lwin); % use rectangular window. other window can also
be used
    P(:,j) = SMOOPER(xz,w');
    if ifNorm==1
        P(:,j) = P/max(P); % normalization, optimal
    end

    Fs = 1/T;
    df = Fs/length(P)/2;
    f = 0:df:Ffs/2-df;

end

P=mean(P,2);
figure(2)

```

```

hold on
plot(f,P,'r')
title('PSD of Control Inceptor Deflection (HF001-1/s)')
xlabel('Frequency (Hz)')
ylabel('(control inceptor deflection)^2/Hz')
INT_PSD=trapz(P)

%%
% M=round(sqrt(length(Input)))
% [cxyM,F]=mscohere(Input,Output,M,0,256)
% figure(1)
% hold on
% plot(F,cxyM,'r')
% title('PSD of Control Inceptor Deflection (Data Set-Last Run)')
% xlabel('Frequency (Hz)')
% ylabel('(control inceptor deflection)^2/Hz')
%
% Gxy=(abs(P1)).^2;
% Gxx=P2;
% Gyy=P3;
%
% Cxy=Gxy./(Gxx.*Gyy);
% plot(f,Cxy)

```

References

- [1] Bailey, R.E. and Knotts, L.H., Interaction of Feel System and Flight Control System Dynamics on Lateral Flying Qualities, NASA Contractor Report 179445, 1990
- [2] Gum, Don R., Modeling of the Human Force and Motion-Sensing Mechanisms, Air Force Human Resources Laboratory-Advanced Systems Division, AFHRL-TR-72-54, June 1973
- [3] Herzog, James H., Matched Control Using the Matched Manipulator Control Technique, *IEEE Transactions on Man-Machine Systems*, Vol. MMS-9, No. 3, September 1968
- [4] Hess, Ronald A. and Zeyada, Y., Modeling Human Pilot Cue Utilization with Applications to Simulator Fidelity Assessment, *Journal of Aircraft*, Vol. 37. No. 4, July/August 2000
- [5] Hess, Ronald A. and Malsbury, T., Flight Simulator Fidelity Assessment in Rotorcraft Lateral Translation Maneuver, *Journal of Guidance, Control, and Dynamics*, Vol. 16, No. 1, January/February 1993
- [6] Hess, Ronald A. and Malsbury, T., Closed-Loop Assessment of Flight Simulator Fidelity, *Journal of Guidance, Control, and Dynamics*, Vol. 14, No. 1, January/February 1991
- [7] Hess, Ronald A., Analyzing Manipulator and Feel System Effects in Aircraft Flight Control, *IEEE Transactions on Systems, Man, and Cybernetics*, Vol. 20, No.4, July/August 1990
- [8] Hess, Ronald A., A Model-Based Theory for Analyzing Human Control Behavior, *Advances in Man-Machine Systems Research*, Volume 2, 1985, pp. 129-175
- [9] Hosman, Ruud J.A.W, Abbink, David A., and Cardullo, Frank M., The Neuromuscular System, *AIAA Modeling and Simulation Technologies Conference*, Toronto, Canada, August 2010
- [10] Johnston, Donald E. and Aponso, Bimal L., Design Considerations of Manipulator and Feel System Characteristics in Roll Tracking, NASA Contractor Report 4111, 1988
- [11] Johnston, Donald E. and McRuer, D.T., Investigation of Interactions Between Limb-Manipulator Dynamics and Effective Vehicle Roll Control Characteristics, NASA Contractor Report 3983, 1986
- [12] Levison William H., Effects of Simulator Delays on Performance and Learning in a Roll-Axis Tracking Task, *Fifteenth Annual Conference on Manual Control*, Wright State University, Dayton, Ohio, 1979
- [13] Magdaleno, R.E. and McRuer, D.T., Experimental Validation and Analytical Elaboration for Models of the Pilot's Neuromuscular Subsystem in Tracking Tasks, NASA Contractor Report 1757, April 1971
- [14] Magdaleno, R.E. and McRuer, D.T., Small Perturbation Dynamics of the Neuromuscular System in Tracking Tasks, NASA Contractor Report 1212, December 1968
- [15] McFadden Inc., Hydraulic Control Loader System Instruction Manual, 1999

- [16] Mitchell, David G. and Aponso, Bimal L., Effects of Cockpit Lateral Stick Characteristics on Handling Qualities and Pilot Dynamics, NASA Contractor Report 4443, June 1992
- [17] Schroeder, Jeffery Allyn, Helicopter Flight Simulation Motion Platform Requirements, NASA/TP-1999-208766, July 1999
- [18] Takats, J., Flight Control System Simulation, *Flight and Ground Vehicle Simulation Update*, 2011
- [19] Wiener, Earl L., Nagel, David C., Human Factors in Aviation, pg. 229-260, Academic Press, 1988
- [20] National Instruments Corporation (2012), *NI LabVIEW Technical Resources: Getting Started, Support, and Downloads*, <http://www.ni.com/labview/technical-resources/>
- [21] The MathWorks (1994-2013), *Documentation Center/Matlab*, <http://www.mathworks.com/products/matlab/>
- [22] The MathWorks (1994-2013), *Documentation Center/Simulink*, <http://www.mathworks.com/products/simulink/>

REPORT DOCUMENTATION PAGE

*Form Approved
OMB No. 0704-0188*

The public reporting burden for this collection of information is estimated to average 1 hour per response, including the time for reviewing instructions, searching existing data sources, gathering and maintaining the data needed, and completing and reviewing the collection of information. Send comments regarding this burden estimate or any other aspect of this collection of information, including suggestions for reducing this burden, to Department of Defense, Washington Headquarters Services, Directorate for Information Operations and Reports (0704-0188), 1215 Jefferson Davis Highway, Suite 1204, Arlington, VA 22202-4302. Respondents should be aware that notwithstanding any other provision of law, no person shall be subject to any penalty for failing to comply with a collection of information if it does not display a currently valid OMB control number.
PLEASE DO NOT RETURN YOUR FORM TO THE ABOVE ADDRESS.

1. REPORT DATE (DD-MM-YYYY) 01-07-2013		2. REPORT TYPE Technical Memorandum		3. DATES COVERED (From - To)	
4. TITLE AND SUBTITLE Investigation of Control Inceptor Dynamics and Effect on Human Subject Performance				5a. CONTRACT NUMBER	
				5b. GRANT NUMBER	
				5c. PROGRAM ELEMENT NUMBER	
6. AUTHOR(S) Stanco, Anthony A.; Cardullo, Frank M.; Houck, Jacob A.; Grube, Richard C.; Kelly, Lon C.				5d. PROJECT NUMBER	
				5e. TASK NUMBER	
				5f. WORK UNIT NUMBER 160961.01.01.01	
7. PERFORMING ORGANIZATION NAME(S) AND ADDRESS(ES) NASA Langley Research Center Hampton, VA 23681-2199				8. PERFORMING ORGANIZATION REPORT NUMBER L-20288	
9. SPONSORING/MONITORING AGENCY NAME(S) AND ADDRESS(ES) National Aeronautics and Space Administration Washington, DC 20546-0001				10. SPONSOR/MONITOR'S ACRONYM(S) NASA	
				11. SPONSOR/MONITOR'S REPORT NUMBER(S) NASA/TM-2013-218026	
12. DISTRIBUTION/AVAILABILITY STATEMENT Unclassified - Unlimited Subject Category 54 Availability: NASA CASI (443) 757-5802					
13. SUPPLEMENTARY NOTES					
14. ABSTRACT The control inceptor used in a vehicle simulation is an important part of adequately representing the dynamics of the vehicle. The inceptor characteristics are typically based on a second order spring mass damper system with damping, force gradient, breakout force, and natural frequency parameters. Changing these parameters can have a great effect on pilot control of the vehicle. A quasi transfer of training experiment was performed employing a high fidelity and a low fidelity control inceptor. A disturbance compensatory task was employed which involved a simple horizon line disturbed in roll by a sum of sinusoids presented in an out-the-window display. Vehicle dynamics were modeled as 1/s and 1/s ² . The task was to maintain level flight. Twenty subjects were divided between the high and the low fidelity training groups. Each group was trained to a performance asymptote, and then transferred to the high fidelity simulation. RMS tracking error, a PSD analysis, and a workload analysis were performed to quantify the transfer of training effect. Quantitative results of the experiments show that there is no significant difference between the high and low fidelity training groups for 1/s plant dynamics. For 1/s ² plant dynamics there is a greater difference in tracking performance and PSD; and the subjects are less correlated with the input disturbance function.					
15. SUBJECT TERMS Control inceptor; Vehicle simulation					
16. SECURITY CLASSIFICATION OF:			17. LIMITATION OF ABSTRACT	18. NUMBER OF PAGES	19a. NAME OF RESPONSIBLE PERSON
a. REPORT	b. ABSTRACT	c. THIS PAGE			STI Help Desk (email: help@sti.nasa.gov)
U	U	U	UU	179	19b. TELEPHONE NUMBER (Include area code) (443) 757-5802